A Study on Rheological Properties of Blood

and Improvements with High-Voltage Plasma Discharge

A Thesis

Submitted to the Faculty

of

Drexel University

by

Jin Mu Jung

in partial fulfillment of the

requirements for the degree

of

Doctor of Philosophy

May 2012

Acknowledgement

I would like to express my greatest gratitude to my adviser Prof. Young I. Cho. His kind help, full support, and sincere advice enabled me to achieve my research goal during my years at Drexel University. His guidance has always led me to the right direction and taught me how to explore solutions to the questions with a creative thinking, a process which was one of the biggest learnings in my life so far.

I also would like to convey my deep appreciation to Prof. Alexander Fridman, with whom I have a great pleasure and luck to have worked. I have been always amazed at not only the depth of his profound knowledge in plasma chemistry but also his broad understanding in both science and engineering.

Also, I am deeply grateful to Profs. Ying Sun, Mikhail Pekker, and Greg Fridman for their valuable advice as committee members. Without their sincere endeavors and support, it would not have been possible to complete my Ph.D. program.

I am very thankful to my friends and colleagues at A.J. Drexel Plasma Institute. During the years at DPI, I have experienced both the value of true friendship and the warmth of encouragement, which will make me smile whenever I look back to the days at DPI. Special thanks to Hyoungsup Kim, Yong Yang, Alla, Yelena, Kamau, Nathan, Natalie and Ivan with their endless help.

I feel thankful to my friends (Jonghyun Oh, Dalhyoung Kim and his family, Hwabok Wee and his family, Hojun Shin, and Hoyeon Lee and his family) who have always offered a true word of encouragement.

Best of all, I can’t find the words to thank my family enough for all the support, understanding, and love during the years of my study.

Table of Contents

List of Figures

List of Tables

Abstract

A Study on Rheological Properties of Blood

and Improvements with High-Voltage Plasma Discharge

Jin Mu Jung

Dr. Young I. Cho

Blood behaves as a shear-thinning non-Newtonian fluid where its viscosity varies due to both the deformability and aggregation of RBCs with the interaction with macro-molecules in blood plasma. The elevated whole blood viscosity (WBV), which indicates the increased frictional resistance between a moving blood and stationary vessel walls, has been suggested as one of the major determinants or risk factors of atherosclerosis diseases (i.e., cardiovascular diseases, stroke, and peripheral arterial diseases etc.) and microvascular disorders (i.e., diabetic retinopathy, nephrophathy, and neuropathy etc.) by causing both the endothelial injury of vessel walls and poor perfusion at capillaries.

In order to investigate the shear-thinning non-Newtonian behavior of blood in regards to the effects of increased wall shear stress and impaired oxygen delivery on various diseases that might be caused by hyperviscosity, the present study was focused on the studies of rheological properties of blood by examining the WBV profiles over a pathologically wide range of shear rates using a scanning capillary tube viscometer (SCTV) and their improvements using high-voltage plasma discharge.

Firstly, a new hematocrit-correction model using the Casson model was proposed to correct the measured WBVs of different blood samples with different hematocrits to a standard hematocrit of 45 %, a process which is needed to compare

the effect of intrinsic rheological properties or other determinants on blood viscosity for different blood samples. Without the measurement of plasma viscosity, the new model showed about 4 to 6 times more accurate and less deviations than the conventional Matrai's model.

Secondly, a new method of measuring the electric conductivity of whole blood was introduced for the purpose of hematocrit determination, demonstrating a simple but accurate hematocrit measurement by employing a low-frequency square-wave voltage signal in a conductance cell, without the usual error associated with the sedimentation of erythrocytes.

Thirdly, a new physical treatment method with the application of high-voltage plasma discharges (i.e. DBD and corona discharge) followed by filtration of the coagulated particles was proposed. The results indicated that WBV could be reduced by 9.1 % and 17.7 % for systolic blood viscosity (SBV) and diastolic blood viscosity (DBV), respectively, from the baseline values when DBD-treated blood plasma was filtered prior to mixing with red blood cells. When treated with the corona discharge for 60 pulses, DBV and LDL concentration dropped by 30.1 % and 31.5 %, respectively, from the baseline values.

Lastly, a new opaque standard viscosity fluid (SVF) was proposed using maltose with 55 % of concentration to replicate a shear-thinning non-Newtonian behavior of blood for different shear rates. The produced viscosity profiles from three different levels of SVFs provided low-, medium-, and high-standard viscosity fluids that can be used for the performance test of any blood viscometers over a wide range of shear rates. The applicability of new opaque SVFs was demonstrated by dye concentration test, repeatability test, and degradation test.

(BLANK PAGE)

CHAPTER 1: INTRODUCTION

1.1 Needs to Study Blood Viscosity

1.1.1 Introduction to Blood Viscosity

Blood viscosity is the frictional resistance between a moving blood and stationary vessel walls, which represents the thickness and stickiness of blood. Since about 45% of blood volume is made up of suspended cellular particles, primarily red blood cells (RBCs), the blood behaves as a non-Newtonian fluid where its viscosity varies with shear rates (i.e., the ratio of flow velocity to lumen diameter). From a rheological point of view, when blood moves at a high velocity during systole, blood viscosity becomes relatively low (shear thinning), with RBCs maximally deformed (ellipsoid) and dispersed to reduce flow resistance. During diastole, blood viscosity increases exponentially as RBCs tend to aggregate, a phenomenon which is caused by the interactions between RBCs and molecules existing in blood plasma [1, 2].

Whole blood has a relatively large range of viscosity, 4-45 cP (40-450 mP) with the change of shear rates. The systolic blood viscosity (SBV) measured at a shear rate of 300 s^{-1} has a normal value of about 3.8 cP (38 mP). The diastolic blood viscosity (DBV) measured at a shear rate of 1 s^{-1} has a normal value of about 20 cP (200 mP), which is about five times greater than the SBV due to the aggregation of RBCs [3].

1.1.2 Significance of Blood Viscosity Related to Cardiovascular Disease

According to the World Health Organization (WHO), cardiovascular diseases were the number one cause of death among the top ten causes of death globally. WHO also reported that, in 2008, an estimated 17.3 million people died from cardiovascular diseases, representing 30% of all global deaths. It was estimated that, by 2030, almost 23.6 million people would die from cardiovascular diseases, mainly from heart disease and stroke (cited from WHO website: www.who.int).

In the United States, mortality data reported by the American Heart Association (AHA) in 2011 showed that 0.8 million deaths of all 2.4 million deaths in 2007 were caused by cardiovascular disease, i.e., one in every three deaths, see Fig. 1-1. It also reported that, on the average, more than 2,000 Americans die of cardiovascular diseases each day, an average of 1 death every 40 seconds [4]. Of deaths due to cardiovascular disease, coronary heart disease and stroke accounted for more than 65 % because of their acute symptoms, see Fig. 1-2.

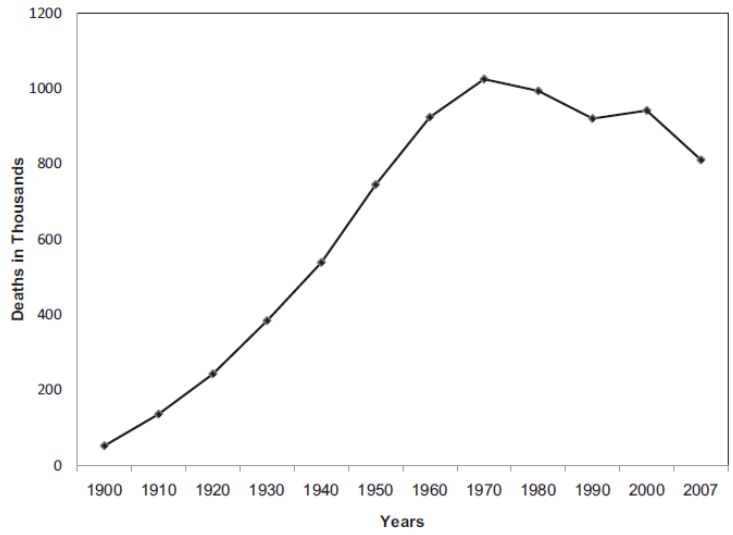

Figure 1-1. Deaths due to cardiovascular disease in the United States between 1900-2007 (source: National Center for Health Statistics & AHA) [4]

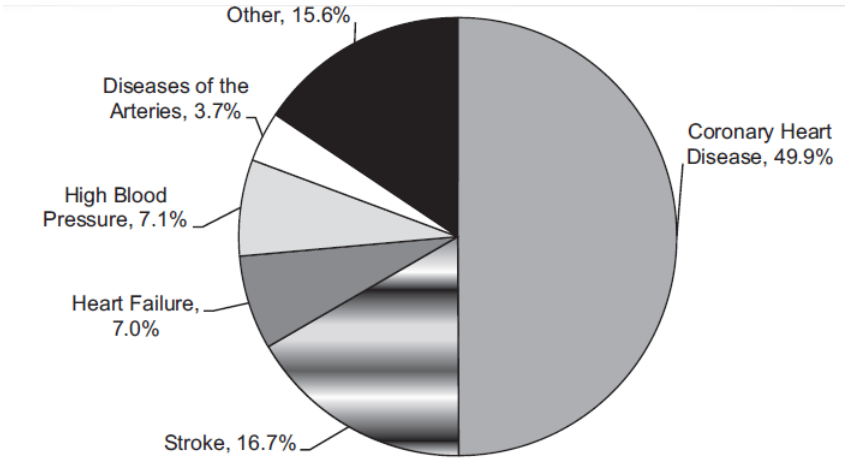

Figure 1-2. Percentage breakdown of deaths due to cardiovascular disease in the United States in 2007 (source: National Heart, Lung, and Blood Institute from National Center for Health Statistics reports and AHA) [4]

Figure 1-3 also shows that deaths by cardiovascular disease claims more lives each year than those by cancer. Referred from the report by Xu et. al. and AHA, in every year since 1900 except for 1918, cardiovascular diseases accounted for more deaths than any other major causes of death in the United States [4, 5].

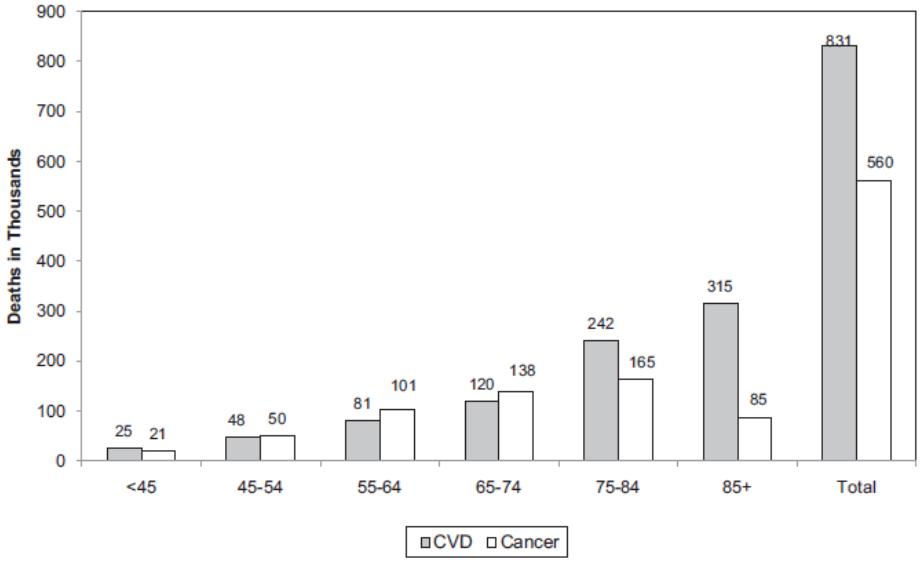

Figure 1-3. Cardiovascular disease deaths versus cancer deaths by age of the United States in 2007 (source: National Center for Health Statistics & AHA & Xu et al) [4, 5]

The risk factors for cardiovascular diseases such as coronary heart disease, cerebrovascular disease, peripheral arterial disease, thrombosis, and pulmonary embolism have been investigated and known to be affected by a number of factors such as fibrinogen, glucose, total cholesterol, LDL cholesterol, triglyceride, blood

pressure, smoking, diabetes etc.[1-4, 6-18].

However, most of researches in the field of cardiovascular disease, especially atherosclerosis and microvascular disorder, which are typically considered as two pathophysiological but contrasting manifestations related to blood flow, have been focused on the histology of blood and vessel wall chemistry [2]. It has been generally recognized that atherosclerosis is an ongoing sterile inflammatory process that begins with functional impairment of the arterial endothelium, whereas microvascular disorder is related to poor perfusion at small micro-vessels, leading to capillary loss [3]. However, the causes of both the endothelial injury of vessel walls and poor perfusion at capillaries have been remained incomplete from a biochemical perspective. Recently, it has become possible to explain the causes by shifting the perspective of understanding from a biochemical approach to a biomechanical one [2, 3].

The key concepts of the biomechanical approach to those diseases related to blood circulation are as follows:

1) The circulatory vascular system can be considered as a closed mechanical piping system in which the energy pumped by the heart must be absorbed by the arterial system [2].
2) A vascular element can be considered as a dynamically responsive organ producing autocrine and paracrine factors that may be regulated functionally by local hemodynamic shear stress [19-25].
3) The microvascular shear stress needs to exceed the yield stress (or

attractive forces between cells and macro-molecules) of blood in order to maintain capillary flow. If not, ischemia and capillary loss may be triggered [3].

Stating from those biomechanical concepts, the initial injury and subsequent events resulting in atherosclerosis could be explained as follows:

The resistance of vasculatures rises with the increase of WBV and thus, systolic pressure must increase to ensure the same circulating blood volume, in other words, for a constant cardiac output to be maintained [2, 26]. In the first phase (according to the protective adaptation theory), compliant arteries respond protectively at the cellular level to overstretching caused by an elevated blood pressure. This over-stretching results in arterial wall thickening, hardening, and subsequent loss of compliance (or called arteriosclerosis). After arteriosclerosis (i.e., the loss of arterial compliance) has developed [2], as blood passes through a bifurcation with a more injurious force, blood decelerates along the outer wall of the bifurcation, greatly reducing the local shear rate at the outer wall [23]. This causes WBV at the outer wall of the bifurcation (i.e., a low-shear-rate area) to be much oscillatory than that at the wall of the main lumen (i.e., a high-shear-rate area). This phenomenon causes endothelial dysfunction, which triggers subsequent vascular remodeling by the activation of endothelium, inflammation, the alteration of lipid metabolism, and finally the progression of atherosclerotic vascular diseases [3, 23]. Thus, atherosclerosis is a geometrically focal [23, 27], site-specific disease which

includes the carotid artery bifurcation, as well as the coronary, infrarenal, and femoral artery vasculatures. On the contrary, the arteries of the arms and breasts, and the veins are free of plaques formation [2].

Adopting the biomechanical concepts mentioned above, the capillary loss, a common outcome of microvascular diseases due to the stasis of blood flow, can also be explained as follows:

The yield stress can be defined as the minimum shear stress required to maintain a continuous flow of blood [28]. The physical origin of the yield stress is the attractive forces (i.e., ion bridges, hydrogen bonds, electrostatic charges, van der Waals forces etc.) between RBCs and the macro-molecules suspended in blood plasma medium. Thus, when the yield stress is greater than the shear forces exerted by the flow itself, hemostasis could occur locally due to the rapid interlocking of cells [3, 16, 29]. Subsequently, capillary loss could occur due to stoppage of oxygen delivery. Unless the shear stress of blood exceeds the yield stress, the perfusion at capillaries may not be maintained, then ischemia and capillary loss could be triggered [3].

The researches concerning the link between the elevated whole blood viscosity (WBV) and related diseases have been increased steadily. Both experimental and clinical data clearly have shown that the flow behavior of blood is a major determinant or risk factor of atherosclerosis diseases (i.e., cardiovascular diseases, stroke, and peripheral arterial diseases etc.) and microvascular disorder (i.e., diabetic retinopathy, nephrophathy, and neuropathy etc.) [1-3].

For specific examples, a positive relation between blood viscosity (or components of blood viscosity) and renovascular/essential hypertension has been reported [9, 30-32]. Blood viscosity has also been implicated as a determinant of hypertensive cardiac hypertrophy and peripheral vascular disease [9, 26, 33]. Moreover, elevated WBV may be a determinant of coronary artery disease, either indirectly because of its relation with systemic hypertension or directly because of its amplification of the resistance, with adverse effects on both clinical manifestations of coronary disease and myocardial oxygen delivery [2, 9, 26, 30-36].

Thus, abnormal (or increased) WBV makes a significant contribution to the pathophysiology of major sources of morbidity and mortality, such as cardiovascular and microvascular disorder, which could be risk factors or biomarkers for prediction, diagnosis, and treatment of those disorders [1-3, 37].

1.2. Methods to Measure Blood Viscosity

1.2.1 Conventional Methods to Measure Blood Viscosity

As the importance of WBV has been continuously increased, various experimental methods have been developed, where in vitro models of in vivo flow situation have been constructed using rotational or capillary viscometers, and relevant information on blood viscosity has been experimentally and clinically investigated [38].

The viscosity of blood has been measured using several types of

viscometers such as a rotational-type viscometer and a capillary-type viscometer [39]. However, those conventional viscometers have allowed the measurement of viscosity at a single point of shear rate [1, 2]. The value of blood viscosity measured at a single shear rate cannot fully describe the behavior of a non-Newtonian fluid, which represents dynamic properties of blood by complicated interactions between the suspended cell and molecules in blood [3]. Thus, it is required to measure blood viscosity over a wide range of physiologically relevant shear rates (i.e. from 1 s^{-1} to 1,000 s^{-1}) in order to understand the behavior of blood as a non-Newtonian fluid, see Fig. 1-4.

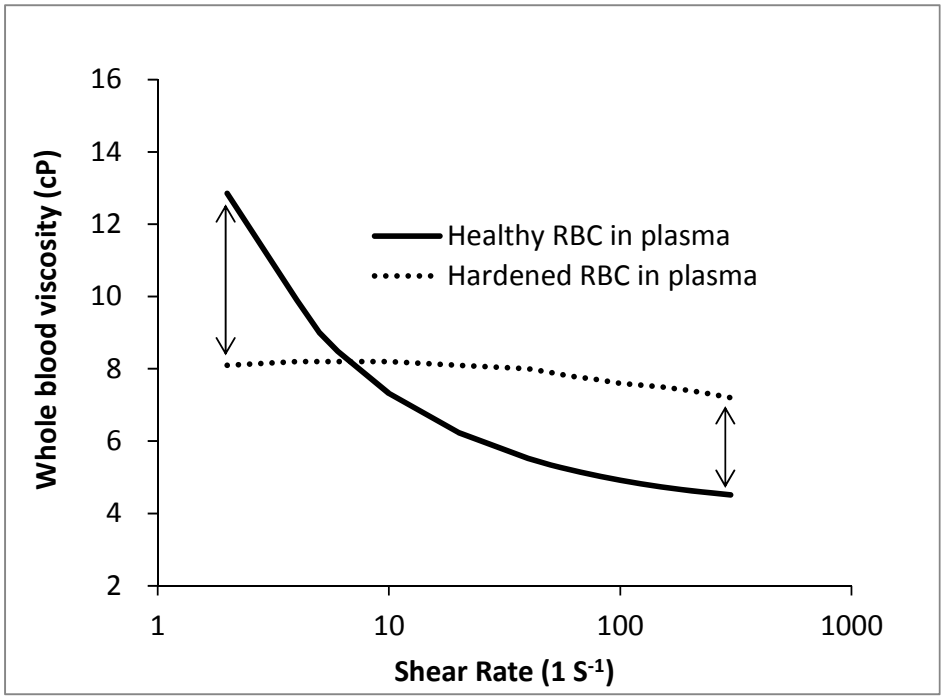

Figure 1-4. Curves of WBV versus shear rates from 1 to 1,000 s^{-1} for normal and hardened RBCs in blood plasma [**1**, **2**]

When a rotating viscometer is alternately used to measure blood viscosity at multiple points of share rates, it is not only a time-consuming but also could influence the validity of viscosity measurement as the blood cells could be ruptured by several sudden changes of shear rates for a relatively long-time measurement. In addition, the structural limitation of a rotating (i.e., spring sensitivity) viscometer provides inaccurate results at physiological shear rates less than 1 s^{-1}. A capillary viscometer was often used to measure plasma viscosity at a single maximum shear rate. Thus, it is not proper to conduct the measurement of whole blood viscosity for multiple shear rates with the capillary viscometer. Furthermore, these two techniques require the direct handling of blood and manual cleaning of the equipment, the processes which could cause a potential risk for the operator to make contact with contaminated blood [2].

Those limitations of conventional viscometers in laboratory measurements have led the researchers to measure whole blood viscosities at several specific points of shear rates (i.e., shear rates of 1, 5, 208 s^{-1}, etc.) instead of a wide range of shear rates [9], limiting clinical applications of blood viscosities.

1.2.1 Scanning Capillary Tube Viscometer (SCTV)

In order to understand the overall characteristics of flow behavior of blood, one needs to measure the viscosity of blood for a pathologically wide range of shear rates (i.e., from 1 to 1,000 s^{-1}), which could be related to a critical risk factor or biomarker for diagnosis and treatment of cardiovascular and microvascular diseases

[1-3]. Depending on these necessities, an automated scanning capillary tube viscometer (SCTV) using a U-shaped disposal tube (Hemathix in USA / BVD in South Korea) has been developed, which can measure the viscosity of whole blood over a wide range of shear rates (i.e., from 1 to 1,000 s^{-1}) by one-time measurement [40-44].

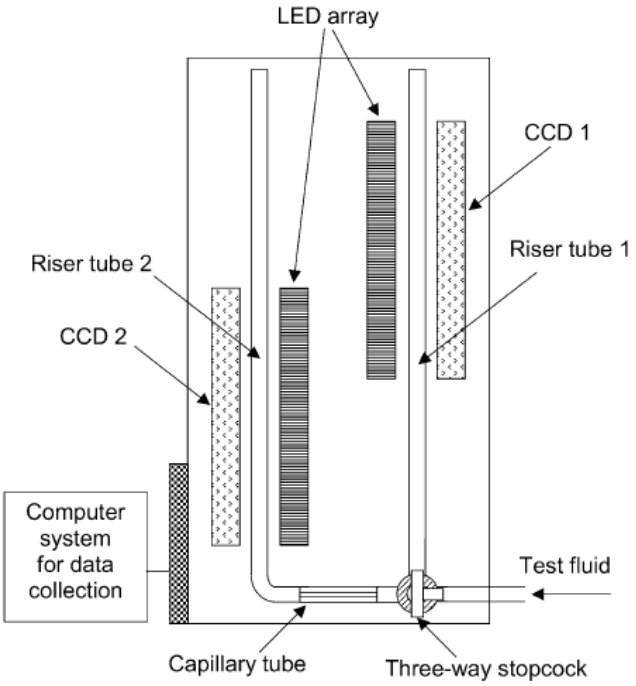

Figure 1-5. Schematic diagram of the SCTV system for blood viscosity measurement used in the present study [**41**, **43**]

As seen in Fig. 1-5, two charge-coupled devices (CCDs) and two light-emitting diodes (LEDs) are vertically installed in the SCTV system to detect height changes of blood along two riser tubes. This system is using a Casson model to mathematically describe the non-Newtonian behavior of blood viscosity using a yield stress term as follows:

$$\sqrt{\tau} = \sqrt{\tau_y} + \sqrt{k}\sqrt{\dot{\gamma}} \quad \text{when} \quad \tau \geq \tau_y \qquad \text{(Eq. 1-1)}$$

$$\dot{\gamma} = 0 \quad \text{when} \quad \tau \leq \tau_y$$

where τ denotes the shear stress by the flow of blood, $\dot{\gamma}$ is the shear rate, τ_y is the yield stress, and k is a Casson model constant.

The mean flow velocity at the riser tube can be obtained as a result of calculating the flow rate at the capillary tube using the expressions of shear rate and pressure drop across the capillary tube from the Casson model. Then, the unknowns, such as a Casson constant, height difference, and additional effect on height difference by surface tension, can be determined through curve-fitting procedure using the height measurements, and the derivative of the height difference at the riser tube [41, 44]. Thus, the apparent viscosity, η, can be calculated as follows [44]:

$$\eta(t) = k + \frac{\left(\frac{\rho g R_e \Delta h_y}{2L_c}\right)}{\dot{\gamma}(t)} + \frac{\sqrt{\frac{2k\rho g R_e \Delta h_y}{L_c}}}{\sqrt{\dot{\gamma}(t)}} \qquad \text{(Eq. 1-2)}$$

where, ρ = the density of blood

g = gravitational acceleration

R_e = Reynolds number

Δh_y = the height of blood at riser tube

L_c = the length of capillary tube

Once the measurement is initiated in the SCTV, the Riser tube 1 is filled with blood up to a pre-determined height. Then, as a three-way valve rotates, the blood in the Riser tube 1 moves to Riser tube 2 through a glass capillary tube. Here, the SCTV system continuously measures the height difference of fluids moving in the two vertical riser tubes, which replicates high shear flow when the height difference is large, and low shear flow when the height difference gradually reduces. Detailed mathematical descriptions are given elsewhere [41, 44].

1.3 Objectives of the Present Study

As the WBV profile over a pathologically wide range of shear rates can be measured using the SCTV, clinical experiments can be conducted in order to investigate the effect of blood viscosity on various diseases that might be caused by hyperviscosity of blood, in regards to the effects of increased shear stress or yield stress and impaired oxygen delivery on the diseases related to blood circulation (i.e. cardiovascular diseases, diabetes, retinal vein occlusion, hemodialysis etc.).

Accordingly, it has also become important on how to utilize the measured blood viscosity information in order to derive meaningful interpretation with experimental and clinical significance.

Thus, the present study was focused on the studies of hemorheological properties of blood related to blood viscosity over a wide range of shear rates. For example, the present study examined a new method to correct the WBV profiles for reliable analysis, the incorporation of the WBV results with other hemorheological properties (i.e. hematocrit) to indicate oxygen delivery index, the improvement (or reduction) of blood viscosity by applying electrical plasma discharges, and the proposal of a standard viscosity fluid for blood viscosity measurements using the SCTV.

The detailed objectives of the present study are as follows:

Objective 1 was to investigate a new procedure for the correction of the measured blood viscosity over a wide range of shear rates (i.e., from 1 to 1,000 s^{-1}) to a standard hematocrit of 45 % using a constitutive equation describing a non-Newtonian behavior of blood, the Casson model.

Objective 2 was to conduct a research and development on an on-line hematocrit conductance cell in order to automatically determine the oxygen delivery index.

Objective 3 was to investigate the feasibility of the improvement of WBV (or reduction of WBV) by applying high-voltage plasma discharge to blood. The mechanism of the change of blood viscosity by the electric plasma discharge was also studied over a wide shear rate range.

Objective 4 was to conduct a research and development on a new standard viscosity fluid for blood viscosity measurements.

CHAPTER 2: A NEW HEMATOCRIT-CORRECTION MODEL

2.1 Motivations and Literature Survey on the Correction of WBV

Hematocrit, the volume fraction of red blood cells in whole blood, is the main determinants of blood viscosity. Depending on the deformability of red blood cells, blood viscosity can increase by approximately 20 % with increase of hematocrit by 10% [2]. Since hematocrit and blood viscosity has an exponential relation, blood viscosity becomes increasingly dominant to hematocrit alterations at higher levels of hematocrit. It is also known that there is about 4% increase of blood viscosity per unit increase of hematocrit at medium to high shear rates [1, 15].

Thus, in order to evaluate the effect of intrinsic rheological properties or other determinant on blood viscosity, it requires estimating the rheological properties of different blood samples with different hematocrits at the same hematocrit value (i.e. 45 % hematocrit). This can be achieved by reconstituting blood samples of different hematocrits to a standard hematocrit (i.e. 45 %) [45] by adding blood plasma to samples with hematocrit over 45 % or removing blood plasma from samples with hematocrit below 45%. However, this procedure could not only cause artifacts during reconstituting hematocrit values, but also be impractical in clinical applications where the likelihood of infection always exists.

Alternatively, Matrai et al. [45] introduced a hematocrit-correction model by adopting plasma viscosity to the correction of the measured WBV to a standard hematocrit of 45 %. The method proposed by Matrai et al. has been widely used for correction at different hematocrits [46]. On this basis, the measured WBV at native

hematocrit could be mathematically corrected to the WBV at a standard hematocrit of 45 % as follows [45]:

$$\frac{\mu_{45\%\,\mathrm{hct}}}{\mu_{\mathrm{PV}}} = \left[\frac{\mu_{\mathrm{native\,hct}}}{\mu_{\mathrm{PV}}}\right]^{\frac{45}{\mathrm{Hct}}} \qquad \text{(Eq. 2-1)}$$

Where $\mu_{45\%\,\mathrm{hct}}$ is the corrected WBV to a standard hematocrit of 45 %, $\mu_{\mathrm{native\,hct}}$ is the measured WBV at native hematocrit, μ_{PV} is plasma viscosity (blood viscosity at 0 % hematocrit), and Hct is the measured native hematocrit [%], respectively [45].

Due to its simplicity in calculating the corrected blood viscosity, Matrai's model has been widely utilized, considering the effects of unequal hematocrit and thus allowing the direct comparison of WBV values at the same hematocrit of 45 % [47].

Lowe et al. [33] performed a study on the association of blood rheological factors, such as WBV, plasma viscosity, hematocrit, fibrinogen, and activation of coagulation in patients with lower limb ischemia. Blood samples were measured in random samples of 1,581 men and women aged 55 to 74 years in Edinburgh, Scotland and the measured WBVs were corrected to a standard hematocrit of 45 % using the Matrai's model. As a results of multivariate analysis, it was found that blood viscosity ($p < 0.05$) and fibrinogen ($p < 0.01$) were independently associated with peripheral arterial narrowing associated with lower limb ischemia in the general population which may be implicated in its pathogenesis [33].

Using another results from the same Edinburgh Artery Study, Amanda et al. [48] also studied the relationship between rheological factors and carotid intima-

media thickness (IMT). During 1988-1989, for baseline, the Edinburgh Artery Study measured whole blood and plasma viscosities, and hematocrit including other critical factors (i.e. fibrinogen, tissue plasminogen activator (tPA), fibrin D-dimer, von Willebrand factor (vWF)) from 1,106 men and women 60 to 80 years old. Then, 5 years of follow-up measurements of IMT had been performed, where the measured WBVs were corrected to a standard hematocrit using the measured plasma viscosity and native hematocrit. The results showed that, in men, blood viscosity and its major determinants were linearly related to IMT, suggesting that blood viscosity was associated not only with incident cardiovascular events but also with the early stages of atherosclerosis [48].

Freyburger et al. [49] investigated the effects of five different plasma substitutes, which were commonly used in preoperative normovolaemic acute haemodilution, on rheological properties such as WBV and plasma viscosity. WBV and plasma viscosity were measured using Contraves LS 30 rotational viscometer at low shear rate, 1 s^{-1}, and high shear rate, 128.5 s^{-1}. The measured WBVs were mathematically corrected using Matrai's model resulting in that the five substitutes had very different effects on red blood cell aggregation and the corrected WBV at low shear rate (mostly dominant by red blood cell aggregation) was reduced in the presence of 4% human albumin (HA) and 3.5% dextran 40 (Dxt 40), but was increased moderately in the presence of 6% dextran 60 (Dxt 60), 6% hydroxyethylstarch 200 (HES), and modified fluid gelatin (Gel) in the following order: HES < Dxt 60 < Gel.

Lee et al. [47] evaluated the pathophysiological abnormalities of stable

angina (SA) and acute coronary syndromes (ACS) promoted by the rheological properties of blood. WBV and plasma viscosity of blood samples collected from 16 healthy, 16 SA, 18 unstable angina (UA), and 19 acute myocardial infarction (AMI) patients were measured and corrected to a standard hematocrit (i.e. 40 %) as shown in Fig. 2-1. The yield stress was calculated using the Casson Equation in order to estimate fluid forces associated with local blood flow. The study showed an association between hemorheological abnormalities and the severity of coronary artery disease [47].

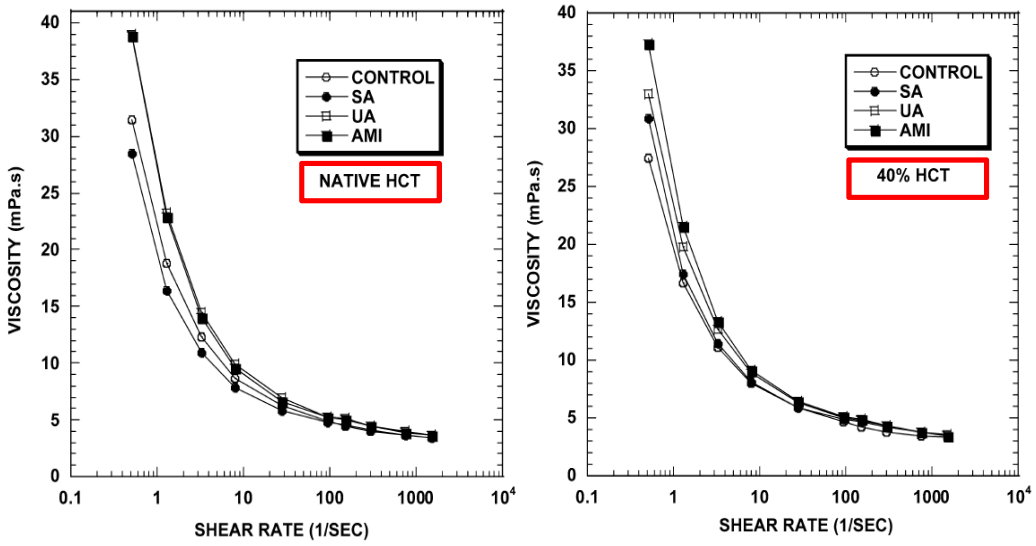

Figure 2-1. Differences in blood viscosity between native hematocrit (left) and corrected hematocrit (right) cases for control, stable angina, unstable angina and acute myocardial infarction patients [47]

At the same manner, Lee et al. also investigated the association of microcirculatory dysfunction in cardiac syndrome X (CSX) with abnormalities of

blood rheology (i.e. blood viscosity and red blood cell aggregation), showing that CSX patients had markedly abnormal blood rheology such as elevated hematocrit-corrected blood viscosity, plasma viscosity and yield stress including higher red blood cell aggregation [50].

Box et al. [46] investigated the effects of blood viscosity, variations in flow rate, and vessel diameter on plaque development which particularly occurs in the recirculation region at a carotid bifurcation where local wall shear stress oscillates. In accordance with the results given by Matrai's model where WBV is exponentially dependent on the increased hematocrit levels, Box et al. proposed to replace the power-law index n in the Carreau-Yasuda (CY) model by hematocrit and performed a numerical simulation by means of the finite element method. As shown in Fig. 2-2, maximum WSS oscillation was found at the edges of the recirculation region at a carotid bifurcation and proposed a possible adoption of the CY model to incorporate the differences of blood viscosity caused by the difference in hematocrits.

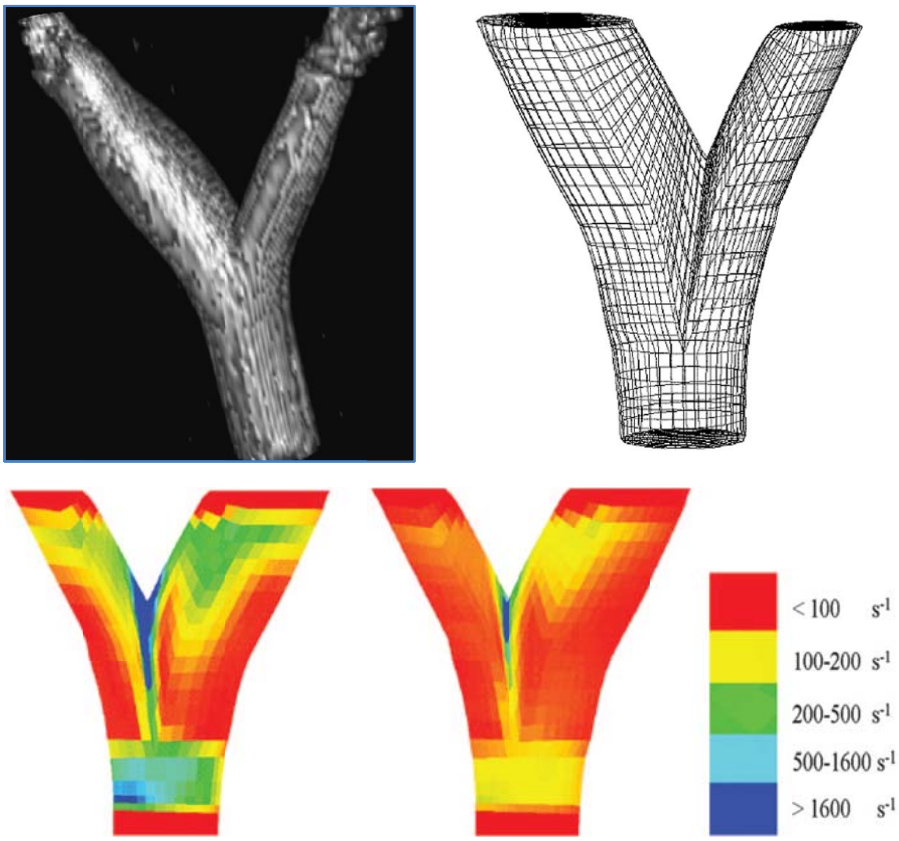

Figure 2-2. Magnetic resonance angiography (MRA) image (top left) and meshed model of a carotid bifurcation (top right) with the results of a numerical simulation for oscillatory wall shear rates during peak systole (bottom left) and middiastole (bottom right) [46]

Vlastos et al. [51] investigated the effect of oral fluid intake on blood rheology. WBV measured at 1, 10 and 100 s^{-1} were also corrected using Matrai's method and the results showed that WBV were reduced at 30 and 120 minutes following hydration, however no significant difference after correction to a standard hematocrit [51].

Michalska-Malecka et al. [52] studied to correlate pathogenetic factors with the hemorheological parameters in age-related macular degeneration (AMD) by

measuring blood viscosity. The studies were performed on 52 patients suffering from AMD. The control group consisted of 42 healthy persons. The measured WBV, corrected WBV, and plasma viscosity increased respectively by 6.9%, 14.6%, and 15.7% higher in the AMD group than healthy group as shown in Fig. 2-3.

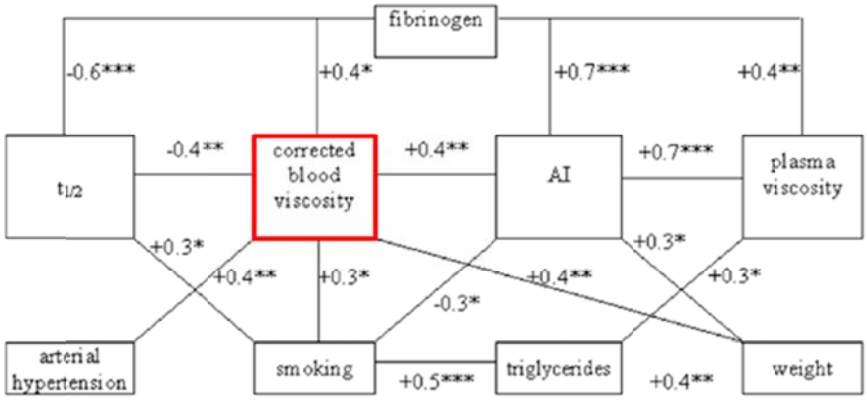

Figure 2-3. Corrected WBV for investigation of the correlation of different pathogenetic factors in age-related macular degeneration [51]

Thus, the Matrai's model has been widely utilized in various researches where the correction of the measured WBV to a standard hematocrit was required. However, plasma viscosity was required to be measured as well as the measurement of WBV and native hematocrit according to the equation given in (eq. 2-1), in order to mathematically calculate the corrected WBV. This means that it requires not only the collection of additional volume of blood for plasma viscosity measurement but

also additional process to separate cells from blood plasma to measure plasma viscosity using either a capillary tube viscometer (i.e. Ostwald viscometer) or a cone-and-plate rotating viscometer (i.e. Brookfield viscometer) [17, 39]. The non-disposable structures of both the capillary tube viscometer and the rotating viscometer need manual cleaning after each measurement, a process which could cause time-consuming and a potential risk for the operator to contact with contaminated blood.

Thus, it is necessary to propose a new hematocrit-correction model that does not require additional measurements of plasma viscosity, but with a WBV alone.

In addition, while Matrai's model was developed based on blood viscosity measured with LS-30 viscometer at two specific shear rates of 0.7 and 94.5 s^{-1} [45], the scanning capillary tube viscometer (SCTV) utilized in the present study was able to produce WBV profile over a wide range of shear rates [41, 43, 44]. Thus, it would be also interesting to investigate the validity of the Matrai's model on the correction of WBV over a wide range of shear rates.

Thus, the objectives of the present chapter was to propose a new procedure to correct blood viscosity to a standard hematocrit (i.e. 45 % hematocrit) without actual measurement of plasma viscosity and investigate the validity of the Matrai's model over a wide range of shear rates (i.e. from 1 to 1,000 s^{-1}).

2.2 Methods

2.2.1 Sample Preparation

Blood samples were obtained from three healthy volunteers into each 200 mL-evacuated glass bottle which contained 2.0 mL of ethylene diaminetetra-acetic acid (EDTA) as an anti-coagulant. Hematocrits of the three blood samples were first measured using a microcenrifuge (StatSpin MP, Iris) to determine the amount of blood plasma required to reconstruct the whole blood samples for 25, 30, 35, 40, 45, 50, 55, and 60 % hematocrit values.

The whole blood in the 200 mL-glass container was then transferred to 10 mL-polyethylene tubes to separate cells using a centrifuge (Fleta 5, Hanil) at 1,500 G of relative centrifugal force (RCF) for 15 min. After the completion of centrifuge, hematocrit values were carefully adjusted into 25, 30, 35, 40, 45, 50, 55, and 60 % (which were considered to be clinically possible ranges of hematocrits) by adding or removing blood plasma according to the following equation to calculate the required volume of blood plasma for reconstructing blood samples to target-hematocrit values:

$$\text{Required volume of plasma (mL)} = \frac{(100 - \text{target Hct}) \times (\text{current Hct})}{10 \times (\text{target Hct})} \qquad \text{(Eq. 2-2)}$$

Since transferring red blood cells directly from the centrifuged 10-mL container to another one could possibly cause hemolysis, which is the destruction of thin and weak membrane surface of red blood cells, blood plasma was added into or removed from the centrifuged 10-mL containers instead of transferring red blood cells.

For example, when hematocrit of blood sample was 48 %, one could calculate additional volume of blood plasma required to prepare a 30 %-hematocrit adjusted sample as follows:

$$\text{Required volume of blood plasma (mL)} = \frac{(100-\text{target Hct}) \text{ x } (\text{current Hct})}{10 \text{ x } (\text{target Hct})}$$

$$= \frac{(100-30) \text{ x } (48)}{10 \text{ x } (30)} = 11.2 \text{ mL} \quad \text{(Eq. 2-3)}$$

Thus, the hematocrit values could be reconstituted by adding 6 mL of additional blood plasma to the original blood sample with 48 % hematocrit. The required volume of blood plasma calculated to adjust for different hematocrit values are given in Table 2-1.

Table 2-1. Examples of the required volume of blood plasma to reconstitute to target-hematocrit values

	Control	Target-hematocrit values to adjust							
	48 %	25 %	30 %	35 %	40 %	45 %	50 %	55 %	60 %
Red blood cell (mL)	4.8 mL	4.8 mL	4.8 mL	4.8 mL	4.8 mL	4.8 mL	4.8 mL	4.8 mL	4.8 mL
Total volume of blood plasma (mL)	5.2 mL	14.4 mL	11.2 mL	8.9 mL	7.2 mL	5.9 mL	4.8 mL	3.9 mL	3.2 mL
Required blood plasma (mL)	-	Add 9.2 mL	Add 6 mL	Add 2.7 mL	Add 2 mL	Add 0.7 mL	Remove 0.4 mL	Remove 1.3.mL	Remove 2 mL

2.2.1 Measurement of WBV and Plasma Viscosity

After the procedure to reconstruct hematocrit values was completed, all the hematocrit-adjusted blood samples were gently mixed using a roller-type mixer in order to have the centrifuged red blood cells uniformly dispersed and mixed evenly with blood plasma. Then, hematocrit values for all the hematocrit-adjusted blood samples were measured again to verify that they were correctly adjusted to the target hematocrit values.

The hematocrit-adjusted blood samples in 10 mL-polyethylene tubes were then divided into two 4-mL plain vacutainers for WBV measurement. WBV was measured at 37^{o}C using the SCTV over a range of shear rates from 1 to 1,000 s^{-1}. Detailed test and viscosity calculation procedures are given elsewhere [43, 44]

In order to measure plasma viscosity, two 10-mL of whole blood samples were taken from a 200-mL evacuated glass bottle and transferred to two 10-mL-polyethylene tubes for centrifuge. After cells in whole blood were separated from blood plasma, blood plasma in the tubes was moved into two 4-mL-plain vacutainers. Dye of about 0.2 % concentration by weight was added to make blood plasma opaque and then the viscosity of blood plasma was also measured using the SCTV.

The effect of adding dye on the change of viscosity had been investigated elsewhere and confirmed that it did not alter the magnitude of fluid viscosity as long as the dye concentration was less than 2 % concentration in volume [43].

2.2.3 Data Analysis

Three different whole blood samples obtained from three healthy volunteers, respectively, were adjusted to 25, 30, 35, 40, 45, 50, 55, and 60 % hematocrit values. In order to increase the accuracy, two samples of a given hematocrit were measured per each case, and the viscosity results were averaged.

The WBV profile generated after WBV measurement contained continuous 10,000 data points over a range of shear rates from 1 to 1,000 s^{-1}, as shown in Fig. 2-4. Due to its difficulties in handling and analyzing all the 10,000 data, several specific points of shear rates (i.e. 1, 2, 4, 5, 6, 10, 20, 40, 50, 60, 80, 100, 150, 200, 250, and 300 s^{-1}) were selected and utilized in both investigating the validity of Matrai's model to the measured WBV profile and proposing a new hematocrit-correction model.

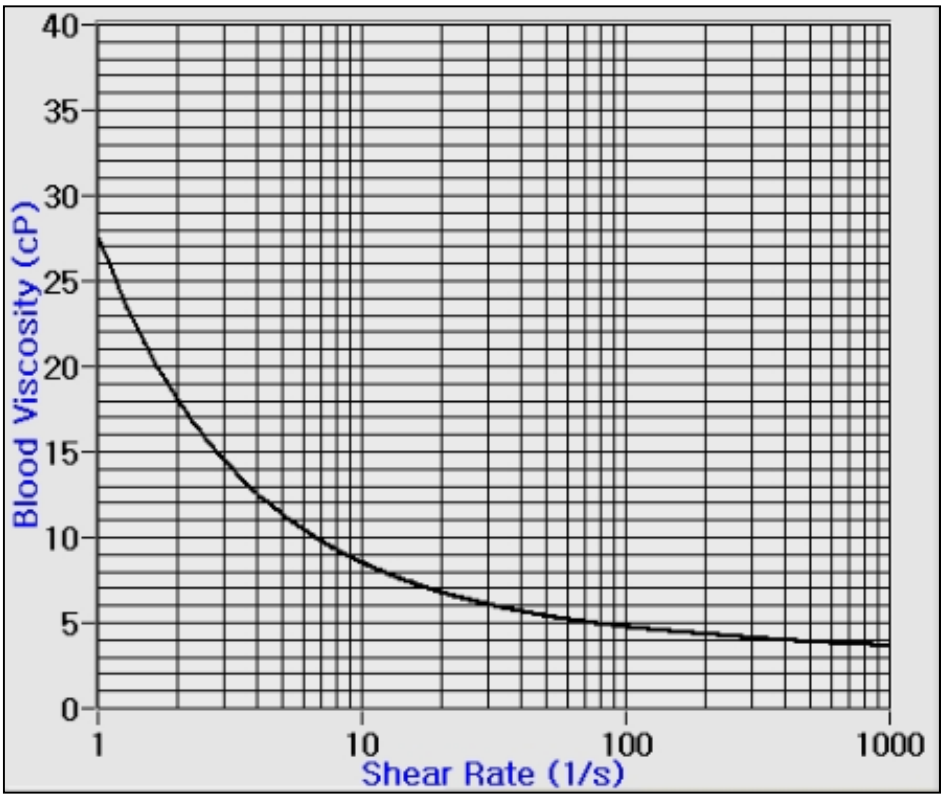

Figure 2-4. A WBV profile obtained from WBV measurement using SCTV [41, 44]

Statistical analysis was performed using a linear regression analysis to evaluate the correlations between the cube root of the measured yield stress, (or the cube root of the Casson constant and hematocrit values. A p-value less than 0.05 was considered to be statistically significant, which was the same as having a 95% confidence interval.

The sum of the error for both the correct WBV using a new model and the one using the Matrai's model was calculated to compare the validity of a new hematocrit-correction model with the Matrai's model.

2.3 Results and Discussion

2.3.1. A New Procedure to Correct the Measured WBV

Human blood is known to have a yield stress, which can be defined as the minimum shear stress required to maintain a continuous blood flow [28, 29] or the limit of the shear stress when the shear rate approaches zero [3]. Such a yield stress is caused by the aggregation of red blood cells at a very low shear rate, and as shear stress overcomes the yield stress, red blood cells disperse and blood starts to flow. In order to describe such a flow model of particles, the Casson model was utilized in the present study. The yield stress can be expressed as shown in (eq. 1-1) [28, 29, 53].

By rearranging (eq. 1-1) regarding to a viscosity term, the following equation can be obtained:

$$\eta(t) = k + \frac{\tau_y}{\dot{\gamma}_w(t)} + \frac{\sqrt{4k\tau_y}}{\sqrt{\dot{\gamma}_w(t)}} \qquad \text{(Eq. 2-4)}$$

Thus, one can obtain blood viscosity by determining the yield stress, τ_y, and the Casson constant, k.

Interestingly, the yield stress and the Casson constant terms are known to be affected by both the particle concentration (i.e. hematocrit) and the viscosity of medium (i.e. plasma viscosity) [28, 29]. From this observation, the present study offers a hypothesis that, by adopting both the yield stress and the Casson constant terms in a new hematocrit-correction model, not only the effect of hematocrit but also

the effect of plasma viscosity could be included in the new model. Thus, one might be able to substitute a direct measurement of plasma viscosity required in the Matrai's correction model.

Several methods have been suggested to determine the yield stress and the Casson constant based on experimental measurements. Merrill et al. suggested that both the yield stress and the Casson constant could be determined by the extrapolation of the measured data to the square root of stress axis on the Casson plot, the square root of the shear stress versus the square root of the shear rate, within 10% of deviation [28, 29].

The SCTV utilized in the present study also used the Casson model to determine blood viscosity by numerically calculating the yield stress and the Casson constant terms over a wide shear rate range. Since the detailed principles of measurement of the SCTV were outlined elsewhere [41, 43], a brief description of the measurement procedure is given below:

Step 1.

The unknowns, such as the yield stress, the Casson constant, height difference including the surface tension, can be determined using the velocity profile measured at the disposable U- tube with two charge-coupled devices (CCDs) and light-emitting diodes (LEDs).

Step 2.

The unknowns are determined by the curve-fitting method from the

experimental data as the sum of the error is minimized.

Step 3.

Then, wall shear rate and viscosity for all data points can be calculated. Thus, by measurement using the SCTV, one can obtain both the yield stress, τ_y, and the Casson constant, k.

According to the hypothesis mentioned above, the correlation between hematocrit and the yield stress (or the Casson constant) obtained during the WBV measurement using the SCTV was investigated.

The yield stress has been generally known that the cube root of the yield stress has a linear relation with hematocrit. Merill et al. [29] showed this correlation with the following equation:

$$\sqrt[3]{\tau_y} = A(H - Hc) \qquad \text{(Eq. 2-5)}$$

Where constant A is 0.008, H is hematocrit, and Hc is a critical hematocrit when no yield stress exists. Similarly, Zydney et al. [54] also provided a constitutive equation of blood viscosity containing the effect of hematocrit, shear rate, and suspending phase:

$$\tau_y = A(H - 0.05)^3 \qquad \text{(Eq. 2-6)}$$

Where constant A is 0.71 [3].

By adopting those concepts suggested from these previous studies, the cube root of the yield stress and the Casson constant obtained from the SCTV measurement were plotted in Figs. 2-5 to 2-7 as a function of hematocrit. The y-axis was plotted with both the cube root of the yield stress and the Casson constant without the consideration of their units, the cube root of millipascal and the cube root of centipoise, respectively.

Prior to further discussion, one needs to set the following assumption in order to simplify the current hematocrit-correction model:

The Casson constant, k, was assumed to be affected by both hematocrit and plasma viscosity as was the yield stress, even though the effects of hematocrit and plasma viscosity on the Casson constant were lower than those on the yield stress. Based on this assumption, the cube root of the Casson constant versus hematocrit was considered to be linear as the yield stress.

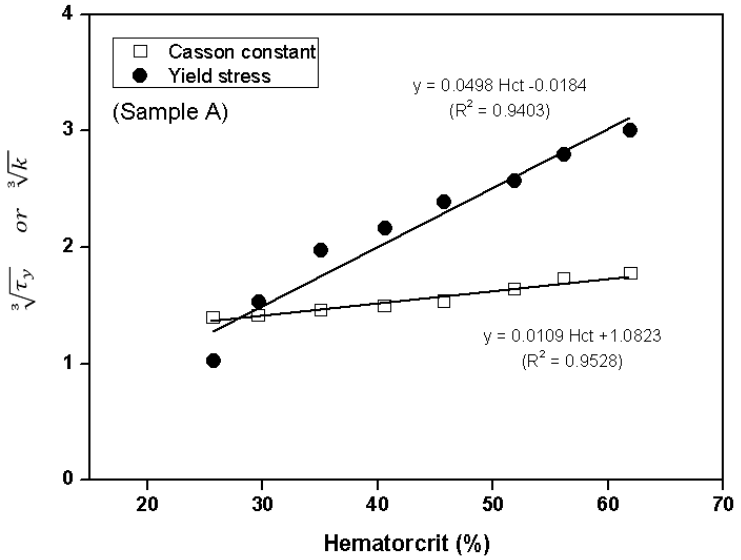

Figure 2-5. The cube root of the yield stress, τ_y, and the cube root of Casson constant, k, plotted on the same y-axis as a function of hematocrit (Sample A)

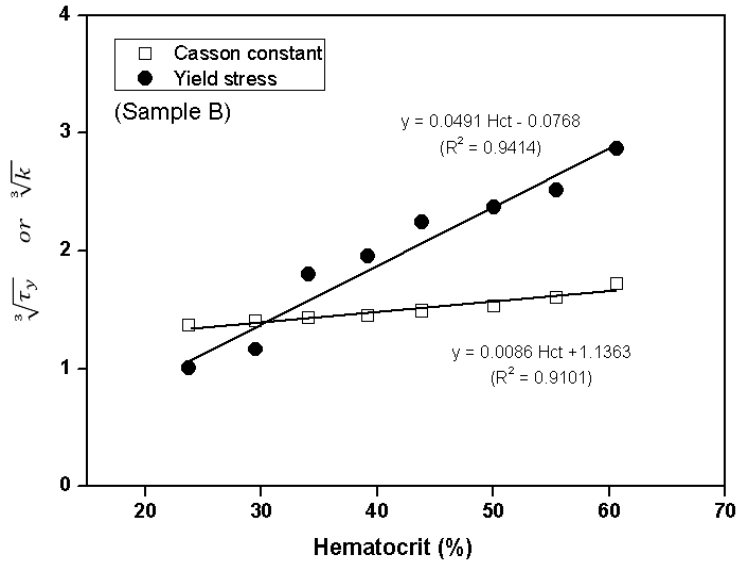

Figure 2-6. The cube root of the yield stress, τ_y, and the cube root of Casson constant, k, plotted on the same y-axis as a function of hematocrit (Sample B)

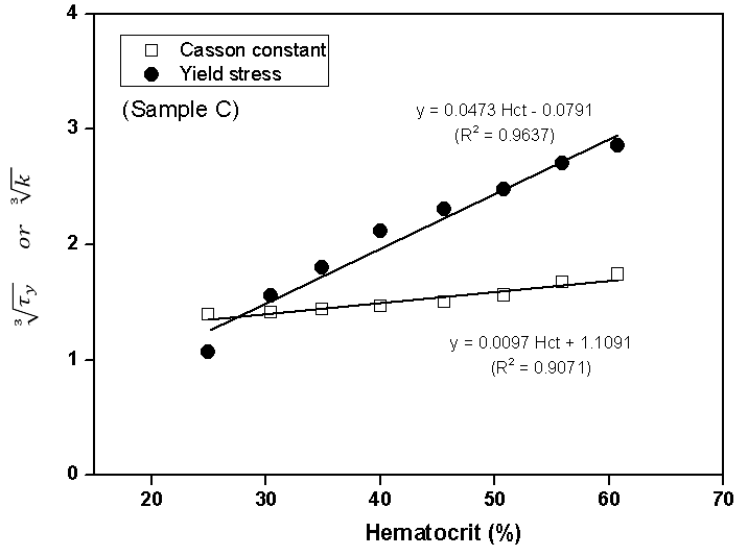

Figure 2-7. The cube root of the yield stress, τ_y, and the cube root of Casson constant, k, plotted on the same y-axis as a function of hematocrit (Sample C)

As seen from Figs. 2-5 to 2-7, two separate linear lines could be produced as a result of linear regression analysis ($P < 0.001$) for three different samples. More importantly, the two lines crossed each other at a certain identical point for all the three samples.

Combining the three figures into one plot as in Fig. 2-8, it could be clearly observed that the two different kinds of linear regression lines, the root cube of the yield stress versus hematocrit and the root cube of the Casson constant versus hematocrit showed almost identical intersections.

Even though the point of intersection among the three samples were not exactly identical, they crossed very close with little difference, for example, within

hematocrit range approximately from 28.4 to 28.9 %, and y-axis approximately from 1.40 to 1.42.

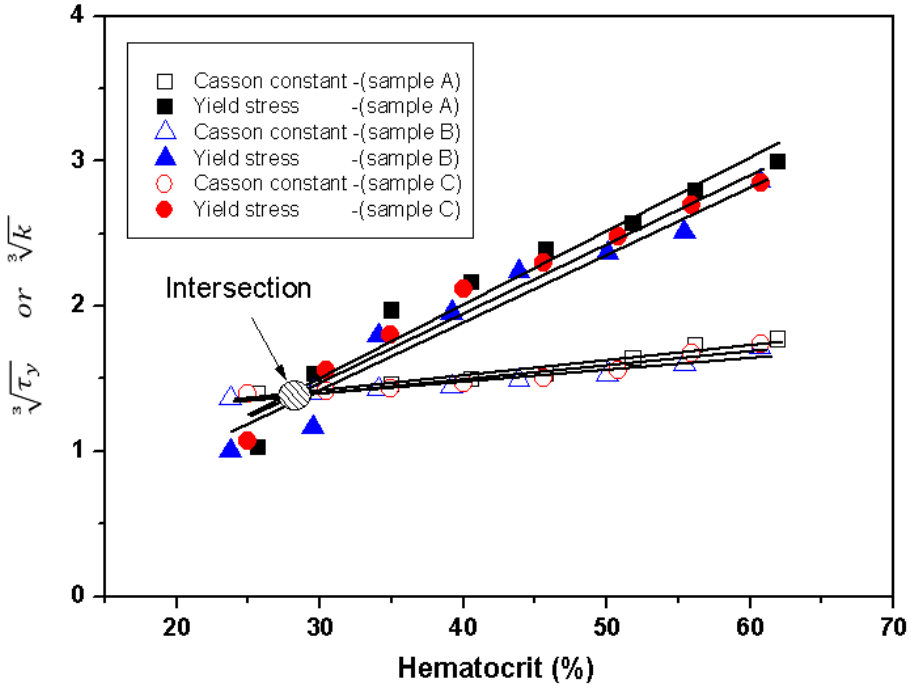

Figure 2-8. The combined plot of the cube root of the yield stress, τ_y, versus hematocrit and the cube root of Casson constant, k, versus hematocrit for Sample A, B, and C

The difference in the slopes among the three curves in Fig. 2-8 could be caused by different plasma viscosities, that is, by different concentrations of plasma viscosity determinants (i.e. fibrinogen, LDL etc.) [33, 55]. Even though the difference

of y-values measured at higher hematocrit values, as the hematocrit decreased, the difference of y-values between the curves became smaller.

The extrapolation of the Casson constants from three different linear regression lines was found to intercept to the y-axis with the values around from 1.0 to 1.2. Furthermore, the yield stresses from the three different linear regression lines were found to extrapolate to the x-axis (indicating a zero yield stress) before the hematocrit value on the x-axis reached zero [14, 28, 29], which was termed as a critical hematocrit [29]. In the present study, the critical hematocrit obtained by the extrapolation of the linear regression lines was from approximately 0.3 to 1.7, which was similar to the values by Merill et al. (i.e. from 1.3 to 6.5) [29].

Based on these findings, A new hematocrit-correction model was proposed with the following procedures:

Step 1.

One assumed that the constant value of the intersection between the cube root of the yield stress versus hematocrit line and the cube root of the Casson constant versus hematocrit line was already experimentally known as Constant $C_1(a, b)$ on the Casson plot, as shown in Fig. 2-9.

Step 2.

The WBV and hematocrit of a blood sample were measured using SCTV and a micro-centrifuge, respectively. During the WBV measurement, the yield stress, τ_y, and the Casson constant, k, could be automatically obtained from

SCTV.

Step 3.

The measured yield stress, τ_y, and Casson constant, k, during the WBV measurement were plotted on the Casson plot with the cube root values, as seen in Fig. 2-9, where A_1 denotes the cube root of the yield stress, $\sqrt[3]{\tau_y}$, and B_1 the cube root of the Casson constant, $\sqrt[3]{k}$, at native hematocrit, respectively.

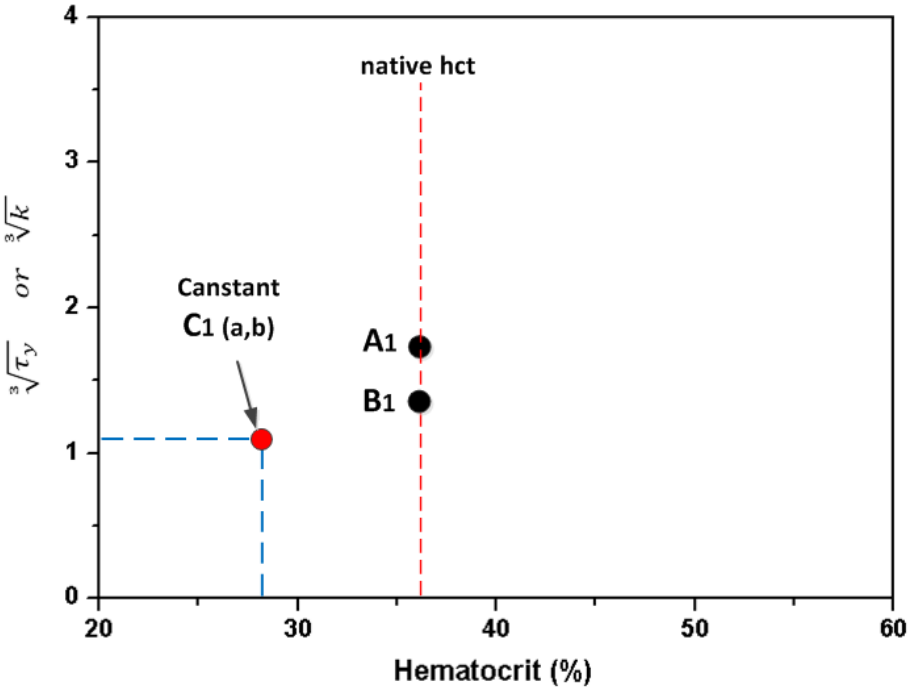

Figure 2-9. Casson plot with Constants C_1, A_1 and B_1

Step 4.

According to the linearity relations discussed in the previous section, the points between Constant, C_1, and the cube root of the obtained yield stress, A_1, at native hematocrit could be connected with a linear line. In the similar way, the points between Constant, C_1, and the cube root of the obtained Casson constant, B_1, at native hematocrit also could be connected with a linear line, as shown in Fig. 2-10.

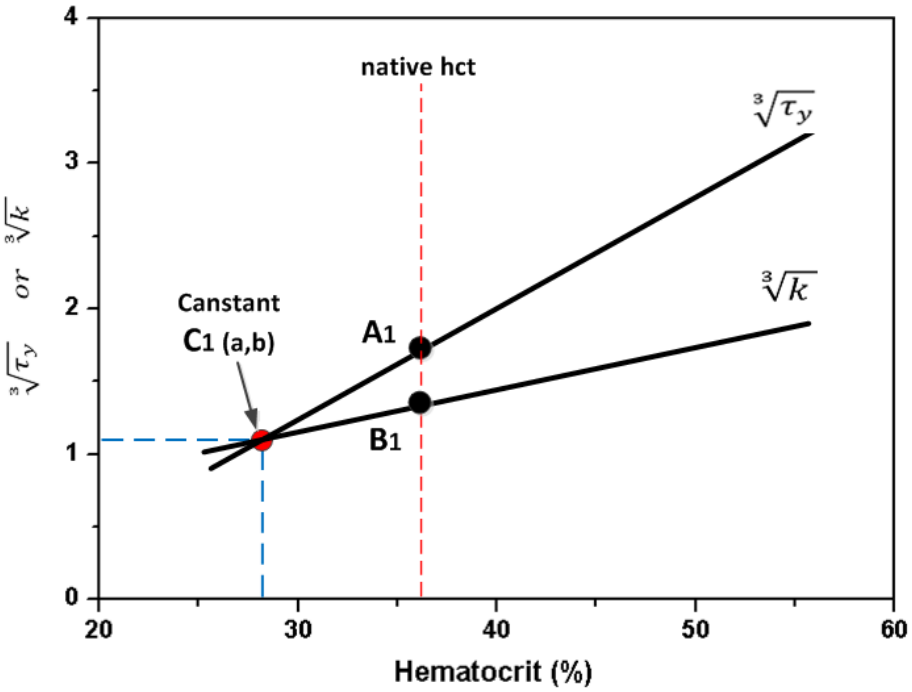

Figure 2-10. Casson plot with two linear lines connecting between Constants C_1 and A_1, Constants C_1 and B_1, respectively

Step 5.

In Fig. 2-11, since the Cartesian coordinates of C_1, A_1, and B_1 on the Casson plot were now known, one could determine the location of points A_2 and B_2 by simple proportional equations, where A_2 is the cube root of the corrected yield stress to a standard hematocrit of 45 % and B_2 is the cube root of the corrected Casson constant to a standard hematocrit of 45 %.

A_2, the calculated cube root of yield stress, $\sqrt[3]{\tau_y}$, at 45 % hematocrit:

$$\frac{\text{native hct}-a}{45-a} = \frac{A_1-b}{A_2-b} \qquad \text{(Eq. 2-7)}$$

$$A_2 = \left[\left(\frac{45-a}{\text{native hct}-a}\right) X(A_1 - b)\right] + b \qquad \text{(Eq. 2-8)}$$

B_2, the calculated cube root of yield stress, $\sqrt[3]{\tau_y}$, at 45 % hematocrit :

$$\frac{\text{native hct}-a}{45-a} = \frac{B_1-b}{B_2-b} \qquad \text{(Eq. 2-9)}$$

$$B_2 = \left[\left(\frac{45-a}{\text{native hct}-a}\right) X(B_1 - b)\right] + b \qquad \text{(Eq. 2-10)}$$

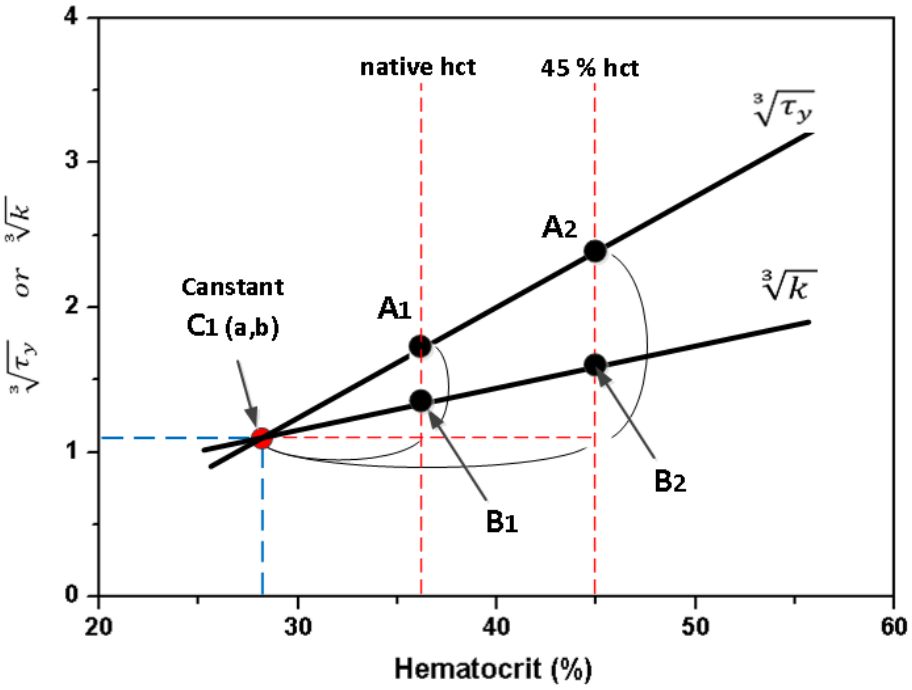

Figure 2-11. Casson plot showing how to determine A_2, the cube root of the corrected yield stress, τ_y, to a standard hematocrit of 45 %, and B_2, the cube root of the corrected Casson constant, k, to a standard hematocrit of 45 %

After cubing and then substituting the calculated yield stress and the Casson constant into (eq. 2-4), the corrected WBV to a standard hematocrit of 45 % could be simply achieved for any shear rate range:

2.3.2 The Comparison of a New Hematocrit-Correction Model to the Matrai's Model

In order to investigate the validity of a new hematocrit-correction model, three different blood samples were collected from three volunteers. The blood samples were adjusted to 25, 30, 35, 40, 45, 50, 55, and 60 % of hematocrits, and their WBVs were measured using SCTV. Plasma viscosity was also measured to correct the measured WBV using the Matrai's model as mentioned in (eq. 2-1).

The measured WBVs for the adjusted hematocrit values were corrected to a standard hematocrit using both the Matrai's model and a new model. The calculated sum of errors for sample A, B, and C are shown in Figs. 2-12 to 2-17.

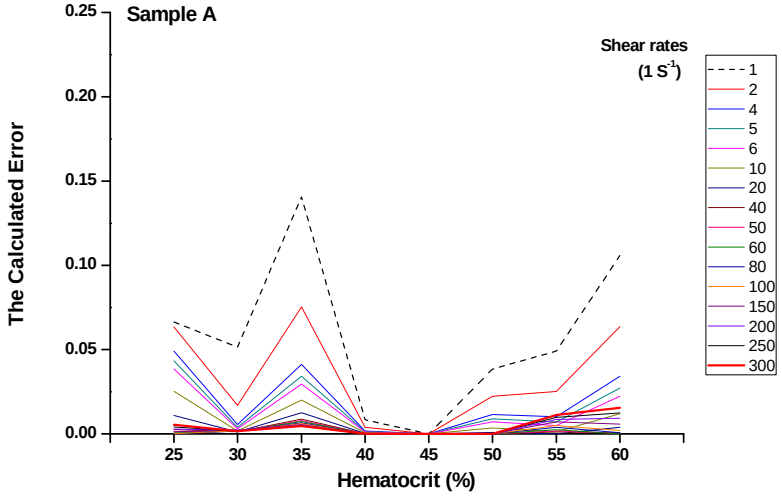

Figure 2-12. Calculated sum of the error for different shear rates after measured WBVs were corrected to a standard hematocrit of 45 % using the Matrai's model [45] (Sample A)

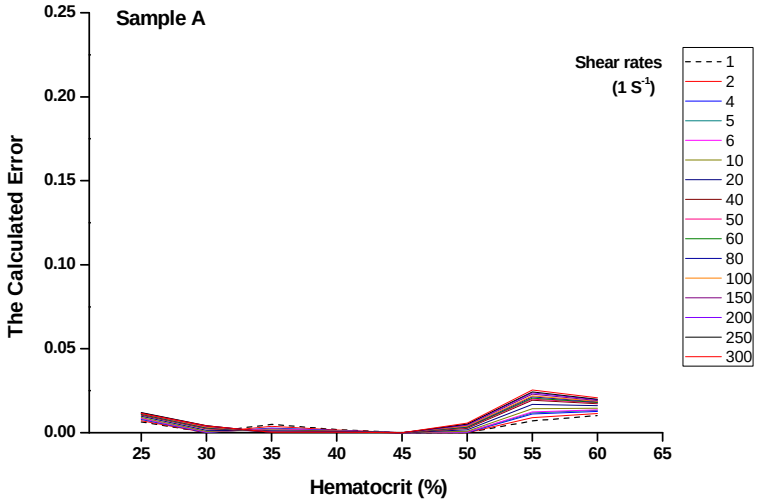

Figure 2-13. Calculated sum of the error for different shear rates after measured WBVs were corrected to a standard hematocrit of 45 % using a new hematocrit-correction model (Sample A)

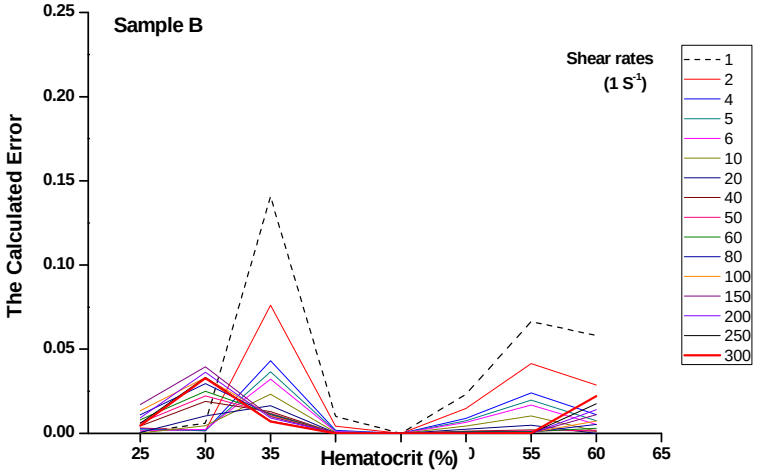

Figure 2-14. Calculated sum of the error for different shear rates after measured WBVs were corrected to a standard hematocrit of 45 % using the Matrai's model [45] (Sample B)

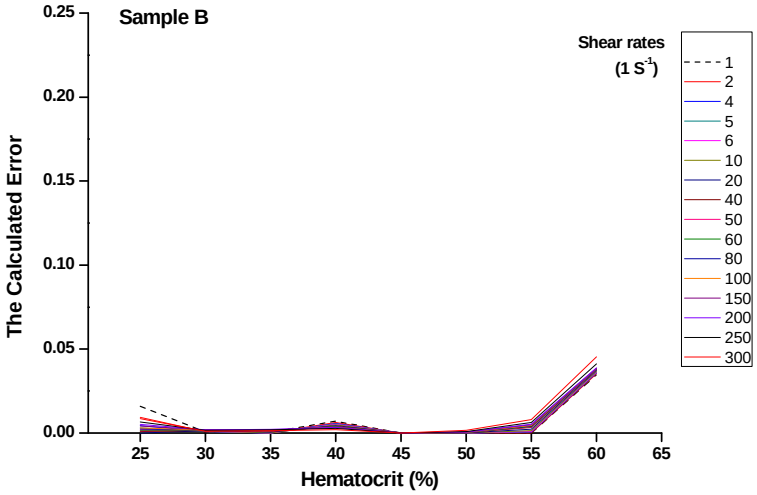

Figure 2-15. Calculated sum of the error for different shear rates after measured WBVs were corrected to a standard hematocrit of 45 % using a new hematocrit-correction model (Sample B)

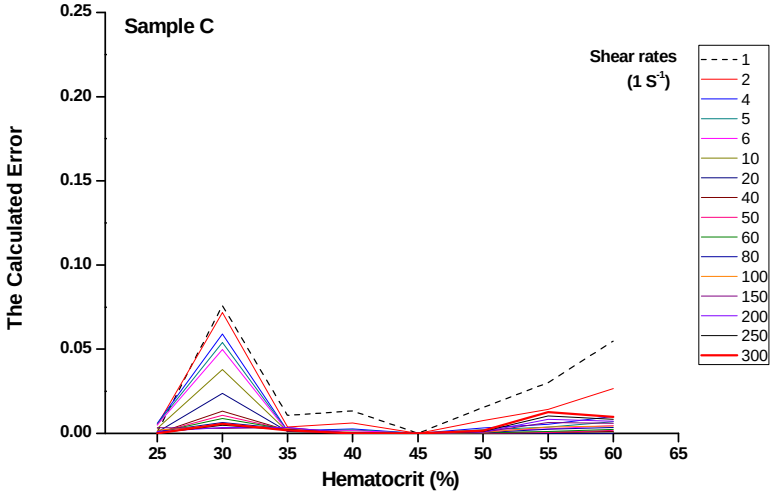

Figure 2-16. Calculated sum of the error for different shear rates after measured WBVs were corrected to a standard hematocrit of 45 % using the Matrai's model [45] (Sample C)

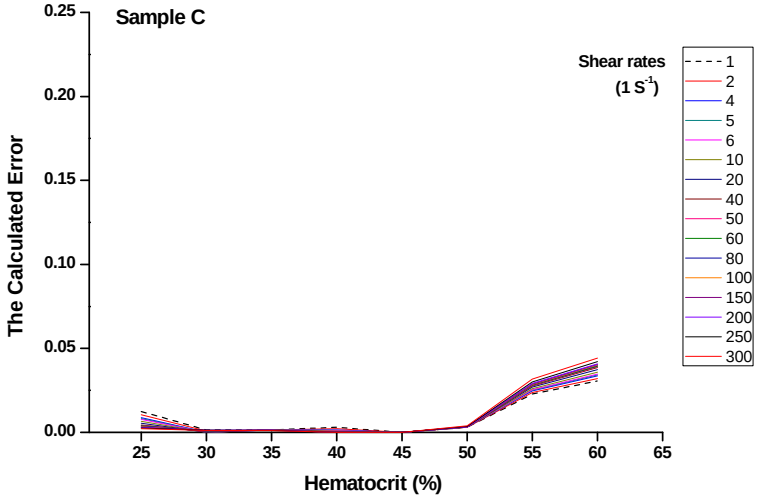

Figure 2-17. Calculated sum of the error for different shear rates after measured WBVs were corrected to a standard hematocrit of 45 % using a new hematocrit-correction model (Sample C)

As seen in Figs. 2-12 to 2-17, the corrected WBVs using the Matrai's model showed larger errors than the corrected WBVs using a new hematocrit-correction model. In case of the Matrai's model, the peaks in the error were observed around from 30 to 35 % of hematocrit ranges with a maximum error up to about 0.15 and the minimum error was shown at around 40 to 45 % of hematocrit. As hematocrit value increased, the error also increased larger at low shear rates than high shear rates.

The corrected WBVs using a new hematocrit-correction model showed stable and low errors around from 30 to 50 % of hematocrits over the entire shear rate ranges. However, as the hematocrit decreased to 25 %, the error slightly increased. A larger increase in error was observed over 50 % of hematocrits.

The increased error at the hematocrit value over 50 % could be explained by the relations between the cube root of the yield stress and hematocrits on the Casson plot. Figure 2-18, referred from Merill's results [29], shows that when the hematocrit increased over 50 %, the yield stress lost its linearity with hematocrit, and the curvature in the correlation was observed over hematocrit value of about 50 % [29]. Thus, the linear correlation between the yield stress and hematocrit described using the Casson model was not valid over about 50 % of hematocrit.

For the errors shown at 25 % of hematocrit, it might be due to the sedimentation of red blood cells, occurring dominantly at the low concentration of red blood cells during WBV measurement. In Fig. 2-8, the data below the linear regression curves at 25% of hematocrit value were deviated in a similar manner for the three samples. Thus, the sedimentation might have caused the error in

determining the yield stress and the Casson constant during WBV measurement, which led to an increase of the error when WBV was corrected to a standard hematocrit.

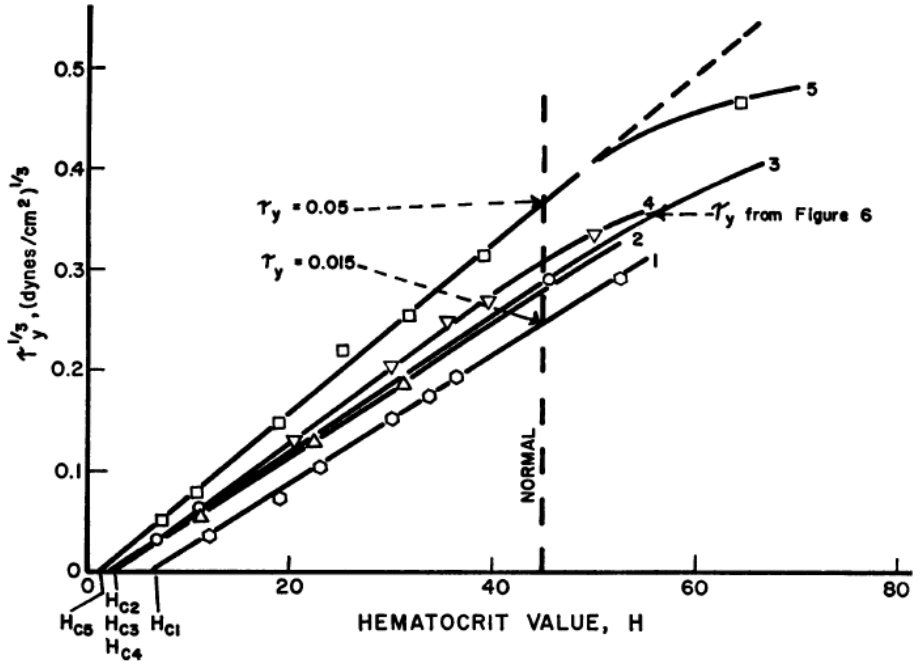

Figure 2-18. Casson plot showing the relations between the cube root of the yield stress, τ_y, versus hematocrit, referred from Merill et al.'s work [29]

The deviation between the experimentally measured WBV at 45% hematocrit and the corrected WBVs according to the two variables (i.e. hematocrit

and shear rate) were calculated to visually display the accuracy of the corrected results.

Firstly, for the Matrai's model, the positive and negative deviations of the corrected WBVs from the measured WBV at 45 % hematocrit were calculated. The results are listed in Tables 2-2 to 2-4, and also plotted to a scatter diagram with connecting lines for different shear rate as shown in Figs. 2-19 to 21.

Note that since a new model was shown to be valid from 30 to 50 % of hematocrit ranges, the comparison of a new model with the Matrai's model was performed within the hematocrit ranges from 30 to 50 %.

As seen in Tables 2-2 to 2-4, the corrected WBVs using the Matrai's model showed under-estimated results at high hematocrits (> 45 %) and low shear rates, and over-estimated results at high hematocrits (> 45 %) and high shear rates. At low hematocrits (<35%), the corrected WBVs varied according to the change of shear rates. From Figs. 2-19 to 2-21, the maximum positive deviation was 27.6 % from the measured WBV at 45 % hematocrit, whereas the maximum negative deviation was -37.5 %.

Table 2-2. Corrected WBVs using the Matrai's model [45] (Sample A) (cP)

Shear rate (1/s)	Hct 30 %	Hct 35 %	Hct 40 %	Hct 45 %	Hct 50 %
	Viscosity (cP)	Viscosity (cP)	Viscosity (cP)	Viscosity (cP)	Viscosity (cP)
1	19.57	29.81	30.14	27.02	23.67
2	12.99	18.82	19.14	17.74	16.18
4	9.35	12.84	12.99	12.35	11.66
5	8.55	11.53	11.63	11.13	10.61
6	7.98	10.62	10.69	10.28	9.86
10	6.75	8.65	8.62	8.39	8.19
20	5.65	6.91	6.79	6.68	6.65
40	4.94	5.83	5.64	5.59	5.64
50	4.77	5.57	5.36	5.32	5.40
60	4.65	5.38	5.16	5.13	5.22
80	4.48	5.12	4.89	4.87	4.97
100	4.37	4.95	4.71	4.70	4.81
150	4.20	4.70	4.44	4.44	4.56
200	4.03	4.53	4.28	4.28	4.41
250	3.88	4.37	4.16	4.17	4.31
300	3.77	4.25	4.07	4.08	4.25

Table 2-3. Corrected WBVs using the Matrai's model [45] (Sample B) (cP)

Shear rate (1/s)	Hct 30 %	Hct 35 %	Hct 40 %	Hct 45 %	Hct 50 %
	Viscosity (cP)	Viscosity (cP)	Viscosity (cP)	Viscosity (cP)	Viscosity (cP)
1	28.86	36.83	29.47	26.79	22.70
2	18.28	22.43	18.73	17.58	15.44
4	12.69	14.77	12.74	12.23	11.08
5	11.49	13.13	11.42	11.02	10.07
6	10.66	12.00	10.50	10.17	9.35
10	8.86	9.56	8.49	8.30	7.75
20	7.27	7.45	6.71	6.60	6.28
40	6.28	6.15	5.60	5.52	5.32
50	6.05	5.84	5.33	5.26	5.08
60	5.88	5.62	5.14	5.07	4.91
80	5.64	5.32	4.87	4.81	4.68
100	5.49	5.12	4.70	4.64	4.53
150	5.25	4.82	4.43	4.38	4.29
200	5.03	4.63	4.28	4.23	4.15
250	4.85	4.46	4.12	4.11	4.05
300	4.72	4.33	4.01	4.00	3.96

Table 2-4. Corrected WBVs using the Matrai's model [45] (Sample C) (cP)

Shear rate (1/s)	Hct 30 %	Hct 35 %	Hct 40 %	Hct 45 %	Hct 50 %
	Viscosity (cP)	Viscosity (cP)	Viscosity (cP)	Viscosity (cP)	Viscosity (cP)
1	19.57	29.81	30.14	27.02	23.67
2	12.99	18.82	19.14	17.74	16.18
4	9.35	12.84	12.99	12.35	11.66
5	8.55	11.53	11.63	11.13	10.61
6	7.98	10.62	10.69	10.28	9.86
10	6.75	8.65	8.62	8.39	8.19
20	5.65	6.91	6.79	6.68	6.65
40	4.94	5.83	5.64	5.59	5.64
50	4.77	5.57	5.36	5.32	5.40
60	4.65	5.38	5.16	5.13	5.22
80	4.48	5.12	4.89	4.87	4.97
100	4.37	4.95	4.71	4.70	4.81
150	4.20	4.70	4.44	4.44	4.56
200	4.03	4.53	4.28	4.28	4.41
250	3.88	4.37	4.16	4.17	4.31
300	3.77	4.25	4.07	4.08	4.25

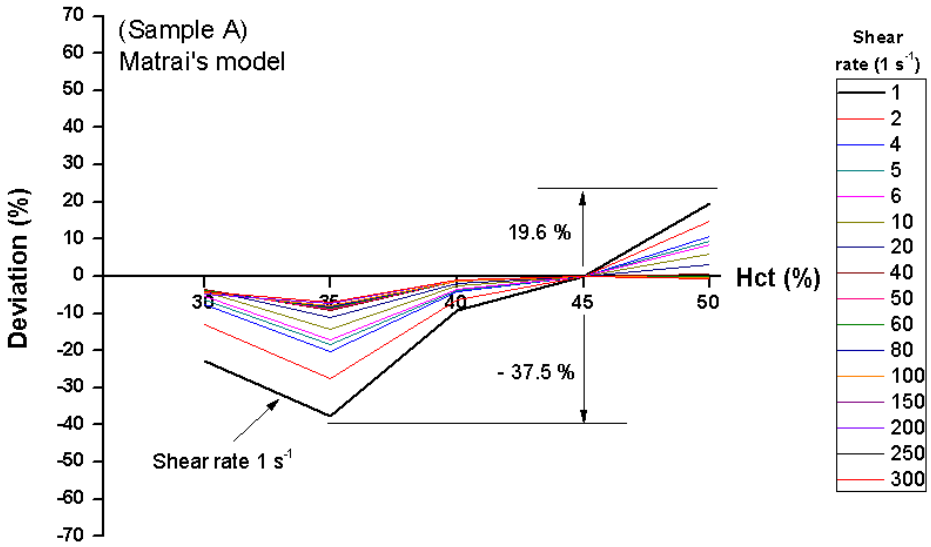

Figure 2-19. Deviations of the corrected WBVs using the Matrai's model [45] from measured WBV at 45 % hematocrit at different shear rates (Sample A)

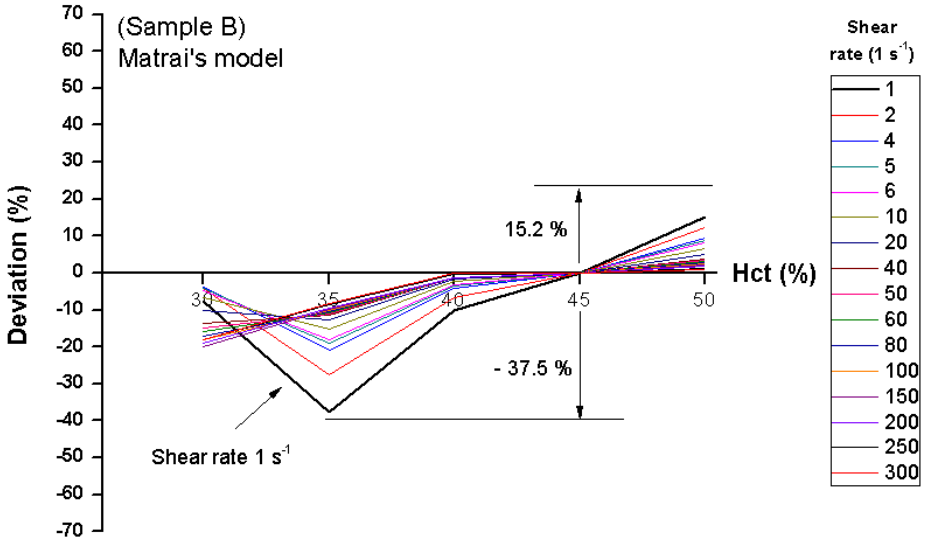

Figure 2-20. Deviations of the corrected WBVs using the Matrai's model [45] from measured WBV at 45 % hematocrit at different shear rates (Sample B)

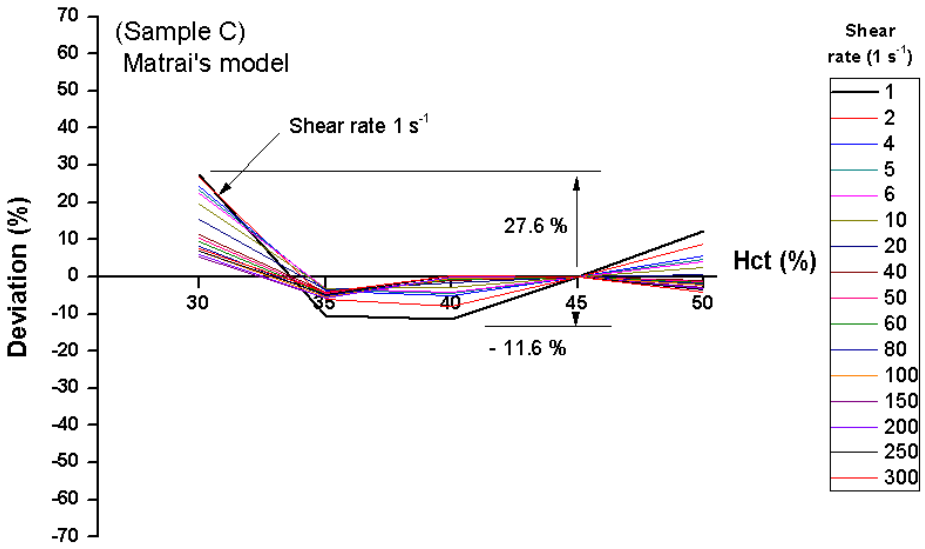

Figure 2-21. Deviations of the corrected WBVs using the Matrai's model [45] from measured WBV at 45 % hematocrit at different shear rates (Sample C)

Secondly, for the new hematocrit-correction model, the positive and negative deviations of the corrected WBVs from the measured WBV at 45 % hematocrit were also calculated. The results are listed in Tables 2-5 to 2-7, and plotted to a scatter diagram with connecting lines for different shear rate as shown in Figs. 2-22 to 2-24.

As seen in Tables 2-5 to 2-7, the corrected WBVs using the new hematocrit-correction model showed less deviation compared to the measured WBV at 45 % of hematocrit over 30 to 50 % hematocrit ranges at the shear rates. From Figs. 2-22 to 2-24, the maximum positive and negative deviations from the measured WBV at 45% hematocrit were 8.5% and -6.7%, respectively, which were about 4 to 6 times lower than those at the Matrai's model.

Table 2-5 Corrected WBV using the present model (Sample A) (cP)

Shear rate (1/s)	Hct 30 %	Hct 35 %	Hct 40 %	Hct 45 %	Hct 50 %
	Viscosity (cP)	Viscosity (cP)	Viscosity (cP)	Viscosity (cP)	Viscosity (cP)
1	30.99	33.36	29.90	31.26	30.86
2	20.19	21.56	19.53	20.34	20.33
4	13.94	14.77	13.53	14.03	14.20
5	12.54	13.24	12.17	12.61	12.81
6	11.54	12.17	11.22	11.61	11.84
10	9.37	9.82	9.12	9.41	9.68
20	7.40	7.70	7.23	7.43	7.73
40	6.16	6.36	6.02	6.17	6.48
50	5.86	6.04	5.73	5.87	6.18
60	5.64	5.81	5.52	5.65	5.97
80	5.34	5.49	5.23	5.35	5.67
100	5.14	5.28	5.04	5.15	5.47
150	4.84	4.96	4.75	4.85	5.17
200	4.67	4.77	4.58	4.67	4.99
250	4.55	4.65	4.47	4.55	4.87
300	4.46	4.55	4.39	4.45	4.79

Table 2-6 Corrected WBV using the present model (Sample B) (cP)

Shear rate (1/s)	Hct 30 %	Hct 35 %	Hct 40 %	Hct 45 %	Hct 50 %
	Viscosity (cP)	Viscosity (cP)	Viscosity (cP)	Viscosity (cP)	Viscosity (cP)
1	28.86	36.83	29.47	26.79	22.70
2	18.28	22.43	18.73	17.58	15.44
4	12.69	14.77	12.74	12.23	11.08
5	11.49	13.13	11.42	11.02	10.07
6	10.66	12.00	10.50	10.17	9.35
10	8.86	9.56	8.49	8.30	7.75
20	7.27	7.45	6.71	6.60	6.28
40	6.28	6.15	5.60	5.52	5.32
50	6.05	5.84	5.33	5.26	5.08
60	5.88	5.62	5.14	5.07	4.91
80	5.64	5.32	4.87	4.81	4.68
100	5.49	5.12	4.70	4.64	4.53
150	5.25	4.82	4.43	4.38	4.29
200	5.03	4.63	4.28	4.23	4.15
250	4.85	4.46	4.12	4.11	4.05
300	4.72	4.33	4.01	4.00	3.96

Table 2-7 Corrected WBV using the present model (Sample C) (cP)

Shear rate (1/s)	Hct 30 %	Hct 35 %	Hct 40 %	Hct 45 %	Hct 50 %
	Viscosity (cP)	Viscosity (cP)	Viscosity (cP)	Viscosity (cP)	Viscosity (cP)
1	27.19	25.83	28.46	27.02	28.56
2	17.85	17.00	18.55	17.74	18.75
4	12.43	11.87	12.81	12.35	13.05
5	11.21	10.71	11.52	11.13	11.76
6	10.35	9.89	10.61	10.28	10.86
10	8.44	8.09	8.61	8.39	8.86
20	6.72	6.46	6.81	6.68	7.05
40	5.63	5.41	5.66	5.59	5.90
50	5.36	5.16	5.38	5.32	5.62
60	5.17	4.98	5.19	5.13	5.42
80	4.91	4.73	4.91	4.87	5.15
100	4.73	4.56	4.73	4.70	4.96
150	4.47	4.31	4.45	4.44	4.68
200	4.31	4.16	4.29	4.28	4.52
250	4.21	4.06	4.19	4.17	4.41
300	4.13	3.99	4.11	4.08	4.33

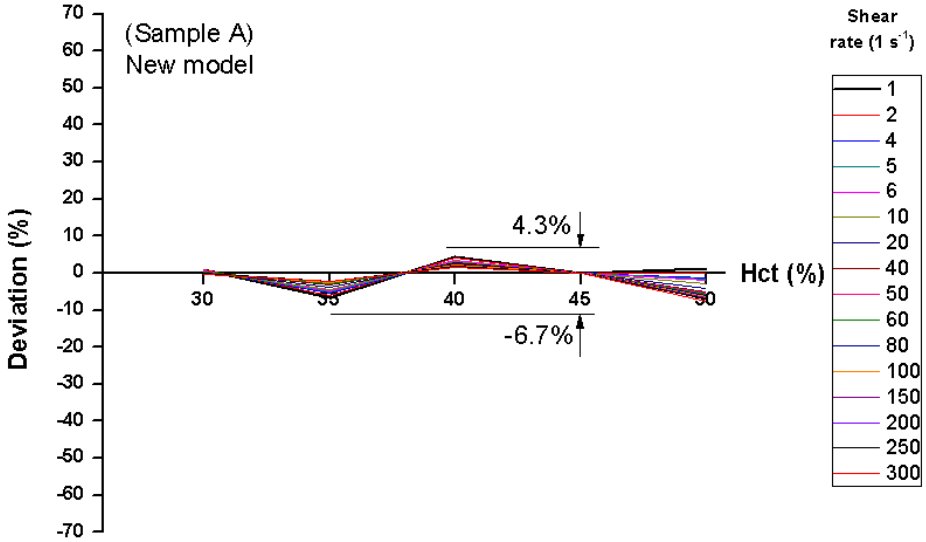

Figure 2-22. Deviations of the corrected WBVs using a new hematocrit-correction model from measured WBV at 45 % hematocrit at different shear rates (Sample A)

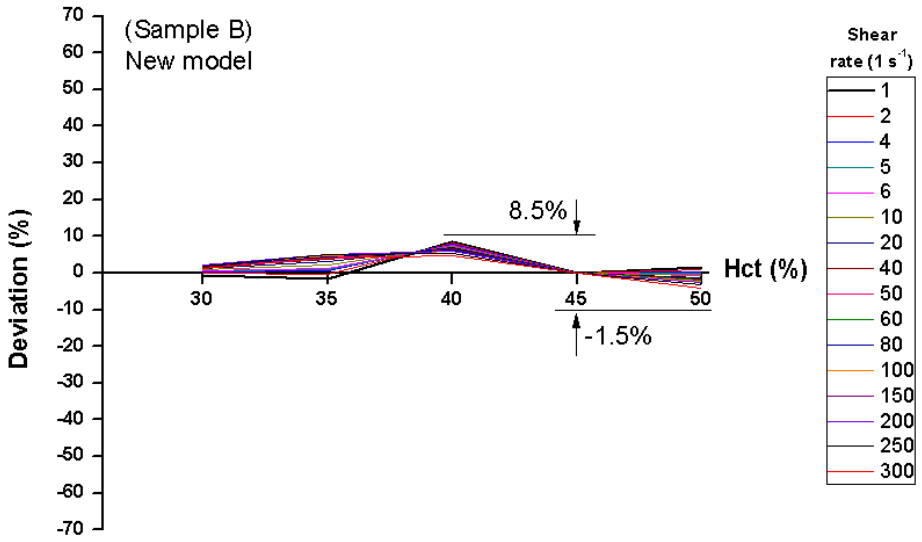

Figure 2-23. Deviations of the corrected WBVs using a new hematocrit-correction model from measured WBV at 45 % hematocrit at different shear rates (Sample B)

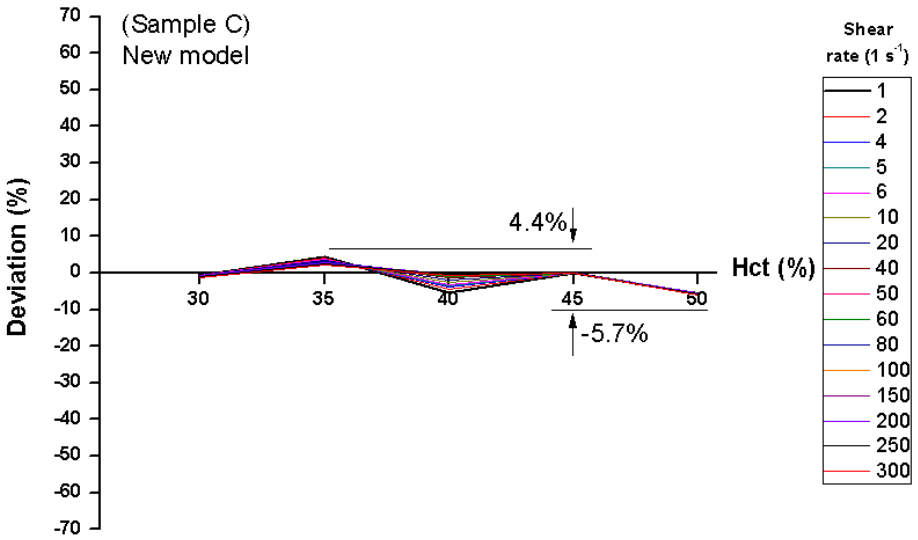

Figure 2-24. Deviations of the corrected WBVs using a new hematocrit-correction model from measured WBV at 45 % hematocrit at different shear rates (Sample C)

Lastly, Figs. 2-25 to 2-33 show the profiles of the WBVs for the hematocrit-adjusted blood samples (i.e. 30, 35, 50, 45, and 50 %), the profiles of the WBVs after correction using Matrai's model, and the profile of the WBVs after correction using a new hematocrit-correction model, which were plotted for comparison for Sample A, B, and C.

Comparing Figs. 2-26 and 2-27, 2-29 and 2-30, 2-32 and 2-33, the validity and difference between the hematocrit-correction models were clearly observed.

When the measured WBVs for different native hematocrits as shown in Figs. 2-25, 2-28, and 2-31, were corrected to a standard hematocrit of 45 %, the WBV profiles by the new hematocrit-correction model were thoroughly plotted close to the WBV profile of 45 % hematocrit in Figs. 2-27, 2-30, and 2-33, while those by the Matrai's model stayed with large deviations from the WBV profile of 45% hematocrit in Figs. 2-26, 2-27, and 2-32.

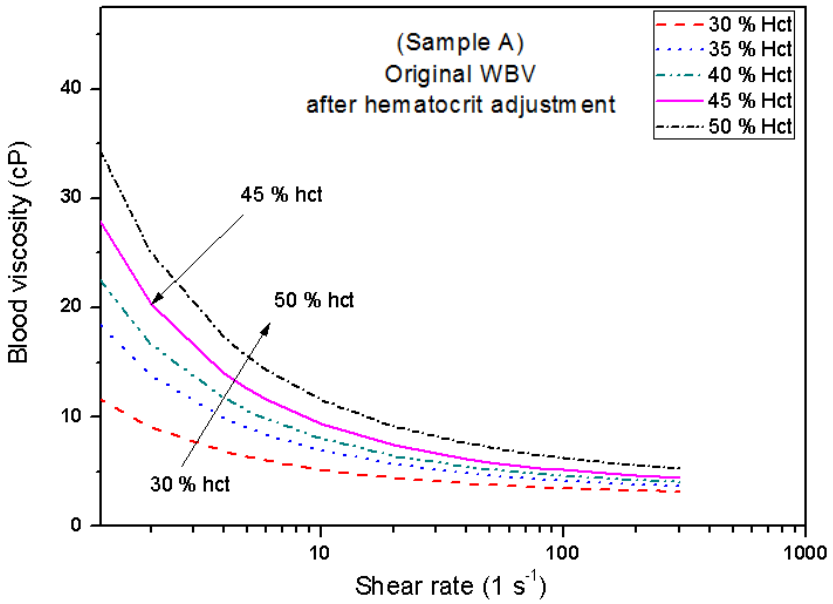

Figure 2-25. Measured WBV profiles of original hematocrit-adjusted bloods (i.e. 30, 35, 50, 45, and 50 %) before the correction to a standard hematocrit of 45 % (Sample A)

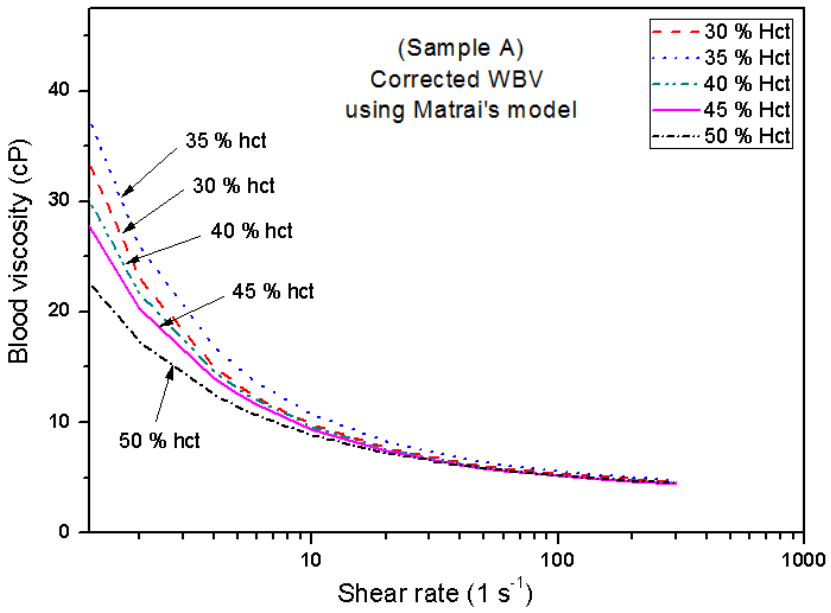

Figure 2-26. Corrected WBV profiles using the Matrai's model [45] (Sample A)

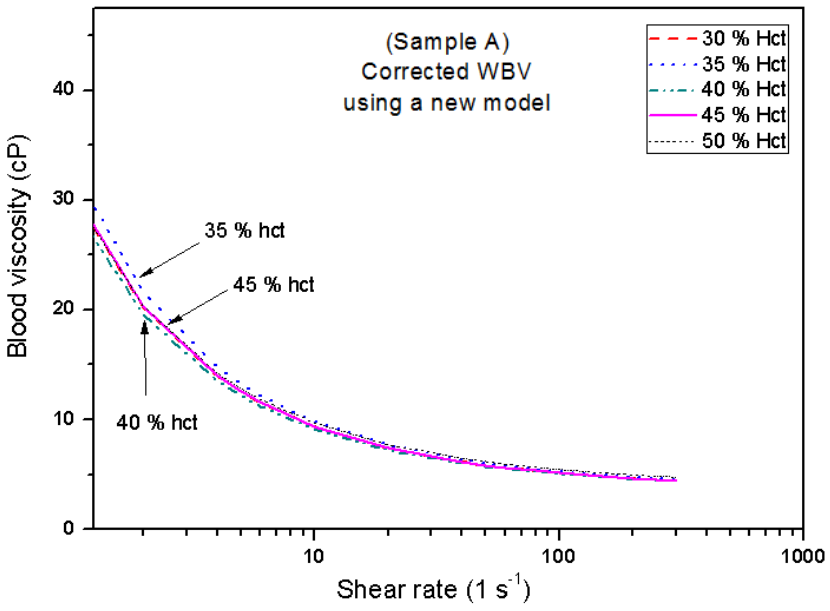

Figure 2-27. Corrected WBV profiles using a new hematocrit-correction model (Sample A)

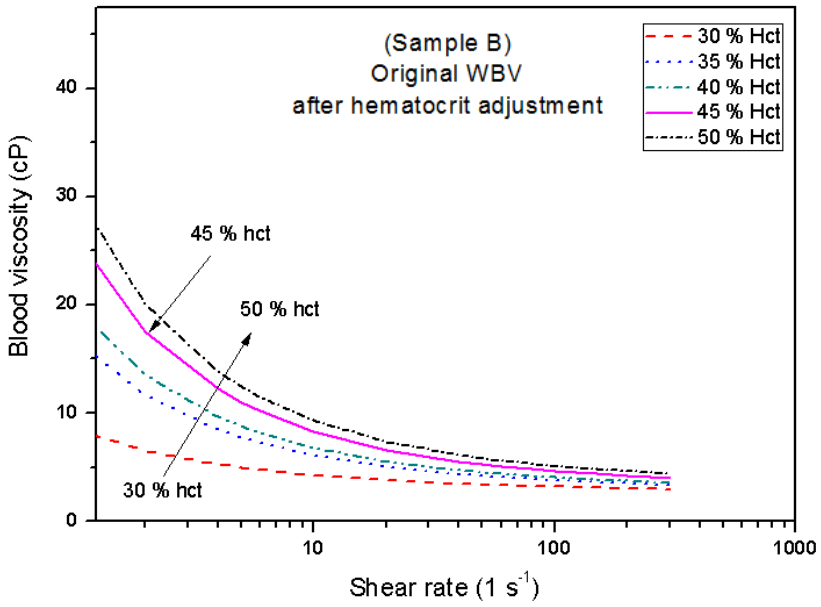

Figure 2-28. Measured WBV profiles of original hematocrit-adjusted bloods (i.e. 30, 35, 50, 45, and 50 %) before the correction to a standard hematocrit of 45 % (Sample B)

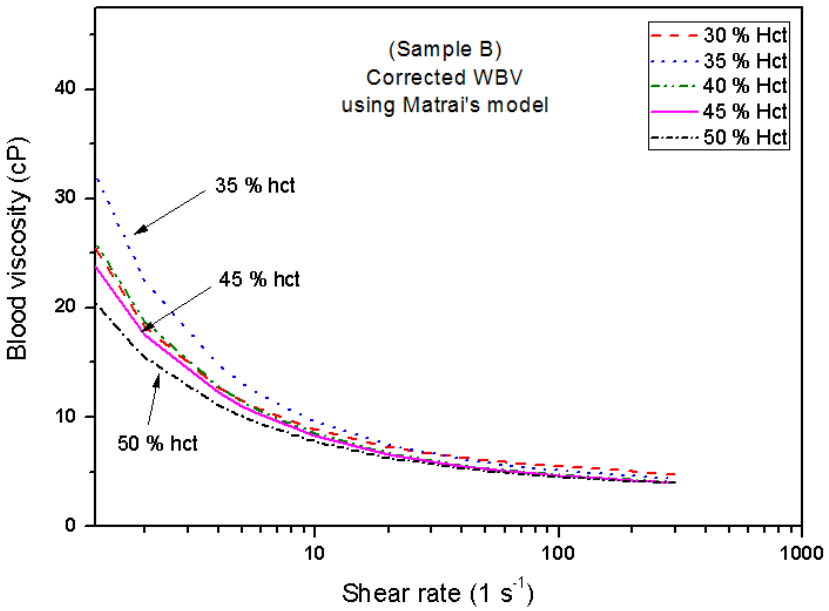

Figure 2-29. Corrected WBV profiles using the Matrai's model [45] (Sample B)

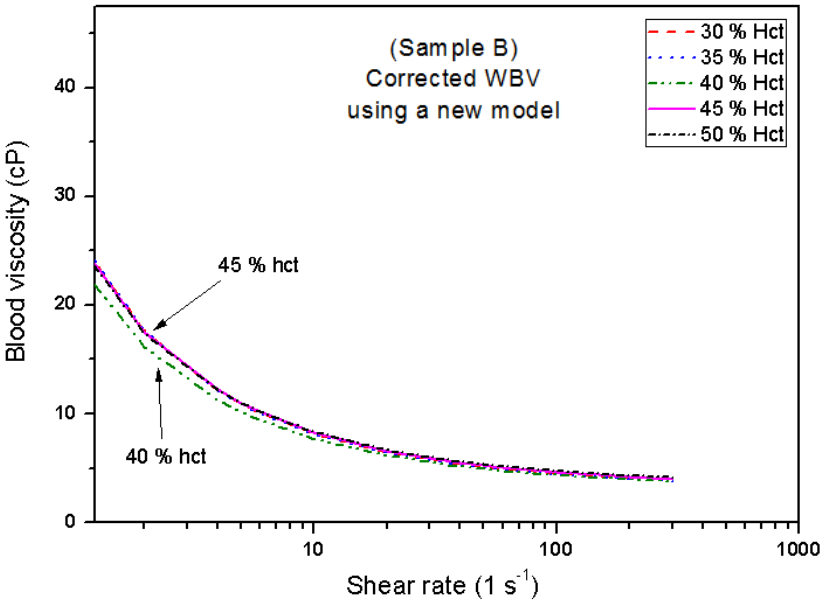

Figure 2-30. Corrected WBV profiles using a new hematocrit-correction model (Sample B)

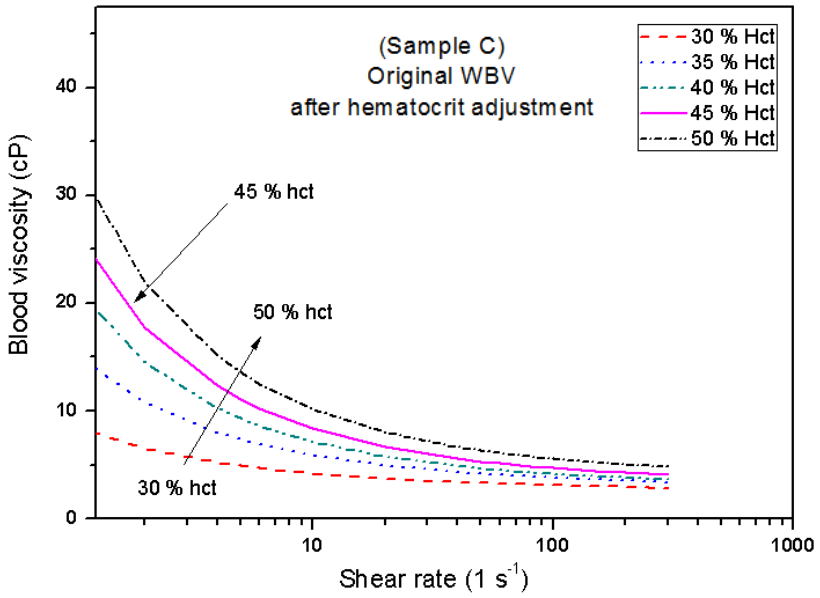

Figure 2-31. Measured WBV profiles of original hematocrit-adjusted bloods (i.e. 30, 35, 50, 45, and 50 %) before the correction to a standard hematocrit of 45 % (Sample C)

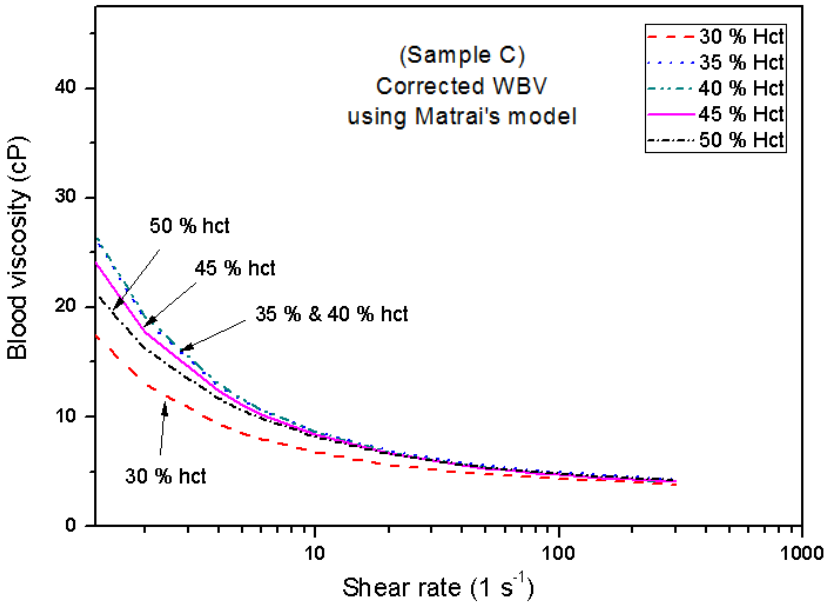

Figure 2-32. Corrected WBV profiles using the Matrai's model [45] (Sample C)

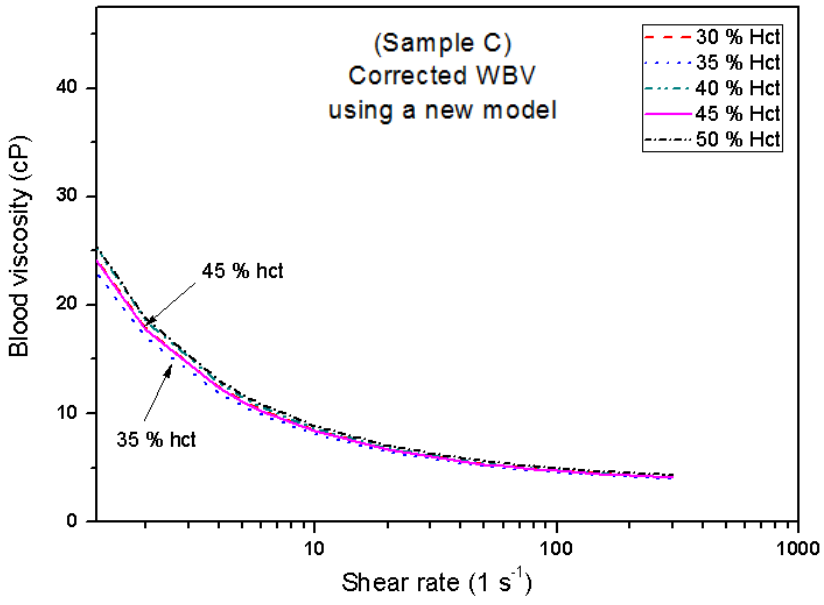

Figure 2-33. Corrected WBV profiles using a new hematocrit-correction model (Sample C)

2.4 Limitations

The validation of the new hematocrit-correction model in correcting the measured WBV at native hematocrit to a standard hematocrit of 45 % was achieved with less errors and deviations over a wide range of shear rates than the Matrai's model. Furthermore, the new model does not require the measurement of plasma viscosity. In general, once the yield stress and the Casson constant could be obtained by either the SCTV or any other viscometers, the corrected WBV could be calculated using the proposed equation given in the present study.

Even though the valid range of the new hematocrit-correction model was limited to hematocrit values of 30 to 50 %, which did not cover a whole range of hematocrit (i.e. from 0 to 100 %), it could be utilized in clinical experiments, where normal hematocrit ranges of men and women are about 36 to 45 % and about 39 to 50 %, respectively.

Further research is recommended to determine the specific characteristics and values of Constant C_1, the intersection of the two linear lines that indicate the cube root of the yield stress and the cube root of the Casson constant as a function of hematocrit on the Casson plot. Thus, one needs to investigate further clinical applicability of the new model whether or not it could show a similar intersection for people with different levels of plasma viscosity, caused by different concentration levels of macro-molecules such as plasma proteins in blood plasma.

CHAPTER 3: A NEW ON-LINE CONDUCTANCE CELL FOR HEMATOCRIT MEASUREMENTS

3.1 Motivations and Literature Survey on Hematocrit Measurement

Hematocrit is defined as the percentage of whole blood volume occupied by red blood cells [56, 57], representing the amount of oxygen in the whole blood [58, 59]. It is one of the important blood properties to assess the oxygen delivery in relation to ischemic diseases [60]. Recently, it is also considered as a marker of oxygen carrying capacity of the blood associated with whole blood viscosity to assess the mortality risk of both cardiovascular, cerebral, and kidney diseases [10, 61-63].

Since the red blood cells contain hemoglobin molecules, the oxygen-delivery capacity to a tissue at a constant flow rate is higher if the hematocrit of the perfusing blood is higher. However, increased hematocrit results in a nonlinear increase of blood viscosity (or flow resistance), and thus the flow rate of blood might be decreased, reducing the amount of blood perfusion to a given tissue. In order to express the relations between WBV and hematocrit, a parameter known as the oxygen delivery index (ODI) is being used, which is defined as the ratio between hematocrit and WBV [1, 3].

$$\mathrm{ODI} = \frac{\text{Hematocrit}}{\text{Blood viscosity}} \qquad \text{(Eq. 3-1)}$$

According to Kaplan-Meier survival analysis performed by Kenyeres et al., ODI showed significant negative correlation with the frequency of hospital admissions ($r = -0.377$, $p = 0.03$), which stated the significance of ODI as a risk factor of cardiac death in coronary heart disease [3, 10].

In order to quantify an optimum balance of ODI, it is required not only to automatically measure the profile of WBV using SCTV but also to determine hematocrit simultaneously.

Several methods to determine hematocrit values in whole blood have been suggested, mainly with an electrical method and a light-emitting method.

The bioelectrical impedance technique has been utilized to determine the conductivity of blood [57, 64-72], which depended on plasma resistance, red cell intracellular resistance, red cell membrane capacitance, and erythrocyte sedimentation [57, 72]. Due to the difficulties in measuring these parameters, the bioelectrical impedance technique could not be done accurately [57, 64-66, 69, 72]. In case of the plasma resistance, a number of studies have employed an alternating voltage signal to minimize an electrolyte effect on the plasma resistance [57, 72]. Such an approach was mostly carried out at a single frequency in a range of 1 kHz -1 GHz [72-74] in a sine-wave form. Even though the sine-wave single frequency method improved the measurement accuracy of the plasma resistance, the electrolyte concentration still affected the resistivity of plasma, but less than the DC voltage signal [72, 75]. Dual or triple frequencies were also utilized to simultaneously

measure the plasma resistance, the red cell intracellular resistance or/and the red cell membrane capacitance [57, 72].

Recently, analytical equations have been developed to take into account the volume or conductance of the cellular particles in the conductance measurement [64, 66, 72, 76]. Even though these mathematical models were well-developed, the final equation for the conductivity of whole blood still contains four variables which must be determined experimentally by independent methods.

$$\rho = \frac{\left(\frac{r}{r_1}\right) - 1}{\left(\frac{r}{r_1}\right) - 1 + f} \qquad \text{(Eq. 3-2)}$$

where r/r_1 is the ratio of the specific resistance of suspension to that of the mixture medium, ρ is the volume fraction occupied by suspended particles, and f is a form factor which depends on the axial ratio of suspended ellipsoids [66, 72, 77]. However, since these studies were conducted in a stationary flow state, erythrocyte sedimentation could cause error in the measurement of the conductivity of whole blood [57, 72]. There was no study to report the conductivity measurement of whole blood which was moving at a constant velocity to prevent the erythrocyte sedimentation.

Thus, this chapter was aimed to propose a new on-line device using a conductance method, which can automatically measure hematocrit and can be easily integrated with the SCTV, specifically to propose a new on-line conductivity cell to measure the hematocrit of whole blood using a low-frequency bipolar square-wave voltage signal to overcome the aforementioned difficulties without the erythrocyte

sedimentation problem.

3.2 Methods

3.2.1 Experimental Setup

The present experimental setup is given in Fig. 3-1 and 3-2, which consisted of a syringe pump, a vacutainer, a temperature-controlled dry bath, short and long needles, a conductivity cell, a power supply, and a signal analyzer. A plain vacutainer (4 mL) filled with whole blood sample was placed at the temperature-controlled dry bath. Whole blood samples with three different hematocrits were used to check the validity of the present method. The syringe pump was used to pressurize air in the vacutainer so that the whole blood was pushed out by the compressed air and introduced into the conductance cell. Both short 21G (3.81 cm in length) and long 18G (15.24 cm in length) needles were inserted into the vacutainer for air infusion and blood outflow, respectively. As the whole blood moved into the conductance cell, the electrical resistivity of the whole blood was determined by applying a square-wave voltage signal across the conductance cell and measuring the resulting current between the two electrodes in the cell.

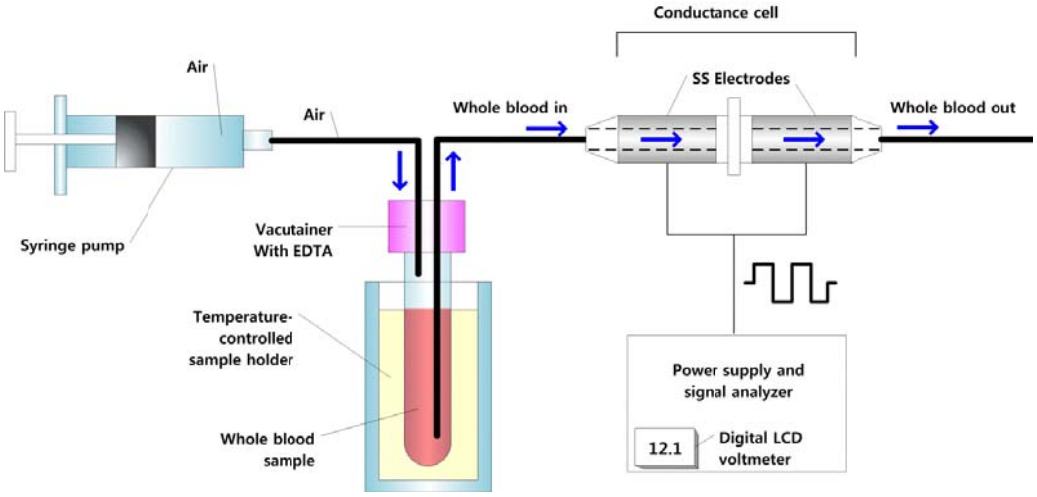

Figure 3-1. Schematic of the present experimental setup

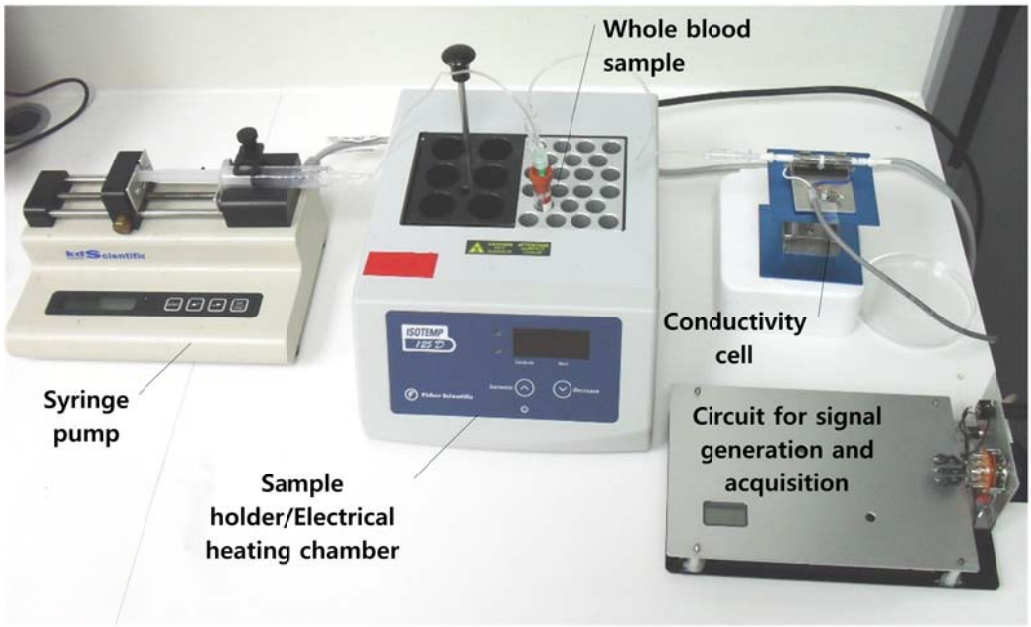

Figure 3-2. Photograph of the present experimental setup

The conductance cell was developed as a tubular assembly (0.635 cm in diameter) as shown in Fig. 3-3 and Fig. 3-4, which had two annular 304L stainless-steel electrodes separated by a polystyrene barrier so that whole blood could continue to flow during conductivity measurements. One of the reasons why the present method used the conductance cell with continuously moving blood was to minimize the measurement error that could have been caused by the sedimentation of cells in whole blood [64]. The blood volume inside the cell was around 1.2 mL. The conductance cell was designed as a disposable unit so that the cell did not have to be cleaned after each test. In addition, the cell was placed into a specially prepared holder (as shown in Fig. 5-3) for electrical insulation, easy connection and removal.

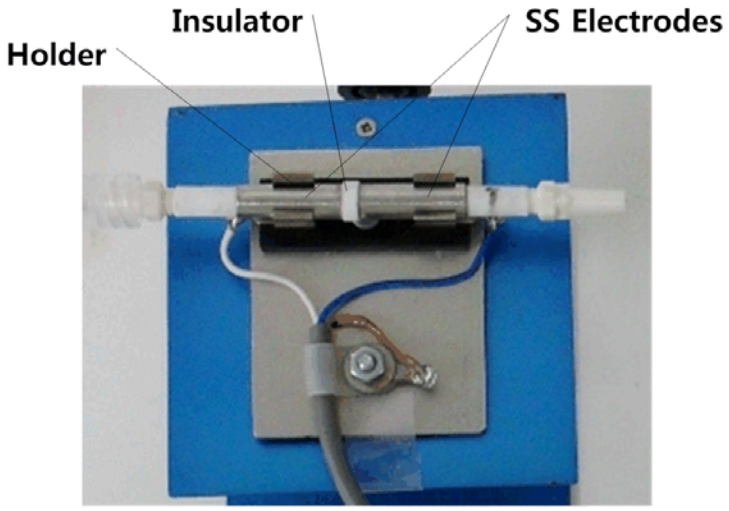

Figure 3-3. Photograph of conductance cell placed in a holder.

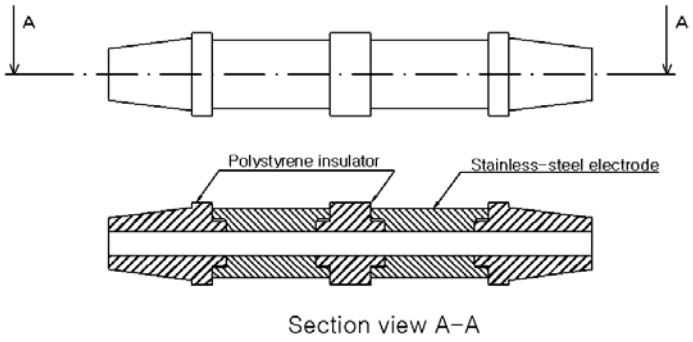

(a) Sectional View

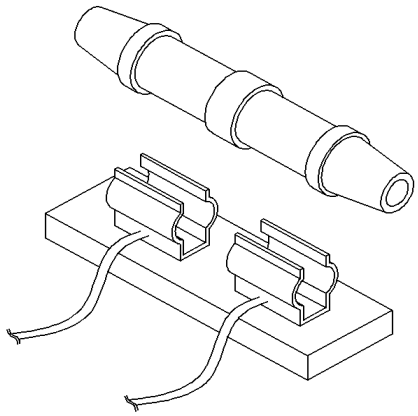

(b) 3D view

Figure 3-4. Sectional (a) and 3D (b) drawings of conductance cell

3.2.2 Description of Power Supply and Signal Analyzer

Figure 3-5 shows the detailed schematic circuit diagram for the present conductance cell to generate a bipolar square-wave voltage signal and measure the resulting current between the two electrodes at the cell. The applied sensing voltage was less than 50 mV so that the reduction-oxidation effect could be minimized on the electrode surfaces. Furthermore, a bipolar voltage was used to minimize the effect of polarization on the cell. The applied voltage had 100-mV peak-to-peak square-wave signal which was centered at zero. In order to achieve the minimal decay in the current waveform due to the dielectric effect of whole blood, a frequency of 5 kHz was employed. The current waveform was corrected by incorporating a peak-reading circuit. Since the cell membrane and the intracellular water became conductive when the frequency was above 100 kHz [57], the present study used a frequency of 5 kHz, where the resistance of erythrocytes remained constant over time.

Some conductance meters used a sine-wave voltage signal at various frequencies [57, 72, 78]. In this case, it was not easy to obtain a stable amplitude voltage signal. In the present study, a CMOS Schmitt trigger relaxation oscillator provided the square-wave voltage signal which was clipped by positive and negative supply voltages. The supply voltages were set by precision 2.5-V Zener diodes. The square-wave signal was scaled to 100 mV with a precision divider and a unity gain follower to provide a low-impedance source which drove the conductance cell.

An op-amp circuit was incorporated to provide 5-mV peak output from several μA input current. A scaling switch was also employed to double or triple the

mV peak output to accommodate a higher resistivity of blood as in polycythemia vera [79, 80], where hematocrit can increase beyond 60%.

A precision rectifier was used as an absolute magnitude converter to convert the bipolar square wave to a DC value which was proportional to an input current. The diodes were placed within an op-amp feedback loop to avoid an approximate 0.7-V drop normally found with a rectifier. A digital meter with a 9-cm digital LCD was utilized with a reading range of 0-199.9 μA at the conductance cell.

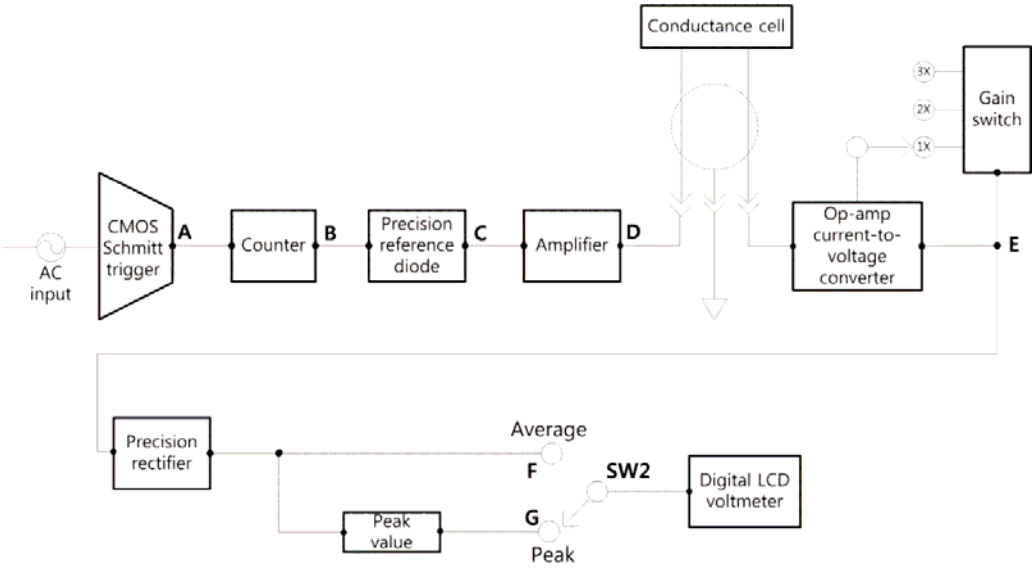

Figure 3-5. Schematic diagram of the circuit in the present conductance cell

3.2.3 Sample Preparation

Normal whole blood of 450 mL anticoagulated with K2 EDTA was obtained from Lampire Biological Laboratories, PA, USA, which was drawn from a healthy donor. Since it was reported that other types of anticoagulants (i.e. heparin and sodium citrate) were found to influence the accurate measurement of the electrical impedance of blood, EDTA was chosen in the present study [72].

In order to investigate the relationship between hematocrit and electrical conductivity, the hematocrit was varied over a range from 20 to 65% which were considered to be the physiological minimum and maximum values, respectively, in human [81-84]. After being mixed gently and homogeneously, the whole blood sample of 450 mL was transferred to 10-mL transparent containers and centrifuged (VanGuard V6500, Hamilton Bell Co.) with a relative centrifugal force of 1,200 G for 15 min. Then, a portion of plasma was either removed or added from the centrifuged containers to produce blood samples at different hematocrits. The hematocrit-adjusted whole blood samples were then transferred to 4-mL vacutainers for the conductivity measurement. In order to check the reliability of the present methods, 20 identical whole blood samples were prepared for repeated measurements for ten different hematocrit cases (i.e., 20, 25, 30, 35, 40, 45, 50, 55, 60, and 65%).

3.2.4 Experimental Procedure

Conductivity, G (mS), can be determined from the inverse of resistance according to the Ohm's law [76].

$$G = \frac{1}{R_{cell}} \quad \text{(Eq. 3-3)}$$

where R_{cell} is the resistance of the conductance cell filled with a test fluid. The specific conductivity C (mS/cm) is defined as

$$C = G \times \frac{d}{A} \quad \text{(Eq. 3-4)}$$

where d is the distance between two electrodes (i.e., 3 mm), and A is the total contact surface area of the two electrodes. Note that the ratio of the distance between the two electrodes to the electrode surface area, d/A, is defined as the cell constant, K (cm^{-1}):

$$K = \frac{d}{A} \quad \text{(Eq. 5-5)}$$

However, the equation of the cell constant does not take into account the effects of both fringe electric field and interfacial resistances on the conductivity. Since it is often difficult to calculate the cell constant including these effects, the cell constant, K, is determined through a separate calibration procedure using a conductivity-standard liquid with a known electrical conductivity [76, 85].Considering the measurement range of the present conductance cell, two different conductivity-standard solutions, 3 mS/cm (Conductivity/TDS Standard, 1534 ppm as NaCl) and 10 mS/cm (5400 ppm as NaCl) (both from Ricca Chemical, TX), were

used for the calibration of the cell constant [76, 85, 86].

The blood samples were thoroughly mixed using a roller mixer to insure the homogeneity of the samples and placed in a vacutainer sample holder at room temperature (25±0.5ºC) [74]. Then, a syringe pump was used to pressurize the air in the vacutainer so that the whole blood could be pushed out to the conductance cell at a constant flow rate of 1.2 mL/min, where the effect of the erythrocyte sedimentation on the conductivity of blood was negligible as shown below. While blood was moving through the cell, the resulting current between the two electrodes at the cell was measured with a signal analyzer and displayed on a digital LCD [64, 87, 88]. Hematocrit was also determined using a microcentrifuge for comparison with the results obtained from the present conductance cell.

In order to investigate the effects of flow rate on the blood conductivity measurement, blood samples at three different hematocrits of 25, 45, and 60 % were used, each at five different flow rates of 0.5, 1.2, 1.8, 2.5, and 3 mL/min at the conductance cell with ID of 0.635 cm.

Prior to each conductivity measurement, the calibration of the electrical circuit was performed by inserting a 1,000-ohm resister (±1% tolerance), confirming that the power supply and signal analyzing unit were in normal operation without any effects of noise, interference or disconnection on the circuit. Then, the hematocrit of each blood sample was measured using the aforementioned microcentrifuge before and after the measurement of blood resistance using the conductance cell, not only to investigate the relationship with the present resistance method but also to check

whether or not the hemolysis of erythrocytes occurred in whole blood sample due to the contact with electrical current and/or the relatively high flow velocity of blood (i.e., up to 0.6 cm/s) inside the conductance cell [57, 64].

3.2.5 Statistical Analysis

Statistical analysis was performed using linear regression analyses to evaluate the correlations and standard error between the conductivity values obtained with the present conductance cell and the conventional microcentrifuge method. A p value less than 0.05 is considered statistically significant, which is the same as having a 95% confidence interval. Analysis of variance (ANOVA) was also performed to determine if the conductivity changed according to flow rates.

3.3 Results and Discussion

The circuit used in this study, as shown in Fig. 3-5, was fabricated in a printed circuit board, as shown in Fig. 3-6 and the resultant signal was generated as shown in Fig. 3-7.

From the circuit diagram in Fig. 3-5, CMOS Schmitt trigger circuit generated an operating signal of 5 kHz. Figure 3-7(a) shows the waveform at Point A in Fig. 3-5. In order to assure that the applied waveform had a duty cycle of exactly 50%, the above signal was fed into a counter. The output of the counter at Point B is shown in Fig. 3-7(b).

Since the amplitude of this square wave was dependent upon power supply voltages, a circuit comprising Zener diodes and a precision reference diode were used. The aforementioned square-wave signal was used to alternately ground each end of the diode to establish an accurate bipolar signal. Both the anode (Light line) and cathode (Dark line) voltages at Point C are shown in Fig. 3-7(c). The voltages shown in Fig. 3-7(c) were summed and set to 100-mV peak-to-peak amplitude by using resistors and the unity gain amplifier. The signal at Point D is shown in Fig. 3-7(d).

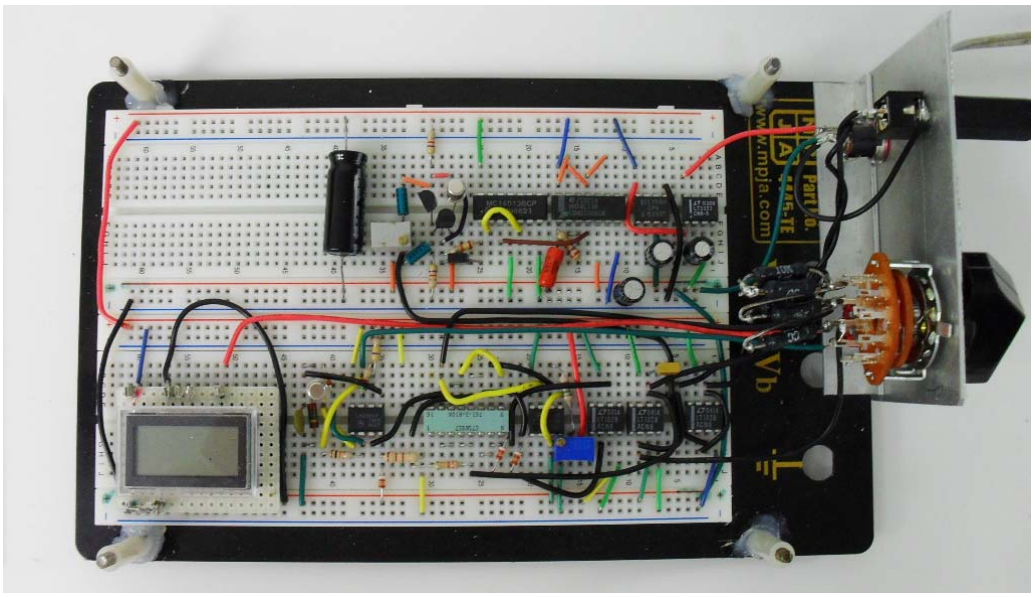

Figure 3-6. Photograph of the fabricated circuit in a printed circuit board used in the present study

The op-amp converted the resulting current of the conductance cell into a voltage with three switchable gain settings. In the 1X position, the output meter was read directly in μA. In the 2X and 3X positions, the meter reading was divided by 2

and 3, respectively. In the 1X position, the resulting saw-tooth signal at Point E is shown in Fig. 3-7(e). The rectifier circuit was comprised to obtain the absolute magnitude of the cell current. Switch SW2 was used to select which signal was to be displayed on the voltmeter between average and peak signals. The waveform of the average value at Point F is shown in Fig. 3-7(f). The digital LCD voltmeter contained a filter to display the average value (i.e., 1.21 V) as shown by an index line in the figure, which was equal to 121-μA cell current.

The peak-value circuit measured the peak value of the current about 10 μS after the cell current changed its direction. At point G, the horizontal dark line trace shown in Fig. 3-7(g) was a DC level which was superimposed on the rectified signal of Fig. 3-7(f). In this case, the peak value was shown as 1.77 V, which was equal to 177-μA peak cell current.

As shown in Fig. 3-7(f), the stable resulting current was achieved from a square-wave voltage signal, and the resulting current was directly proportional to the electric conductivity of blood. The measurements were found to be stable and noise free as shown in Figs. 3-7(a) to (f) and did not exhibit variations from the sedimentation of red blood cells as long as the whole blood kept moving through the horizontally-positioned conductance cell.

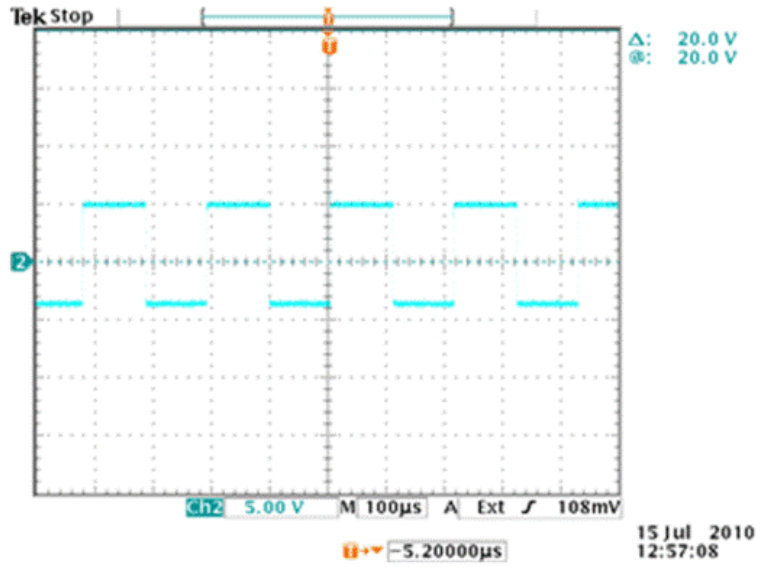
Tek Stop
Δ: 20.0 V
@: 20.0 V
Ch2 5.00 V M 100µs A Ext 108mV
-5.20000µs
15 Jul 2010
12:57:08

(a)

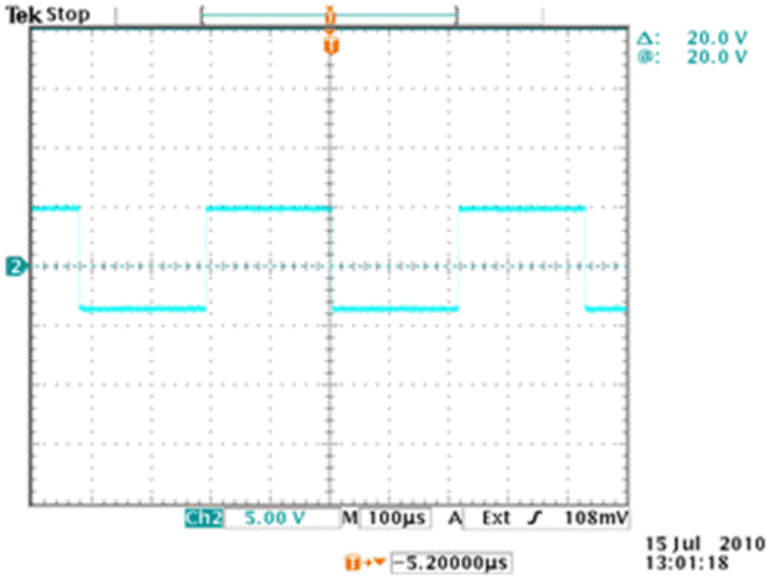
Tek Stop
Δ: 20.0 V
@: 20.0 V
Ch2 5.00 V M 100µs A Ext 108mV
-5.20000µs
15 Jul 2010
13:01:18

(b)

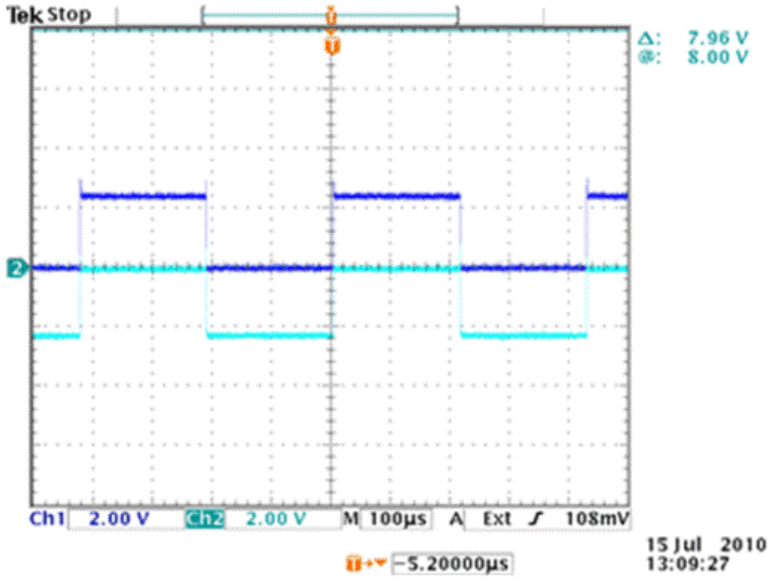
Tek Stop
Δ: 7.96 V
@: 8.00 V
Ch1 2.00 V
Ch2 2.00 V
M 100µs A Ext 108mV
-5.20000µs
15 Jul 2010
13:09:27

(c)

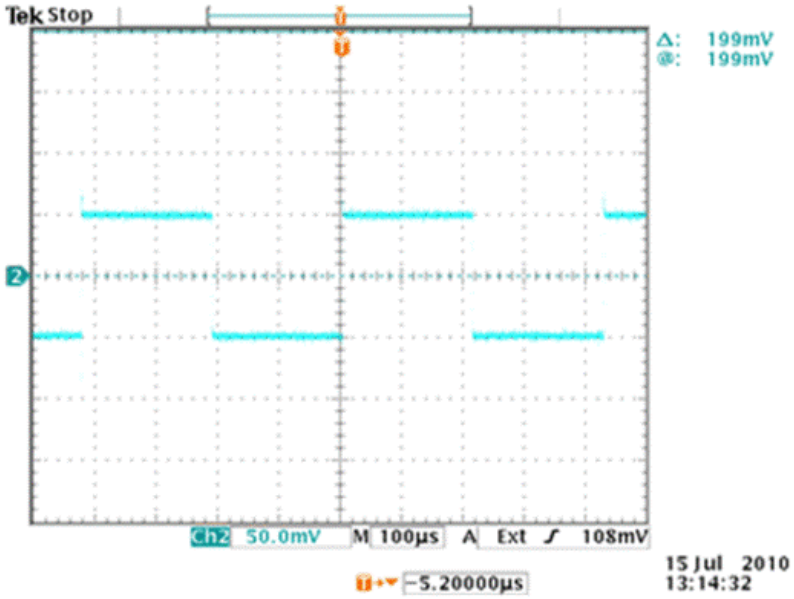
Tek Stop
Δ: 199mV
@: 199mV
Ch2 50.0mV
M 100µs A Ext 108mV
-5.20000µs
15 Jul 2010
13:14:32

(d)

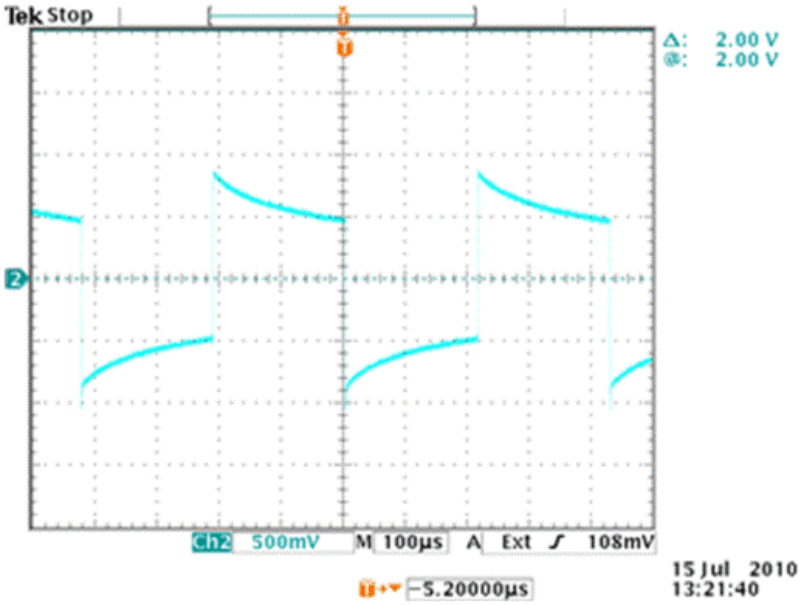
Tek Stop
Δ: 2.00 V
@: 2.00 V
Ch2 500mV M 100µs A Ext ƒ 108mV
-5.20000µs
15 Jul 2010
13:21:40

(e)

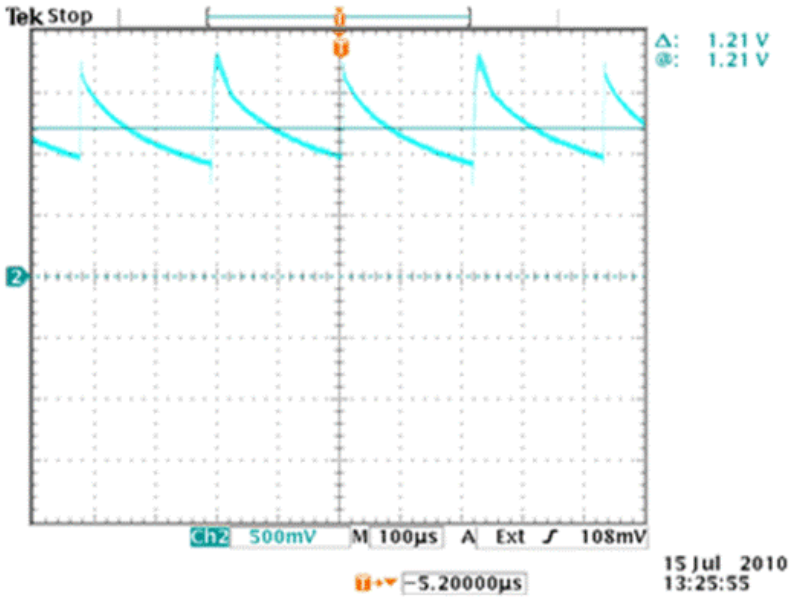
Tek Stop
Δ: 1.21 V
@: 1.21 V
Ch2 500mV M 100µs A Ext ƒ 108mV
-5.20000µs
15 Jul 2010
13:25:55

(f)

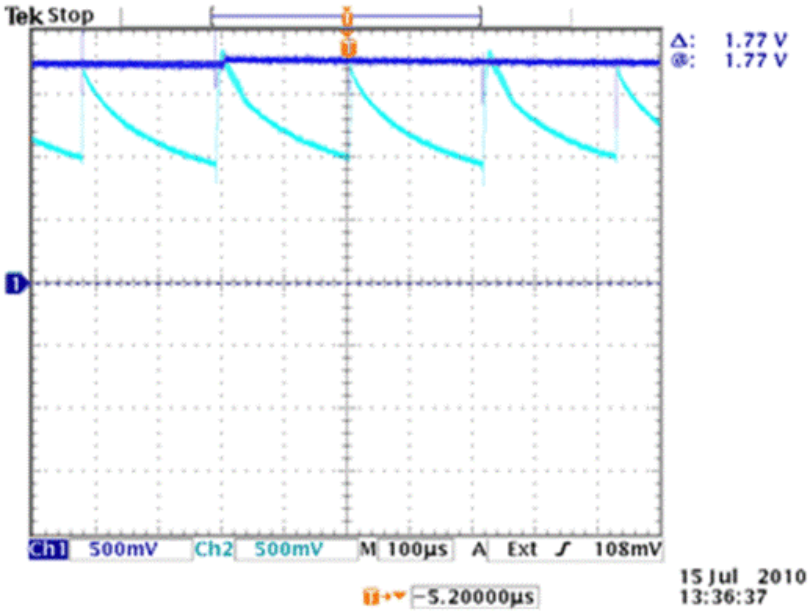

(g)

Figure 3-7. Signals generated from the circuit in the present conductance cell. (a) Point A; (b) Point B; (c) Point C; (d) Point D; (e) Point E; (f) Point F; and (g) Point G.

The cell constant, K, was determined with conductivity-standard liquids which had known electrical conductivities. From eqs. (3-3)-(3-5), the cell constant, K, can be expressed by the following equation:

$$K = R_{cal} \; X \; C_{cal} \qquad \text{(Eq. 3-6)}$$

where R_{cal} is the resistance of the cell measured at a specific electrode separation when the cell was filled with calibration liquid [76], and C_{cal} was the known electrical conductivity of the conductivity-standard fluid.

For the two conductivity-standard fluids of 3 and 10 mS/cm, the cell constants were found to be 18.520±1.867 and 18.505±1.013 cm^{-1}, respectively. The standard deviation in the case of the 3-mS/cm standard fluid was about 1.8 times larger than that for the case of 10-mS/cm. This difference can be attributed to the resolution of LCD reading with one decimal point, which was ±0.5% (for 3,000-μS/cm standard fluid) and ±1% (for 10,000-μS/cm standard fluid) deviations from the respective mean values. The mean value of the cell constant from the two calibration tests with two conductivity-standard fluids was 18.513±1.464 cm^{-1}.

Hematocrits measured for each blood sample before and after each conductivity measurement did not give any significant difference between the two hematocrit values ($p > 0.05$), confirming that no hemolysis occurred during the present conductivity measurement procedure [57, 64].

Using the cell constant, K, obtained from the aforementioned calibration procedure, the current was measured for each blood sample using the present conductivity cell, and then the conductivity of whole blood was calculated. Figure 3-8 shows the values of measured current (closed square) and specific conductance (open triangle) versus hematocrit obtained from microcentrifuge over a range of hematocrit. The measured current was found to decrease linearly with increasing hematocrit.

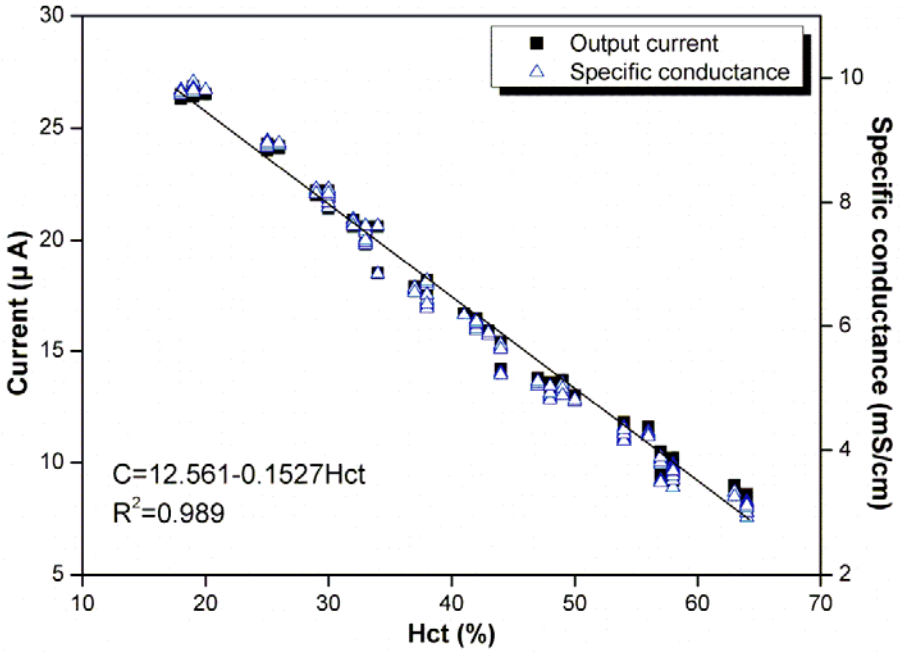

Figure 3-8. Output current and specific conductance measured at the present conductance cell over a range of hematocrits obtained with a microcentrifuge. C = specific conductance (mS/cm).

Figure 3-9 shows changes in the conductivity of blood as a function of flow rates from 0.5 to 3.0 mL/min (i.e., from 0.027 to 0.16 cm/s) inside conductance cell for three different hematocrit samples of 25, 45, and 60 %. The specific conductance for the case of 25%-hematocrit sample was 8.326 mS/cm at a flow rate of 0.5 mL/min. As the flow rate increased to 1.2 mL/min, the specific conductance increased to 8.933 mS/cm. Further increase in the flow rate up to 3.0 mL/min almost did not change the specific conductance. Similar trends were observed for higher hematocrit samples of

45 and 60%, although the rate of change of the specific conductance as the flow rate increased from 0.5 to 1.2 mL/min was much smaller compared to that in the case of 25% hematocrit.

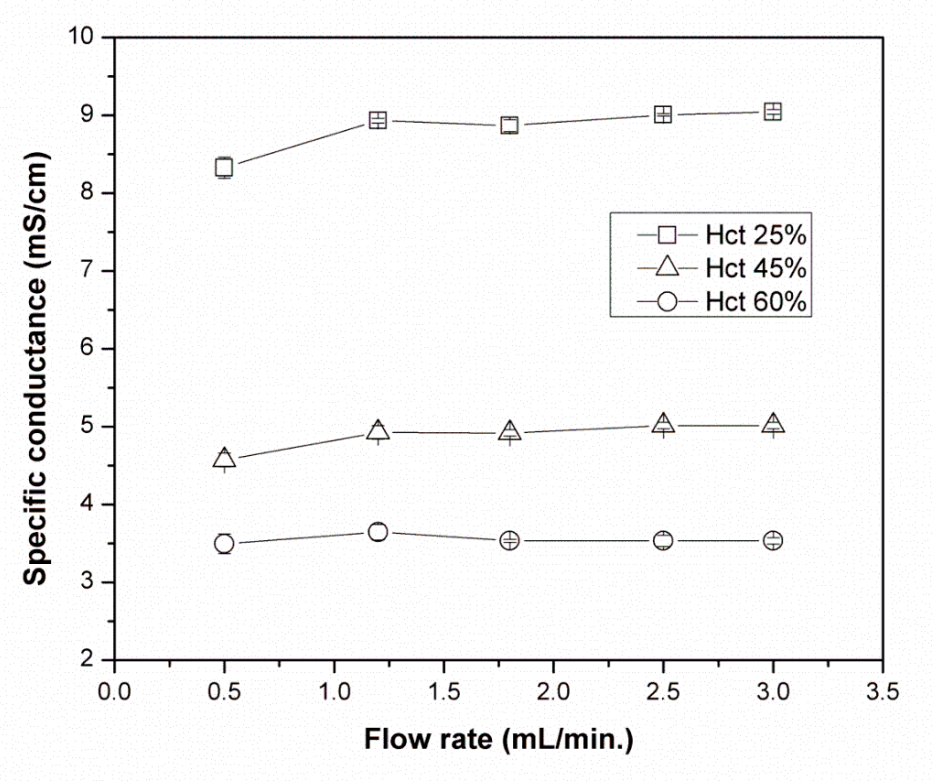

Figure 3-9. Specific conductivity measured from the present method using a conductance cell versus flow rates for three different hematocrits

The present study proposed a new method to measure the conductivity of whole blood. A conductance cell was fabricated to generate a low-frequency bipolar

square-wave voltage signal between two cylindrical electrodes. By the utilization of alternating bipolar signal, the electrolyte effect which altered the resistivity of plasma could be reduced, and hence the accuracy of conductance measurement was increased.

By applying a relatively low-frequency voltage signal (i.e., 5 kHz), the resistance of blood was able to remain constant without a decay in the current waveform due to dielectric effects of blood cells, so that the red blood cells could be considered as a non-conductive substance. The capacitive effect of the cell membrane could be minimized in response to the applied square-wave signal which provided a constant alternating voltage [76, 85, 86]. The difficulty often caused by the sedimentation of red blood cells was minimized in the present conductance cell as the whole blood continuously moved through the cylindrical electrodes [64].

Linear regression analyses of 200 data points (i.e. ten different hematocrits and 20 repeated runs for each hematocrit) were conducted to calculate the correlation and standard error between the conductivities measured from the present method and hematocrits determined from microcentrifuge. The coefficient of correlation and R value in Table 1 showed an excellent linear relationship between the two methods, and the variability in the data set was small as manifested by $R^2 = 0.989$ ($p < 0.001$). The resulting equation after the regression analysis can be given by the following equation:

$$C = 12.561 - 0.1527\,\mathrm{Hct} \qquad \text{(Eq. 3-7)}$$

where C is the specific conductance (mS/cm) , and Hct is the hematocrit of whole blood (%).

Table 3-1 also shows several correlations between the impedance and hematocrit. Cha et al. [57] reported an equation based on the data measured at room temperature, using linear, exponential, and Maxwell-Fricke expressions [57, 72, 77, 89, 90]. Considering the accuracy of the equations with the coefficient of correlation R and standard error SE, the present model, also shown at the bottom of Table 3-1, was found to have the least standard error with a similar coefficient of correlation compared to the previous correlations [57, 72, 77, 89, 90]. This could be attributed to the square-wave voltage signal, which minimized the errors from the electrolyte effect on the plasma resistance and the capacitive behavior of red cell membrane, as well as the error associated with the erythrocyte sedimentation

Table 3-1. Previous correlations to determine hematocrit as a function of impedance and the new correlation proposed by the present study

Models		Coefficient of Correlation, R	SE
Maxwell-Fricke [57, 72, 77, 89, 90]	$\mathrm{Hct} = 100 \cdot \left(1 - \frac{149.1}{R_p + 107.4}\right)$	0.984	1.75
Exponential [57, 72, 77, 89, 90]	$\mathrm{Hct} = \frac{100}{2.98} \cdot \ln\left(\frac{R_p}{43.0}\right)$	0.981	1.86
Linear [57, 72, 77, 89, 90]	$\mathrm{Hct} = 100 \cdot \left(\frac{R_p + 22.5}{425.5}\right)$	0.945	3.15
Dual-frequency [57]	$\mathrm{Hct} = 100 \cdot \left[0.142 \cdot \ln(\frac{R_p}{R_h}) + 0.155 \cdot \ln(X_h) - 0.157\right]$	0.989	1.41
Square wave [Present study]	$\mathrm{Hct} = -\frac{100}{15.27} \cdot \frac{K}{R_{sq}} + 82.259$	0.989	1.01

* SE is standard error, R_p is the resistance of plasma measured at a low frequency below 100 kHz, R_h is the resistance at a high frequency of 1 MHz, X_h is the reactance measured at a high frequency of 1 MHz, R_{sq} is the resistance measured using square-wave voltage signal, and K is the cell constant.

In measuring the blood conductivity of whole blood, the electrical resistance was found to increase with the sedimentation of erythrocyte [91]. The current measured from the present conductance cell was found not stable when whole blood was stationary, but continuously decreased with time in spite of the horizontal design of the conductance cell. The observed instability could be attributed to the sedimentation red blood cells. The effect of the sedimentation on the resistance of blood affected the conductance measurement at a small flow rate as manifested in Fig.

3-9, where the specific conductance value had a minimum value at the minimum flow rate of 0.5 mL/min for the case of 25%-hematocrit sample and reached an asymptote only after the flow rate increased above 1.2 mL/min (i.e., 0.06 cm/s). Any cell geometry other than the horizontal cylindrical electrodes could result in the over-estimation of conductivity due to the sedimentation of erythrocytes [64].

The statistical estimation with ANOVA provided the threshold flow where the erythrocyte sedimentation affected the conductivity of blood to be below 1.2 mL/min. For flow rates less than 1.2 mL/min, the measured conductivity was much smaller than those obtained at a flow rate of 1.2 mL/min or greater ($p = 0.048$).

The effect of flow on the conductivity of the blood can be qualitatively explained by the orientation and deformation of red blood cells [87, 88]. When blood moves through a cylindrical tube, the shear stress produced from the motion of blood orients the red blood cells such that their long axes align parallel to the direction of the blood flow. The pathway of a low-frequency AC could alter the orientation and alignment of the red blood cells. Consequently, the electrical conductivity in the flow direction of blood could increase [87, 88]. However, in the present study, such an effect on the conductivity of blood could be minimized by applying a bipolar square-wave voltage signal not to the direction of flow but to the whole volume of blood.

The results given in Fig. 3-9 indicate that the on-line measurement of hematocrit is feasible. For example, when a blood sample is drawn from a patient, hematocrit could be measured at site if the present conductance cell is attached between the outlet of a needle and a syringe. In addition, hematocrit could be

measured in a capillary tube viscometer if the conductance cell is inserted at the supply line of blood sample connected to the viscometer [41, 57].

3.4 Limitations

A new on-line conductance cell might have limitations in measuring hematocrit accurately for blood samples with impaired blood cells by hemolysis or diseases such as sickle-cell disease, sphyrocytosis, etc.

The accuracy of the current conductance method was achievable as we avoided the behaviors of red cells to become conductive or/and capacitive by applying specific signals. However, if red cells are physically damaged, it has a doubt whether or not the principles of the current method could be applied properly for an accurate measurement of hematocrit, which requires further clinical trials.

CHAPTER 4: PLASAMA DISCAHRGE TREATMENT TO IMPROVE HEMORHEOLOGYCAL PROPERTIES

4.1 Motivations and Literature Survey on Reduction of Blood Viscosity

There are a number of variables for the WBV, which include hematocrit, plasma proteins (i.e., fibrinogen, immunoglobulin, and albumin), total cholesterol, low-density-lipoprotein (LDL) cholesterol, high-density-lipoprotein (HDL) cholesterol and triglyceride [1, 18, 28]. In addition, the aggregation and deformability of erythrocytes critically affect the WBV [18, 92]. Since both the plasma proteins and LDL molecules influence the aggregation of erythrocytes [8, 13, 93, 94], it is important to keep both levels within the respective normal ranges. For example, lipid-lowering statin drugs have been widely used to keep the LDL cholesterol within the normal range (i.e., 62-130 mg/dl) [95-102]. Statins are powerful cholesterol-lowering drugs in clinical practice and have a life-saving potential in properly selected patients, particularly those with severe hyperlipidemia and atherosclerotic disease [103, 104]. Results from randomized clinical trials have demonstrated a decrease in congested heart diseases (CHD) and total mortality, reductions in myocardial infarctions, revascularization procedures, stroke, and peripheral vascular disease [103, 105]. However, statins are prescribed for less than half of the patients who should receive this therapy, unfortunately, because fear of liver and muscle toxicity, a side effect which remains a major impediment to the appropriate use of these drugs [106, 107].

In recent years, many new medical applications, including the sterilization of living tissue without damage, blood coagulation, the induction of apoptosis in

malignant tissues, and the modulation of cell attachment are being developed utilizing non-thermal plasma discharges in atmospheric pressure [108-116]. It was demonstrated that selective coagulation of fibrinogen, which is one of the major viscosity determinants in blood, could be induced by the application of dielectric barrier discharges (DBD) in air [108]. Hence it is hypothesized that the hemorheological properties of blood may be improved by lowering the levels of fibrinogen or/and LDL molecules in blood plasma through electrical plasma-assisted coagulation and the subsequent filtration of the coagulated particles from the treated blood plasma. Hence, the objective of the present chapter was to investigate the feasibility of reducing whole blood viscosity through two types of electrical plasma treatment, dielectric barrier discharge (DBD) and corona discharge, of blood plasma and subsequent filtration.

4.2 The Effect of DBD Treatment on Blood Viscosity

4.2.1 Methods

The DBD system used in the present study was identical to the one used by Kalghatgi et al. [108], which was atmospheric pressure dielectric barrier discharge and is illustrated in Figs. 4-1 and 4-2. The DBD system was operated with one dielectric-covered powered electrode and the other grounded electrode. Discharge was ignited when the powered electrode approached the surface of the sample to be treated at a distance of less than 3 mm, the phenomenon which depended on the waveform, duration, and polarity of the driving voltage [109]. A pulsed high voltage

of 35kV (peak to peak) with alternating polarity at 1 kHz frequency was applied between the quartz insulated copper electrode and the surface of the sample (blood plasma) to generate DBD. The power applied to the present DBD system was analyzed by measuring the current passing through the discharge gap and the voltage drop in the gap when the discharge was generated. The current and voltage signals were acquired and recorded by a two-channel digital phosphor oscilloscope (DPS) (TDS5052B, 500 MHz bandwidth, 5 GS/s sample rate, Tektronix, Inc). The surface power density which corresponded to the applied power was around 1.5 W/cm^2 [108, 109, 117].

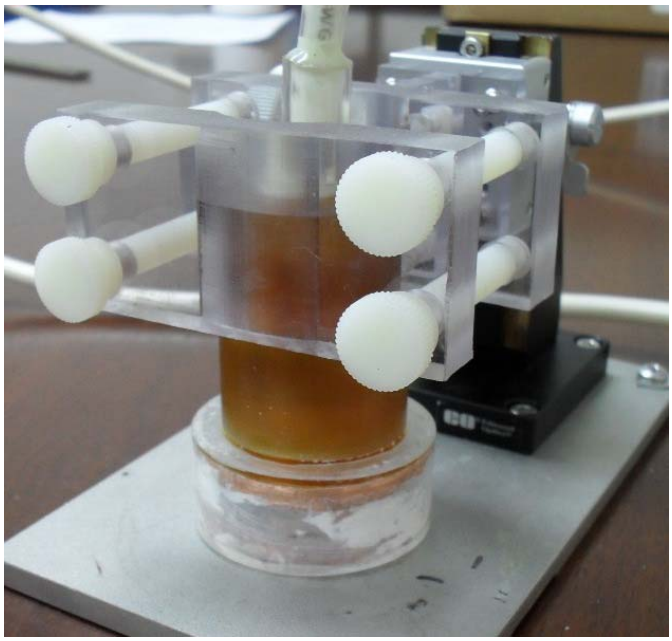

Figure 4-1. Application of DBD to a blood plasma sample

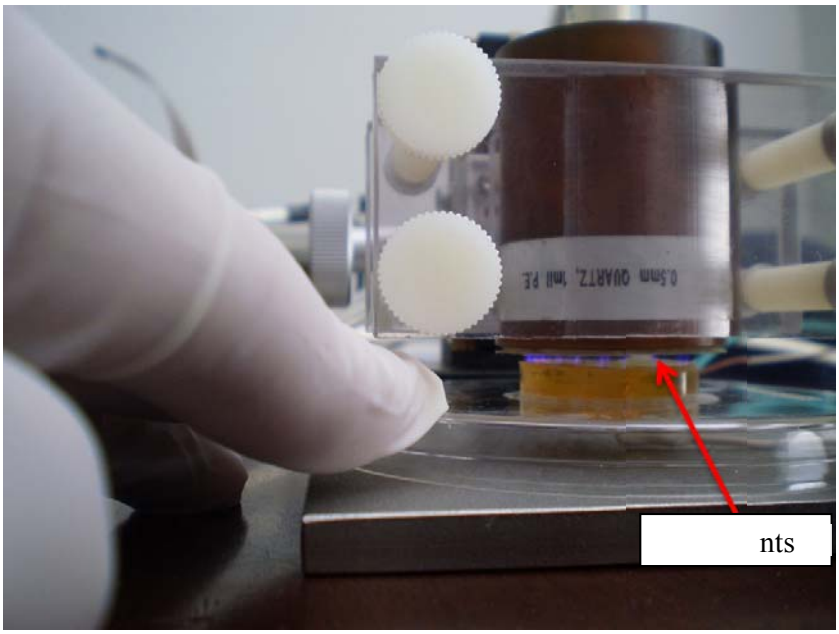

Figure 4-2. Photograph of filaments generated by DBD to blood plasma sample

The electrode was constructed of a 25 mm diameter copper rod enclosed in polytherimide (Ultem®). A 1 mm thick fused quartz was used to prevent an arc formation by limiting the current in the DBD discharge. The presence of the insulating layer prevented the buildup of high current and subsequent heating of the gas in the discharge gap so that biological samples could be treated without thermal damage. The gap between the bottom of the dielectric quartz glass covering the copper electrode and the surface of the blood plasma sample was adjusted to be 2 mm using a precision vertical positioner shown in Fig. 4-3. To treat the sample with DBD, 4 mL of blood plasma were placed in the sample holder (see Fig. 4-3) which was

composed of a 25-mm-diameter copper rod inserted into polytherimide (Ultem®) shell. The bottom of the copper rod inside the sample holder was placed on a 21 mm thick polycarbonate plate as the grounded base electrode [108, 117].

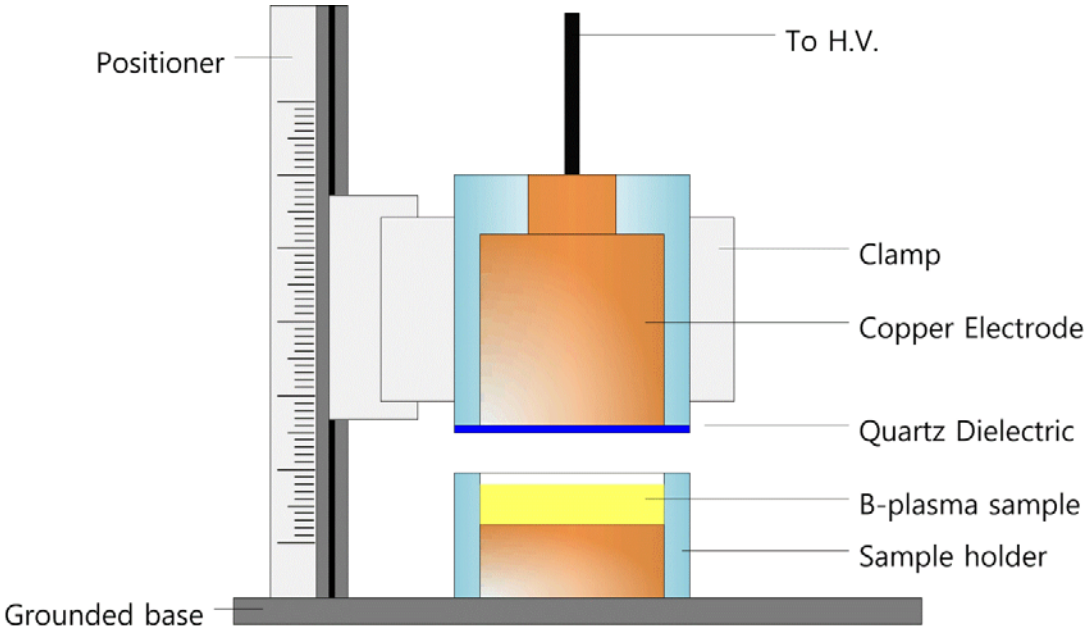

Figure 4-3. Schematic of the experimental setup for the DBD treatment of blood plasma

Human whole blood of 150 mL with 1.5 mL of ethylene diaminetetraacetic acid (EDTA) as an anti-coagulant was obtained from Lampire Biological Laboratories (Pipersville, PA) in a glass bottle. Both the WBV and hematocrit for the

blood sample were measured to determine the baseline data prior to the DBD treatment. The whole blood in the 150 mL of bottle was then transferred to several 10 mL-polyethylene tubes to prepare blood plasma from whole blood using a centrifuge (VanGuard V6500, Hamilton Bell Co.) with 1,200 G of relative centrifugal force (RCF) for 15 min.

The blood plasma viscosity was measured before DBD treatment for the baseline data. Each blood plasma sample separated from whole blood was then treated with DBD for 1, 2, 4, and 8 min to investigate the effect of DBD treatment on the rheological properties of blood plasma and whole blood. Temperature change was monitored before and after the DBD treatment.

The viscosity of the blood plasma after DBD treatment was measured again with viscometers (see below) to compare the change in the plasma viscosity before and after DBD treatment. In order to evaluate the change in the WBV due to the coagulated particles generated by DBD treatment, some of the DBD-treated blood plasma samples were mixed back with the original erythrocytes which had been separated in the previous step, and the WBV was measured. For the last step, to investigate whether or not the WBV could be reduced by the filtration of the coagulated particles from the DBD-treated blood plasma, some of the DBD-treated blood plasma samples was filtered using a syringe filter (25 mm, pore size 0.20 μm, Nylon, Millipore) and then mixed back with the centrifuged erythrocytes, and the viscosities of the mixed whole blood samples were measured.

Here, hematocrit concentration was also measured to examine any possible

plasma loss or hemolysis during the transfer of blood, the centrifugation of blood cells, the DBD treatment, the filtration process of DBD-treated blood plasma, and the remixing of the DBD-treated blood plasma with the centrifuged erythrocytes.

WBV was measured at 37^{o}C using the SCTV over a range of shear rates from 1 to 1,000 s^{-1}. Detailed test and viscosity calculation procedures are given elsewhere [41]. The viscosity of the DBD-treated blood plasma was also measured using Brookfield viscometer (LV-III with CP-42, Brookfield Engineering Lab.) at two different shear rates of 225 and 450 s^{-1}. The temperature of the test sample at Brookfield viscometer was maintained at a constant temperature of 37^{o}C with a constant temperature water bath and circulator. Since some plasma volume could be lost during the DBD treatment and filtration, the WBV was normalized to a standard hematocrit of 45% using a standard hematocrit-correction method [45].

The mean and standard deviations for both whole blood and blood plasma viscosities were calculated. WBV was reported both at the observed (native) hematocrit and normalized hematocrit of 45% [45].

4.2.2 Results and Discussion

Prior to DBD treatment, the WBV profiles of control blood samples were measured using the SCTV and viscosity values at five different shear rates of 1,000, 300, 100, 10, 1 s^{-1} were obtained for numerical comparison after DBD treatment. All the obtained WBVs including the baseline mean and standard deviation values were

normalized to standardized hematocrit of 45%. The normalized WBV of untreated blood varied from 35.38 to 301.01 mP when shear rate decreased from 1,000 to 1 s^{-1}.

Table 4-1. The Change of whole blood viscosity after DBD treatment (1 cP = 10 mP)

DBD Treatment time	Shear rate	(Uncorrected) Whole blood viscosity (Means ± SD) (mP)	(Normalized) Whole blood viscosity (Means ± SD) (mP)
No treatment	1,000 s^{-1}	34.65 ± 1.63	35.38 ± 3.28
	300 s^{-1}	38.60 ± 3.39	39.29 ± 2.48
	100 s^{-1}	44.85 ± 4.74	45.68 ± 2.82
	10 s^{-1}	83.85 ± 11.95	86.08 ± 8.13
	1 s^{-1}	286.90 ± 53.60	301.02 ± 56.17
DBD treated (1 min.)	1,000 s^{-1}	33.79 ± 3.38	38.99 ± 0.82
	300 s^{-1}	37.25 ± 3.87	41.92 ± 0.83
	100 s^{-1}	43.21 ± 6.25	47.89 ± 0.59
	10 s^{-1}	82.94 ± 11.51	93.23 ± 5.10
	1 s^{-1}	291.25 ± 49.75	326.12 ± 44.05
DBD treated (2 min.)	1,000 s^{-1}	43.73 ± 7.45	41.47 ± 5.06
	300 s^{-1}	46.35 ± 7.41	43.87 ± 4.71
	100 s^{-1}	52.63 ± 6.56	49.66 ± 3.11
	10 s^{-1}	101.28 ± 12.95	93.56 ± 4.08
	1 s^{-1}	370.35 ± 62.98	327.75 ± 27.74
DBD treated (4 min.)	1,000 s^{-1}	39.50 ± 7.91	38.28 ± 4.48
	300 s^{-1}	43.50 ± 7.77	42.19 ± 3.90
	100 s^{-1}	50.27 ± 7.86	48.75 ± 3.04
	10 s^{-1}	99.33 ± 17.95	95.28 ± 6.14
	1 s^{-1}	353.97 ± 64.75	336.47 ± 45.00
DBD treated (8 min.)	1,000 s^{-1}	46.27 ± 9.26	44.50 ± 3.79
	300 s^{-1}	49.30 ± 9.92	47.36 ± 3.79
	100 s^{-1}	55.23 ± 9.54	53.23 ± 2.01
	10 s^{-1}	104.90 ± 15.66	101.01 ± 5.86
	1 s^{-1}	383.83 ± 60.19	368.10 ± 65.41

When blood plasma was treated with DBD, a white layer formation was found on the top surface of the treated blood plasma samples and at the interfacing edge with a copper surface, whereas the blood plasma without DBD treatment did not exhibit any white particle formation on the sample surface after being exposed to open atmosphere for the same duration (see Fig. 4-4). The viscosity of blood plasma treated with DBD measured with Brookfield viscometer at two different shear rates, 225 and 450 s^{-1} is shown in Fig. 4-5. The viscosity of blood plasma showed irregular values in accordance with the DBD treatment time for both shear rates.

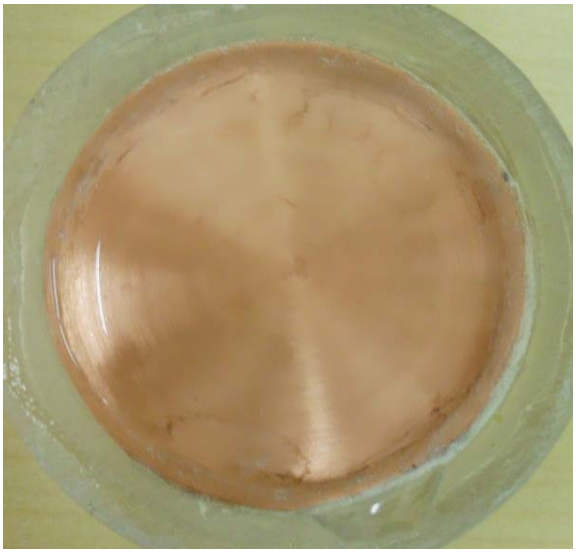

(a)

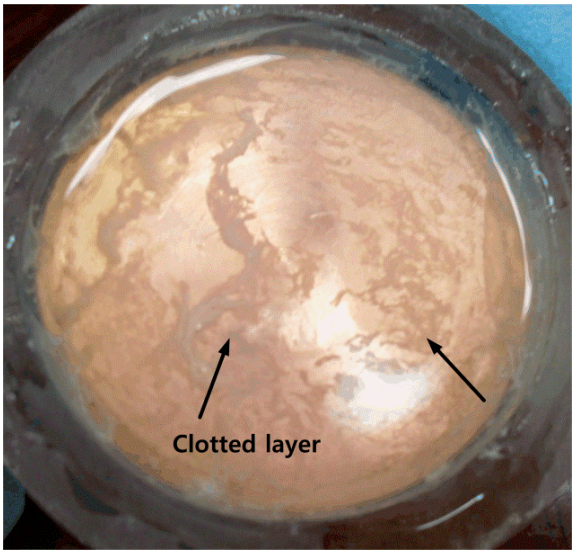

(b)

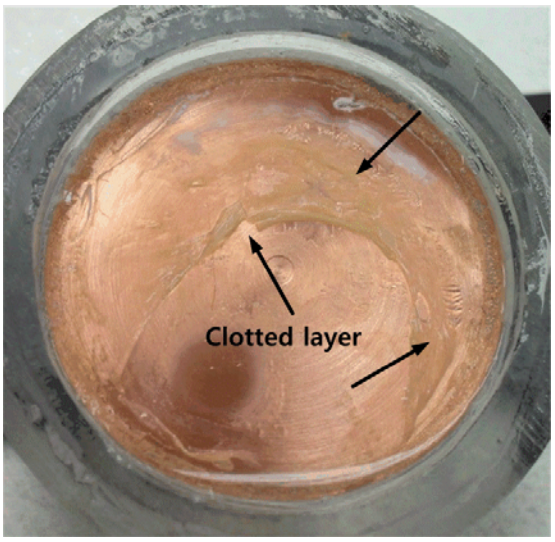

(c)

Figure 4-4. Photographs of the formation of white layer in blood plasma sample with DBD treatment: (a) blood plasma before DBD treatment showed no coagulation, (b) blood plasma treated with DBD for 4 min. exhibited a partially coagulated layer, and (c) blood plasma treated with DBD for 8 min. Showed white clotted layer on the surface of copper surface

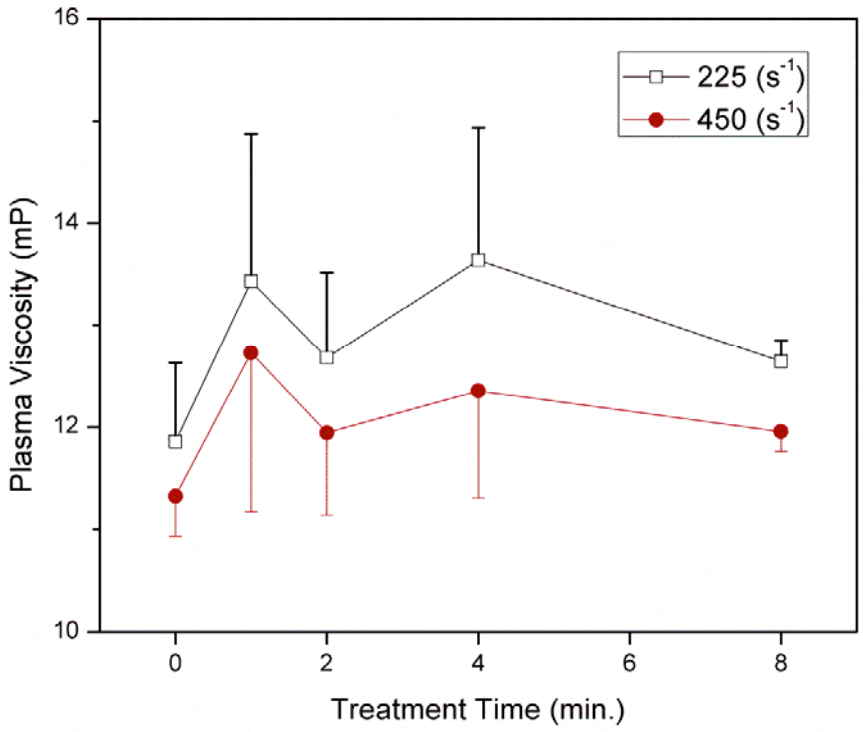

Figure 4-5. Variations in the viscosity of blood plasma at two different shear rates, 225 and 450 s^{-1} at four different DBD treatment times together with baseline data

The values of WBV for the blood samples mixed with blood plasma treated by DBD are given in Fig. 4-6 at five different shear rates at each treatment time (i.e., 1, 2, 4, and 8 min). Over the range of shear rates, the normalized WBV increased with increasing DBD treatment time. WBV measured at a high shear rate of 300 s^{-1} is usually termed as systolic whole blood viscosity (SBV), whereas WBV measured at a

low shear rate of 1 s^{-1} is termed as diastolic whole blood viscosity (DBV) as WBV varies during a cardiac cycle like blood pressure. As shown in Fig. 4-6, DBV values were significantly higher in DBD-treated samples (i.e. 368.10 ± 65.41 mP for 8-min DBD treatment case) than untreated control samples (301.02 ± 56.17 mP). SBV values were also elevated from 38.60 ± 3.39 mP for control to 49.30 ± 9.92 mP (for 8-min DBD treatment case).

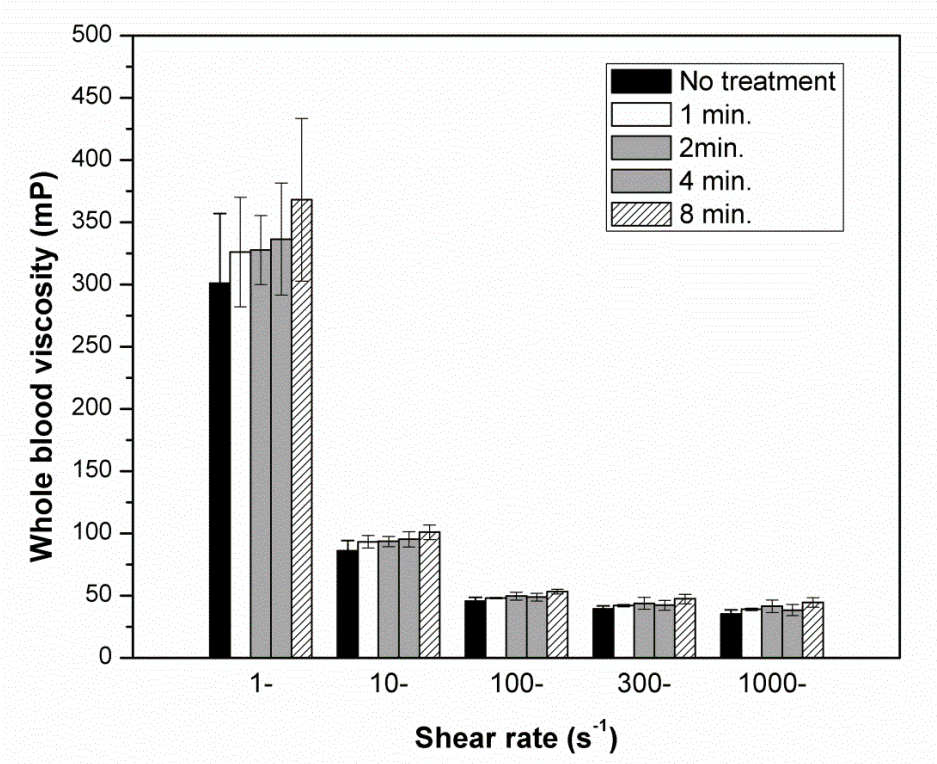

Figure 4-6. Variations in the viscosity of whole blood at four different DBD treatment times together with baseline data

WBVs of blood samples remixed with DBD-treated blood plasma, which was filtered before being mixed with the original red blood cells are shown in Figs. 4-7 and 4-8. For SBV values shown in Fig. 4-7, the systolic blood viscosity after 8-min DBD treatment without filtration increased by 5.5% from the baseline value of 41.0 mP. When the DBD-treated plasma was filtered and then remixed with red blood cells, the systolic blood viscosity decreased by 9.1% from the baseline SBV of 41.0 mP. The diastolic blood viscosity of blood treated by DBD but without filtration was elevated with increasing DBD treatment time. For example, the DBV of blood increased by 29.9% from the baseline value of 340.7 mP (see Fig. 4-8). When the DBD-treated plasma was filtered then remixed with red blood cells, the DBV of blood for 8-min treatment case decreased by 17.7% from the baseline value of 340.7 mP.

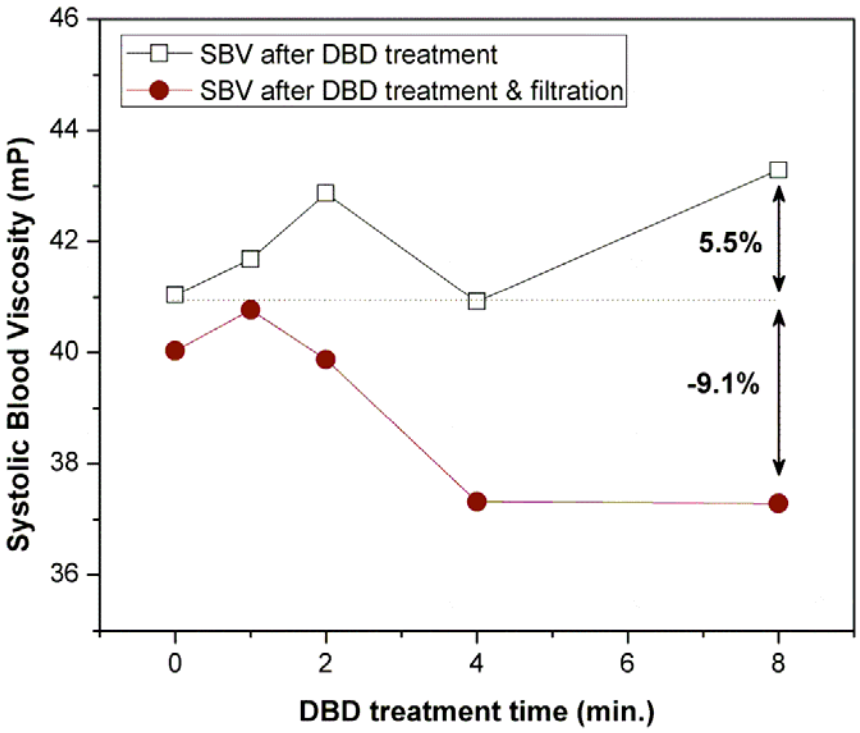

Figure 4-7. Variations in the systolic blood viscosity of whole blood after DBD treatment with and without filtration

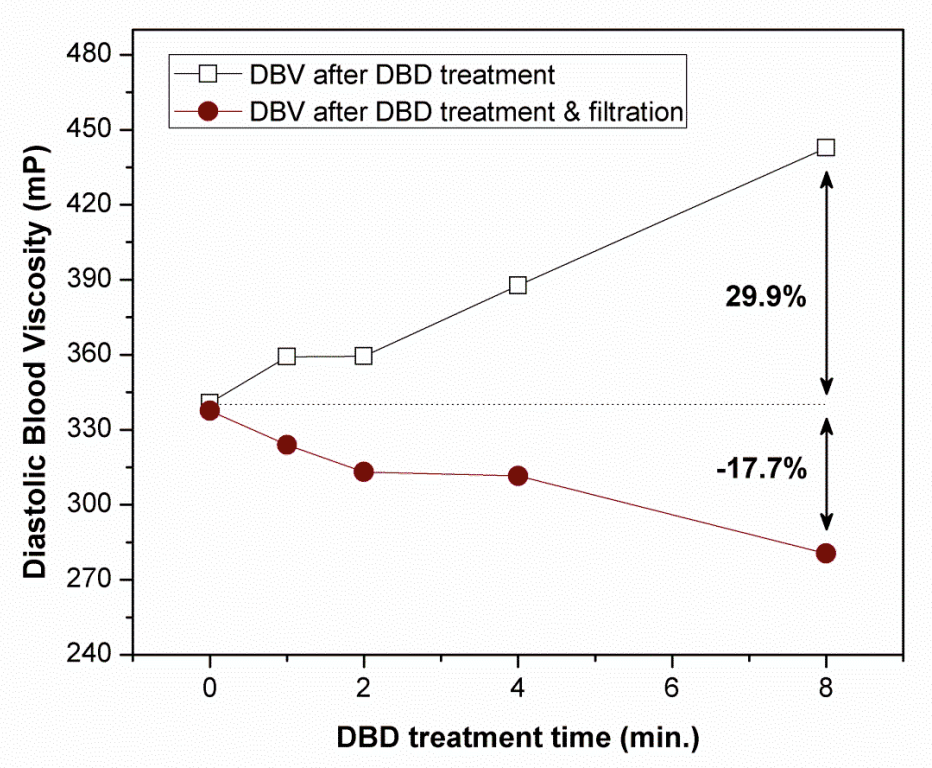

Figure 4-8. Variations in the diastolic blood viscosity of whole blood after DBD treatment with and without filtration

When blood plasma was treated by DBD, a white clot layer was formed at the top of blood plasma sample (see Fig. 4-4), suggesting that the plasma proteins and lipids in blood plasma might have precipitated into coagulated particles through DBD treatment. Accordingly, if these coagulated particles are removed, one may anticipate some improvement in the rheological properties of whole blood. Note that the size of fibrinogen (diameter of 5-7 nm and length of 48 nm) and LDL molecules (approximately 22 nm) are too small to be removed by filter [118-120].

Although DBD discharge employed in this study is non-thermal, there could be about 20 % of thermal energy to be transferred from filamentary discharge to the blood plasma sample due to energy distribution of input power to the metallic electrode [121, 122], a phenomenon which could create the white layer of coagulated particles by heating effect. To test this possibility, temperature measurement was performed before and after the treatment of the samples with DBD, and no significant change in temperature was observed, suggesting that the coagulated particles must have come from the oxidation and subsequent coagulation by active species generated by DBD. In addition, there was no change in hematocrit between before and after DBD treatment, indicating no significant evaporation in blood plasma during the DBD treatment procedure.

Two important buffer systems exist in blood plasma, dihydrogen phosphate buffer and carbonic acid buffer. The dihydrogen phosphate buffer resists a drop in pH, while the carbonic acid buffer resists a rise in pH [123]. It has been known that when non-thermal plasma discharge is applied to liquids, it generates a significant amount of hydrogen ions, which change the acidity of liquids. The effect of DBD discharge on phosphate buffered liquids which is similar to the buffering system of blood plasma has been investigated and confirmed that when about 5-mL phosphate buffered solution was treated with DBD discharge, the phosphate buffer system prevented the acidification of the liquids, while treating smaller volume (i.e. less than about 1.5 mL) for longer than about 10 min. could be susceptible to the acidification of DBD discharge [112, 124]. In the present study, the 4-mL blood plasma sample was treated with DBD discharge for maximum 8 min., thus we assumed that the

acidification of 4-mL blood plasma sample could not be significantly affected by DBD plasma discharge.

The blood mixed with the blood plasma treated by DBD without filtration showed significant increase in WBV. This can be attributed to the fact that plasma proteins and lipids formed large groups of coagulated particles of micron size, increasing frictional resistance to flow over the entire range of shear rates. Since the coagulated particles are visible (i.e., large in size), they could be relatively easily removed with filtration, a process which helped reducing WBV as the plasma proteins and lipids are the key determinants of WBV.

The SBV of blood with DBD treatment and filtration decreased by about 9.1% from the baseline value, whereas the DBV dropped by 17.7% from the respective baseline values, both representing significant improvements in rheological properties. The reason why the DBD treatment improved the DBV more than the SBV is as follows: The SBV is usually affected by erythrocyte deformability while DBV is affected by the erythrocyte aggregation. Since the plasma proteins (i.e., fibrinogen and immunoglobulin) and LDL molecules are instrumental in the RBC aggregation [13, 94], their removal by the DBD treatment and filtration should mitigate the erythrocyte aggregation, subsequently reducing the DBV.

In terms of the mechanism of DBD treatment in the precipitation of plasma proteins and lipids from blood plasma, Kalghatgi et al. [108] reported that DBD treatment might have activated some of protein coagulation process which resulted in rapid fibrinogen aggregation. It was also mentioned that the selective coagulation of

proteins was observed – not of albumin but of fibrinogen only [108]. We can hypothesize that this coagulated fibrinogen and subsequent removal might have affected the WBV of blood with DBD-treated blood plasma.

In addition, oxidized LDL molecules are known adhere to arterial wall surfaces, playing a key role in the progression of atherosclerosis [125, 126]. In a similar manner, from the reduction of DBV, we can indirectly hypothesize that LDL molecules in blood plasma might have been oxidized by DBD treatment, and the oxidized LDL molecules may tend to precipitate and coagulate, a phenomenon which requires further investigation. Since LDL molecules are one of the important variables in WBV [127-129], their removal with DBD treatment and filtration should not only help reducing WBV [130] but also reducing the progression of atherosclerosis.

4.3 The Effect of Corona Discharge Treatment on Blood Viscosity

4.3.1 Methods

An experimental setup was prepared to generate a pulsed corona discharge as shown in Figs. 4-9 and 4-10. This system was originally constructed with three components (i.e. a high-voltage dc power supply, a spark-gap switch, and a point-to-plain electrode) and could be utilized to generate a pulsed corona, arc or spark discharge with capacitors according to its application. When the spark-gap switch was triggered, the capacitor bank (8.5nF) charged by a pulsed power supply could

initiate a pulsed discharge between electrodes [131].

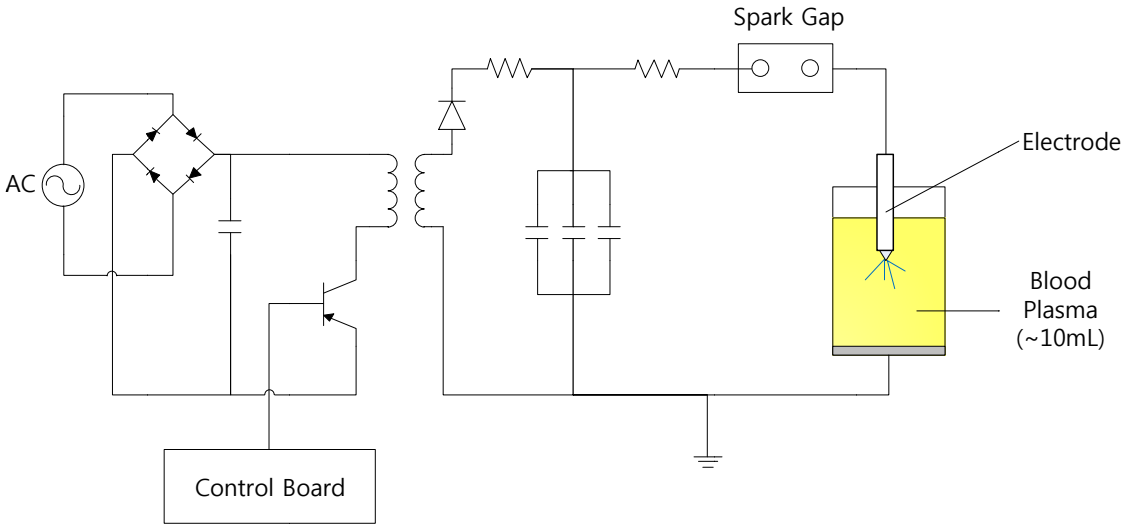

Figure 4-9. Experimental layout for the generation of a pulsed corona discharge in blood plasma [131]

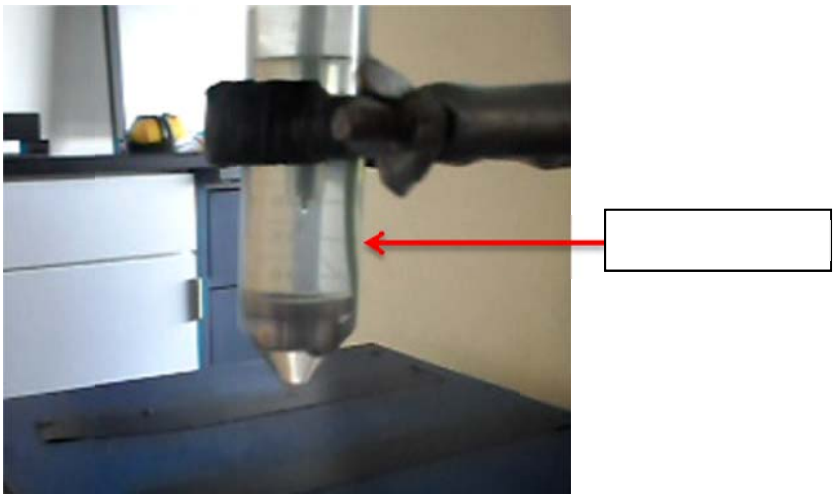

Figure 4-10. Application of a pulsed corona discharge to blood plasma

A corona discharge could be generated when the ionized region (or the potential gradient of electric field) around an electrode became high enough to grow, but limited to a certain radius. Thus, streamer filaments did not propagate across the electrode gap. If the potential gradient became too high, it could generate electrical breakdown and form an arc or spark discharge. One prepared a point-to-plane geometry of electrodes and immersed in a 10-mL cylindrical container filled with blood plasma. A tungsten needle electrode (3 mm in outer diameter and 150 mm in length) was prepared as an anode and completely insulated from surrounding blood plasma except for the 2-mm tip of the needle.

In order to generate a pulsed corona discharge and avoid electrical breakdown, the gap between the electrodes was maintained to be 30 mm, and the tip of the tungsten needle electrode was mechanically grounded to 0.5 mm in the radius of curvature at the tip of the anode. The electric field on the needle tip could be estimated by the following equation:

$$E \sim U/r_c \qquad \text{(Eq. 4-1)}$$

where U and r_c are the applied voltage and radius of curvature of the needle, respectively [132, 133]. By maintaining the gap between the electrodes and the radius of curvature of the needle tip relatively large, a pulsed corona discharge could be generated without breakdown.

In order to prepare blood samples, 200 mL of normal whole blood was obtained from a volunteer and collected in a glass container, which had contained 2 mL of ethylene diaminetetraacetic acid (EDTA) as an anti-coagulant.

The whole blood sample in a glass container was gently and homogeneously mixed. Then, it was transferred to 10-mL polyethylene transparent tubes for the separation of cells from whole blood by centrifuge so that one could obtain blood plasma. After completion of centrifuge (VanGuard V6500, Hamilton Bell Co.) for 15 min with a relative centrifugal force (RCF) of 1,200 G, the separated blood plasma from whole blood was transferred to another empty 10-mL transparent container for corona discharge treatment.

Same as the previous DBD experiment, WBV was measured at 37^{o}C using the SCTV over a range of shear rates from 1 to 1,000 s^{-1}. Detailed test and viscosity calculation procedures are given elsewhere [41].

The experimental procedure for corona discharge treatment to blood plasma was shown in Fig. 4-11. The WBV profile over a range of shear rates from 1 to 1,000 s^{-1} was measured in order to determine the baseline values before the blood samples were centrifuged. Hematocrit was also measured to confirm that no hemolysis took place while the blood cells were centrifuged, transferred, and mixed back with blood plasma.

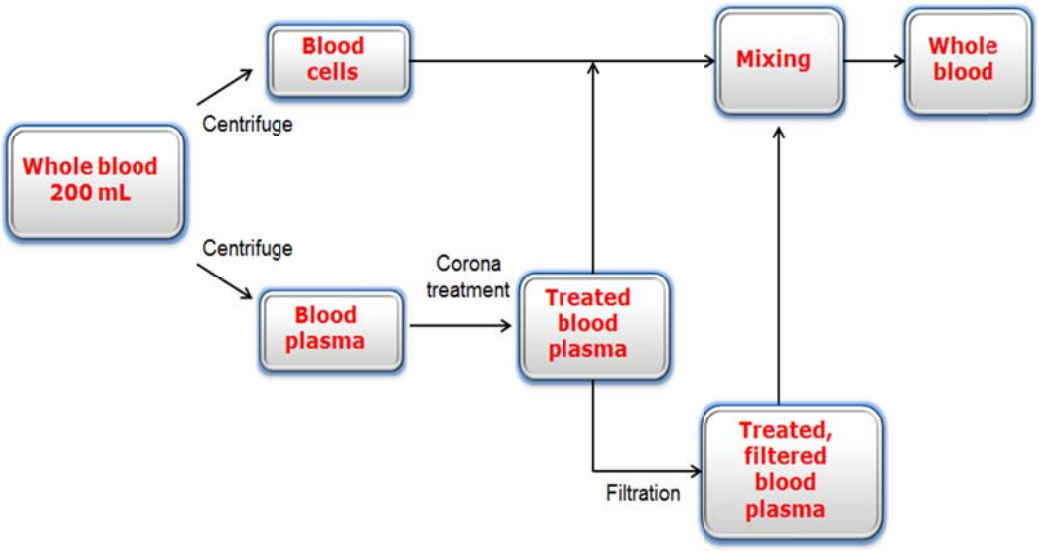

Figure 4-11. Flow chart describing the experimental procedure for corona discharge treatment to blood

After the completion of centrifuge, but before the application of a pulsed corona discharge treatment, the viscosity of blood plasma was measured in order to obtain the baseline profile of blood plasma viscosity. Then, each blood plasma sample was treated with a pulsed corona discharge for 15, 30, 60, and 90 s. The temperature change of blood plasma was monitored during the treatment since the coagulation of blood plasma could have occurred by the influence of heating instead of plasma-assisted chemical reaction.

As mentioned in the previous DBD treatment to blood plasma, the viscosity of blood plasma after the corona discharge treatment was measured again to compare

the change of plasma viscosity before and after the corona discharge treatment. Then, the corona-treated blood sample was filtered using a syringe filter (25mm, pore size 0.20 μm, Nylon, Millipore) to investigate whether or not the coagulated particles could be removed by filtration. The blood plasma samples treated with a pulsed corona discharge and then filtered were mixed back with red blood cells to measure the profiles of WBV.

The change of LDL concentration in whole blood between before and after filtration was monitored using an LDL measuring equipment (Cardio Check Monitor and LDL Direct Cholesterol Test Strips, POLYMER Technology systems) to check if LDL was removed by the coagulation using a pulsed corona discharge and subsequent filtration.

The mean and standard deviations for whole blood viscosity, blood plasma viscosity, and LDL values were calculated. WBV was reported at the normalized hematocrit of 45% for comparison [45].

4.3.2. Results and Discussion

Figure 4-12 shows the profiles of WBV after a pulsed corona discharge treatment. Once blood plasma samples were separated from whole blood, they were treated with a pulsed corona discharge. Then, they were mixed back with the separated blood cells to investigate the effect of corona discharge on WBV. As seen in Figs. 4-12 and 4-13, WBV at low shear rate ranges showed a large increase as the

treatment time of a pulsed corona discharge increased. For example, DBV (at a shear rate of 1 s^{-1}) increased by 42.6% from 297.69 mP to 424.53 mP after corona discharge treatment for 90 pulses.

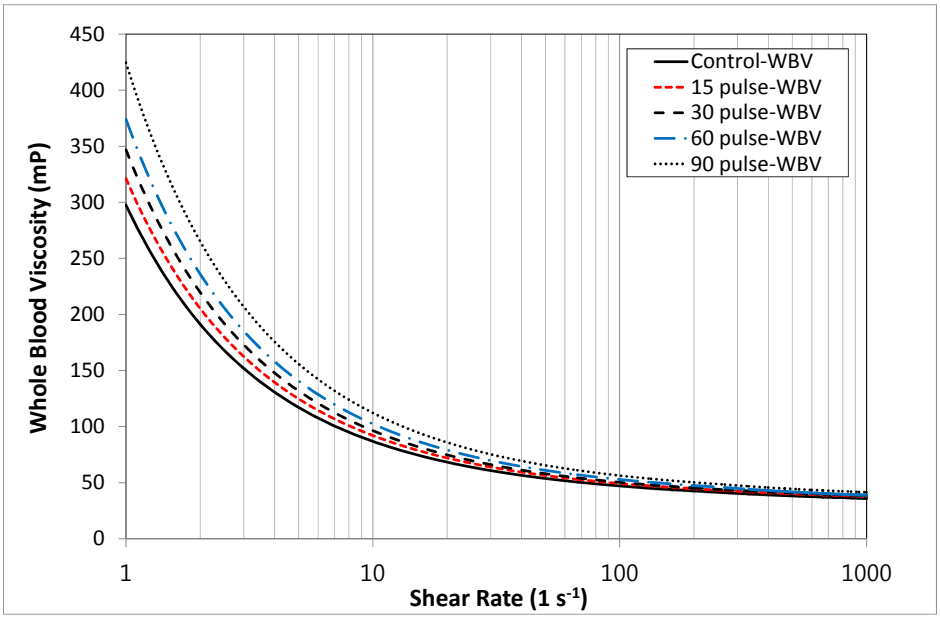

Figure 4-12. Profiles of WBV over a shear rate range from 1 to 1,000 s^{-1} after blood plasma treated by corona discharge was mixed back with blood cells

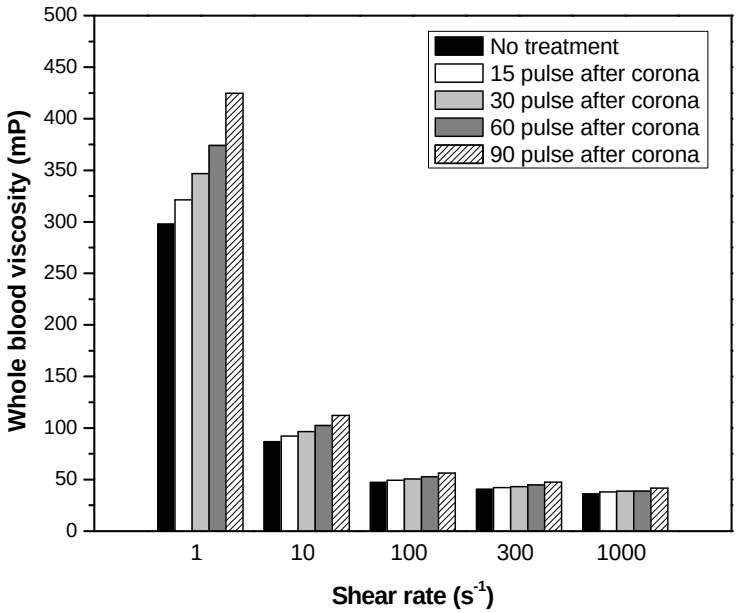

Figure 4-13. Comparison of WBVs at shear rates of 1, 10, 100, 300, and 1,000 s^{-1} blood plasma treated by corona discharge was mixed back with blood cells

Figure 4-14 shows the profiles of WBV over high shear rate ranges from 100 to 1,000 s^{-1} after corona-treated blood plasma was mixed back with blood cells. As shown in Fig. 4-13, the WBV at high shear rate ranges also increased as the blood plasma sample was treated for longer pulses, i.e. 15, 30, 60, and 90 pulses of corona discharge. However, the increased amounts of WBV at high shear rate ranges were smaller than those at low shear rate ranges. For example, the SBV (at a shear rate of 300 s^{-1}) showed an increase by 17.2 % from 40.53 mP to 47.50 mP after the blood plasma was treated for 90 pulses with corona discharge, whereas the DBV (at a shear

rate of 1 s^{-1}) increased by 42.6 %, 2.5 times higher than the SBV. This indicated that a pulsed corona discharge could affect greater to the WBV at low shear rate ranges than that at high shear ranges, a finding which was similar to the results of DBD discharge to blood plasma in the previous experiment.

The fluidity of blood depends not only on the volumetric fraction of blood cells (i.e. hematocrit), but also on the behavior of those cells under shear forces (i.e. deformability, orientation, and aggregation of red blood cells).

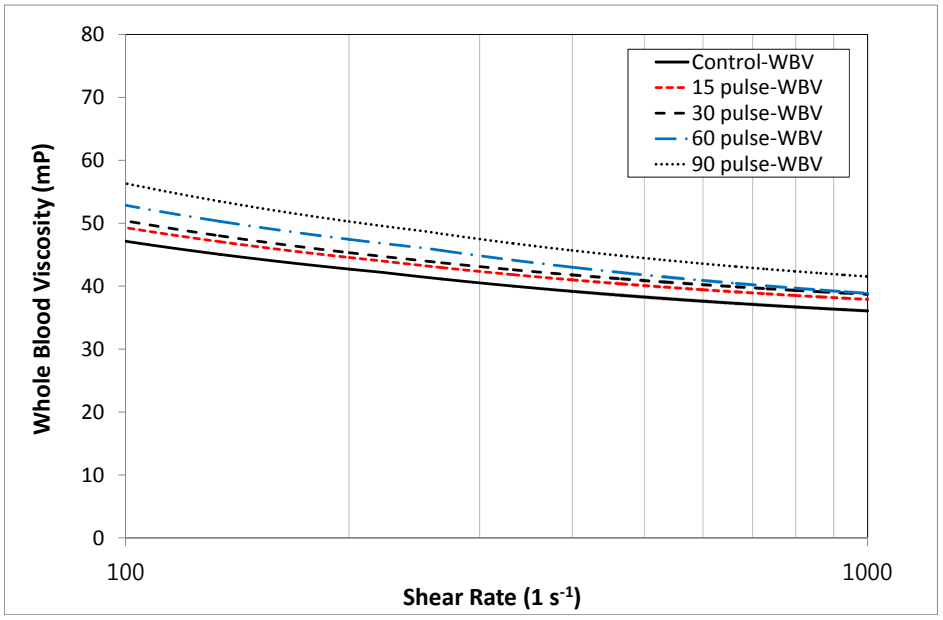

Figure 4-14. Profiles of WBVs over high shear rate ranges from 100 to 1,000 s^{-1} after blood plasma treated by corona discharge was mixed back with blood cells

At low shear rates, several studies have indicated that the erythrocyte tends to aggregate into linear arrays and form three-dimensional structures like stacks of coins, a phenomenon which is known as Rouleaux formation [134]. Because of the increased effective particle size by the erythrocyte aggregation, the disturbance of flow streamlines becomes more pronounced, and accordingly blood viscosity is significantly increased at the low shear rates. Thus RBC aggregation becomes a major determinant of blood viscosity under low shear conditions [135].

The aggregation has been known to be strongly affected by the concentration of macromolecules such as fibrinogen and low density lipoprotein (LDL) cholesterol molecules in blood plasma [18, 128, 134, 136, 137]. According to Bridging model theory, one of the widely accepted models explaining the mechanisms of RBC aggregation, the RBC aggregation occurs when a bridging macromolecule with a diameter greater than 19 nm binds to two erythrocytes, such that the distance between two erythrocytes is maintained to be about 19 nm [127, 137-140].

In case of fibrinogen, a long chain molecule with a length of approximately 47-48 nm, it adheres to the membrane surface of erythrocytes [141] and establishes a cross-linking network structure when RBCs are near at low shear conditions. For LDL cholesterol molecules, since the diameter of LDL cholesterol molecules is about 18-30 nm, they can easily bind to two adjacent erythrocytes, and form the RBC aggregation, and thus increase blood viscosity at low shear rates [137, 138]

Therefore, the phenomena that the WBV at low shear rates had been increased significantly after blood plasma was treated with pulsed corona discharge

might be explained follows: when the macromolecules are treated with a pulsed corona discharge, the discharge enhances the coagulation of macromolecules, and thus the size of macromolecules increases greater than their original size. Then, the coagulated macromolecules might bind to the erythrocyte membrane, enhancing the formation of aggregation, and thus increasing WBV particularly at low shear rates.

At high shear rates, it has been known that RBC deformation is the primary factor affecting WBV [135, 142] as the increased shear force disaggregates the Rouleaux formation. RBCs, highly specialized cells, respond to the applied forces by extensive change of their shape, with the degree of deformation under a given force, which is known as deformability. These cells behave as elastic bodies and their shape is reversible when the deforming forces are removed [135, 143]. Cytoskeleton which is a network of proteins lying just beneath the cell membrane is accepted as a major contribution to the rigidity of RBC membrane, thus the maintenance of normal mechanical behavior of RBC depends on a low cytosolic calcium level adjusted by an active ATP-dependent calcium pump under RBC membrane [135, 144]. LDL cholesterol also can decrease the erythrocyte deformability by increasing the cholesterol-to-phospholipid ratio at the erythrocyte membrane [127, 137] even though its contribution to deformability is less than that to aggregation. In addition, glucose, osmolality, and dehydration adversely affect the rigidity of erythrocyte membrane [137].

Considering the determinants of the erythrocyte deformability mentioned above, the reason of WBV increase at high shear rate ranges, as seen in Figs. 4-13

and 4-14, could be suggested as follows: the coagulated LDL by corona discharge treatment might play a significant role in the increase of WBV at higher shear rates by promoting the rigidity of erythrocytes as mentioned above. Another possibility may be suggested that the increased size of macromolecules could attribute to the increase of plasma viscosity as the concentration of macromolecules in suspension medium increases, thus causing an overall increase of WBV profiles over all shear rate ranges.

Thus, the present study hypothesized that the coagulated macromolecules by corona treatment, such as fibrinogen and LDL cholesterol, might have affected both the erythrocyte aggregation at low shear rates and the erythrocyte deformation at high shear rates, both of which might have attributed to the increase of plasma viscosity and resulted in the increase of WBV at overall shear rates. In order to verify the hypothesis, the blood plasma treated with the corona discharge was filtered using a syringe filter, and then mixed back with RBCs.

Here, a syringe filter with 200 nm in pore size was used to investigate the effect of the corona discharge on the size growth of macromolecules, of which the normal size is 47-48 nm for fibrinogen and 18-30 nm for LDL cholesterol.

Figure 4-15 shows the profiles of WBV over a shear rate range from 1 to 1,000 s^{-1} after blood plasma was treated with the corona discharge and filtered, then mixed back with blood cells. The profiles of WBV showed an overall drop after filtration, representing the improvements in hemorheological properties. As clearly seen in Fig. 4-16, the longer time the blood plasma was treated with the corona

discharge, the greater reduction of WBV was achieved after the filtration. However, the decrease in WBV was mostly observed at low shear rate ranges, for example, DBV (at shear rate 1 s^{-1}) dropped by about 30.1% (from 297.69 mP to 207.96 mP) from the baseline value, whereas the SBV (at 300 s^{-1}) showed no significant change in blood viscosity from baseline value. As shown in Fig. 4-17, at high shear rate ranges (i.e. from 100 to 1,000 s^{-1}), no increase or decrease in WBV profiles was observed.

Note that the blood plasma sample treated with 90-pulse corona discharge was not able to be completely filtered using a 200 nm-syringe filer since the coagulated particles were so large to clog the filter membrane after about 3 mL out of 10 mL-blood plasma volume had been filtered.

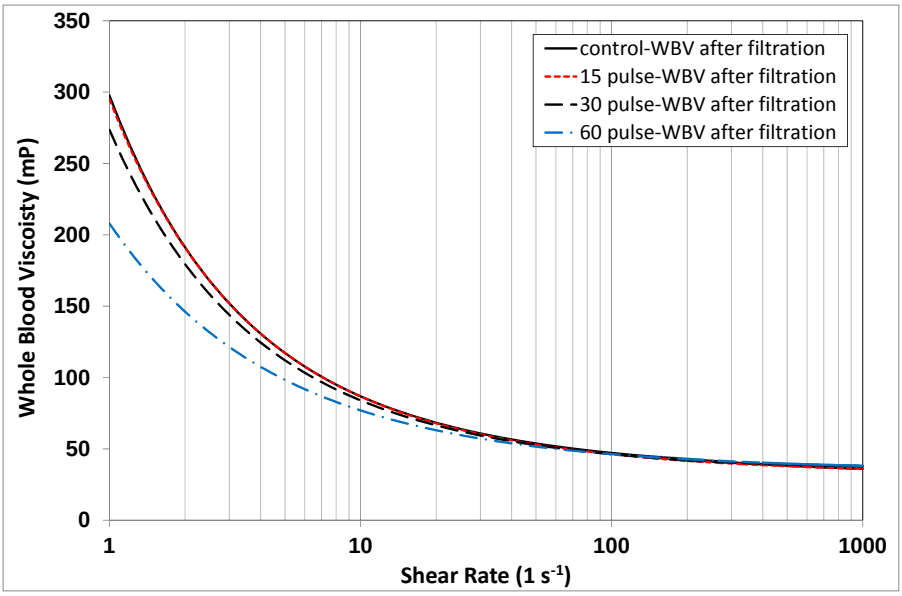

Figure 4-15. Profiles of WBV over a shear rate range from 1 to 1,000 s^{-1} after blood plasma was treated with corona discharge, filtered, and then mixed back with blood cells

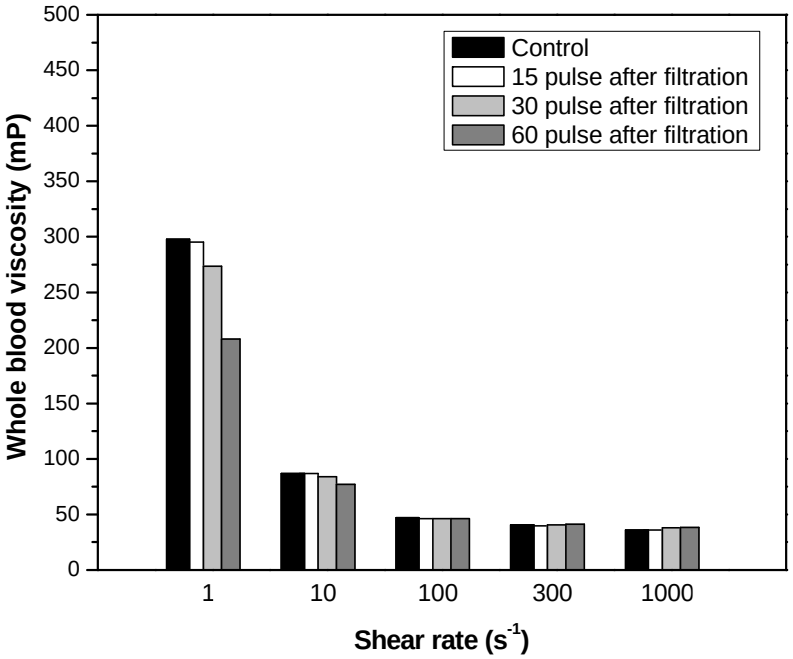

Figure 4-16. Change of WBVs for shear rates of 1, 10, 100, 300, and 1,000 s^{-1} after blood plasma was treated with corona discharge, filtered, and then mixed back with blood cells

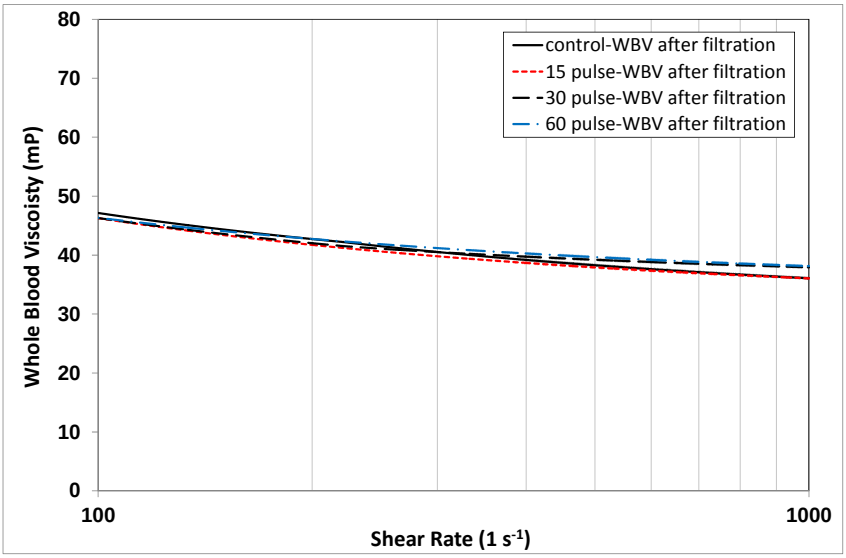

Figure 4-17. Profiles of WBVs over a high shear rate range from 100 to 1,000 s^{-1} after blood plasma was treated with corona discharge, filtered, and then mixed back with blood cells

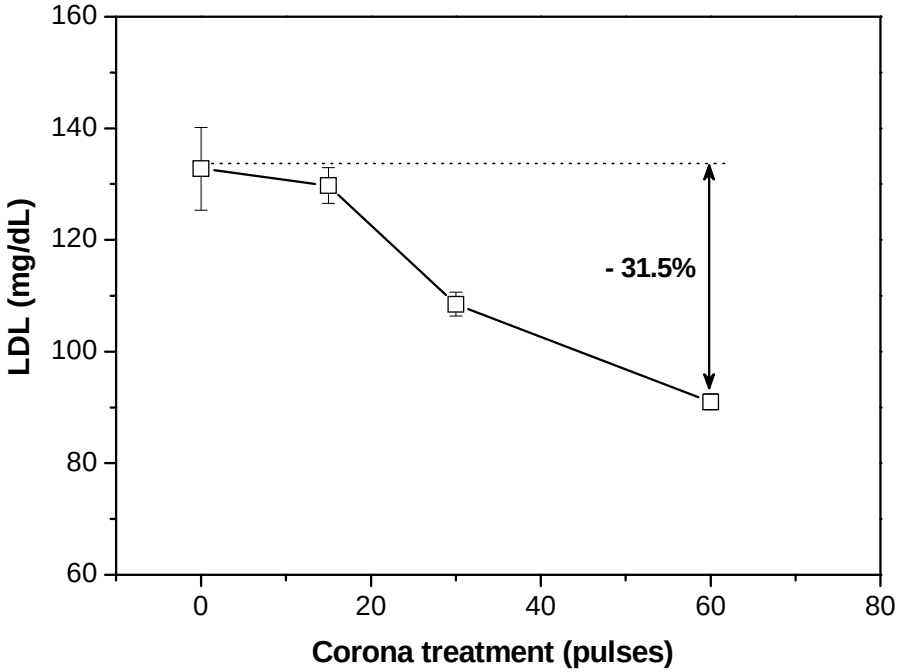

Figure 4-18. Change of LDL after filtration for 15-, 30-, and 60-pulse corona treated blood plasma

The change of LDL was also monitored during the experiment, and Fig. 4-18 shows the reduction of LDL after filtration.

After the concentration of LDL was initially measured before the centrifuge of whole blood, the centrifuged blood plasma was treated with the corona discharge for different pulses, then filtered using a syringe filter. The filtered blood plasma was mixed back with blood cells, and then LDL was measured again to investigate the effect of both corona treatment and filtration on the removal of LDL in blood.

The rate of LDL reduction became larger as the treatment time increased,

which made possible to indirectly assume that the longer blood plasma was treated with the corona discharge, the more oxidized LDL molecules greater than 200 nm in diameter existed, large enough to be filtered. For example, LDL in the corona-treated blood plasma for 60 pulses dropped by 31.5% from 132.79 to 90.00 mg/dL.

The graphs showing the effect of filtration on the change of WBV (i.e. DBV and SBV) are shown for comparison in Figs. 4-19 and 4-20, respectively. For DBV case, the linearly increased DBV with an increase of corona treatment time had a significant drop after filtration. This reduction became bigger as it was treated with a longer time. However, for SBV case, even though SBV increased as it was treated with the corona discharge, it showed almost no change in SBV after filtration.

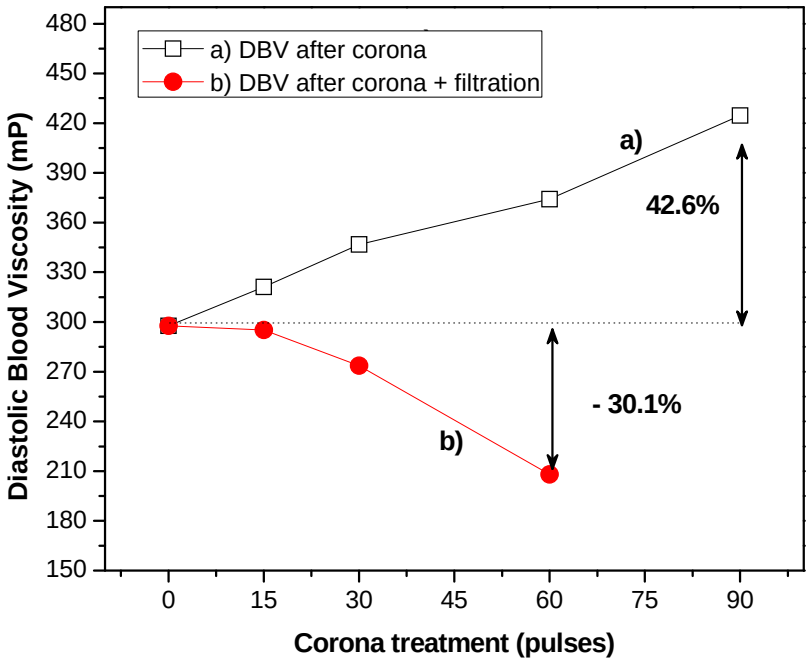

Figure 4-19. Changes of DBV at shear rate 1 s^{-1}: a) blood plasma was treated with corona discharge, then mixed back with blood cells, and b) blood plasma was treated with corona discharge, filtered, and then mixed back with blood cells

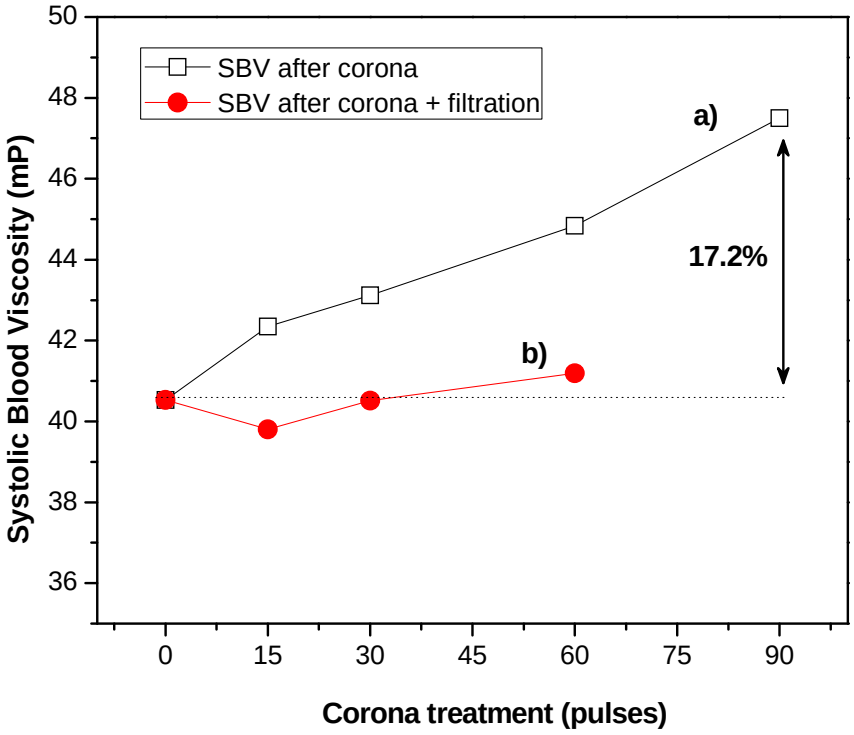

Figure 4-20. Changes of SBV at shear rate 300 s^{-1}: a) blood plasma was treated with corona discharge, then mixed back with blood cells, and b) blood plasma was treated with corona discharge, filtered, and then mixed back with blood cells

Reminding the hypotheses discussed in the previous section, for DBV, the coagulated macromolecules (i.e. fibrinogen and LDL) might enhance the erythrocyte aggregation at low shear rates due to their large diameter or length, resulting in the increase of DBV.

In the present experiment, as one removed the coagulated macromolecules

(i.e. oxidized LDL) using a filter, one could achieve a significant reduction of DBV compared to the baseline value. In other words, as the coagulated LDL molecules were removed, the erythrocyte aggregation was reduced accordingly, thus decreased the frictional resistance of blood flow in small vessels at low shear rates.

For SBV at high shear rate, one could hypothesize that the coagulated LDL molecules could affect to the erythrocyte rigidity, increasing blood viscosity at high shear rates. If the erythrocyte deformability thus had been affected by the coagulated LDL molecules, SBV should have decreased at least lower than the baseline value as the coagulated LDL had been removed by a filter. However, as shown in Fig. 4-20, even though the coagulated LDL was reduced, no significant difference was observed in SBV compared to the baseline value, a finding which explained that the above hypothesis was not appropriate for the SBV at the high shear rates.

Instead, the increase of WBV at low shear rates could be explained as follows: the coagulated macromolecules (i.e. fibrinogen and LDL) might enhance the level of plasma viscosity as the concentration of the macromolecules increases after the corona treatment. Such an increase of plasma viscosity could affect the overall fluidity of whole blood shown in Fig. 4-20 that the increased SBV after the corona treatment had returned to the baseline value after the removal of the coagulated LDL molecules by filtration.

In order to verify that the coagulated macromolecules could promote an increase of plasma viscosity, thus enhancing an overall increase of WBV, blood plasma samples were prepared and treated with the corona discharge for 90 pulses.

Plasma viscosity was measured after the corona discharge treatment was completed as well as after filtration process was completed using a syringe filter. However, instead of using a 200-nm syringe filter used in the previous experiment, a 3-µm syringe filter larger in pore size was used to avoid the clogging of a filter during filtration.

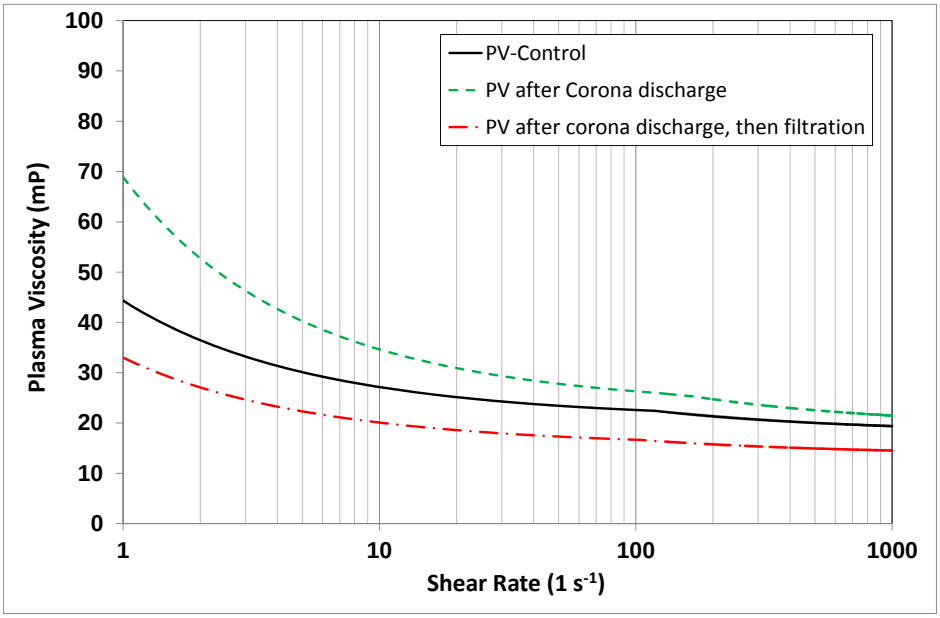

Figure 4-21. Changes of plasma viscosity for 3 cases; control, after corona discharge treatment but before filtration, after corona discharge and filtration

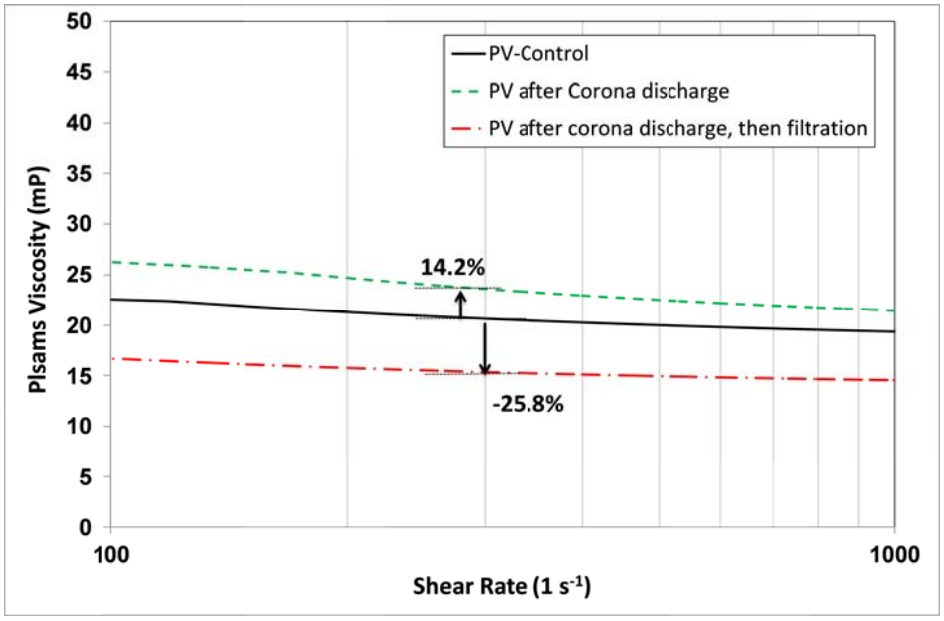

Figure 4-22. Changes of plasma viscosity for shear rates from 100 to 1,000 s^{-1} for 3 cases; control, after corona discharge treatment but before filtration, after corona discharge and filtration

Figure 4-21 shows an overall increase of blood plasma viscosity after blood plasma was treated for 90 pulses. Increased blood plasma viscosity due to the coagulated macromolecules after the corona treatment was able to be reduced below the baseline value by the subsequent filtration.

In Fig. 4-22, after blood plasma was treated with the corona discharge for 90 pulses, its viscosity increased by about 14.2 % at a shear rate of 300 s^{-1}. When the corona-treated blood plasma sample was then filtered, the result showed a significant

reduction in blood plasma viscosity by -25.8% from the baseline value.

Generally, the viscosity of blood plasma, a highly concentrated protein solution, is determined by water-content and macromolecular components [55]. The level of blood plasma viscosity increases when the protein in blood plasma has less spheroid shape, higher molecular weight, and higher concentration [55]. Thus the increase of blood plasma viscosity after the corona treatment might have been promoted by the same reasons, i.e., enhanced by the coagulation of macromolecules in blood plasma with the corona treatment.

Blood plasma is considered as a Newtonian fluid, where viscosity is independent on shear rates. Such Newtonian characteristics of blood plasma can be observed in Fig. 4-21, showing a nearly constant viscosity over shear rates from 10 s^{-1} to 1,000 s^{-1}.

However, for shear rates below 10 s^{-1}, the plasma viscosity showed non-linear behavior, rather close to the characteristics of non-Newtonian fluidity. Any fluids with suspended particles could have the yield stress. The yield stress in the blood plasma can be determined as the minimum limit of shear stress to initiate the flow of fluids [3]. It is caused by the interactive forces between suspended particles in fluid. Thus, blood plasma, a highly concentrated protein solution, might also have a yield stress due to weak but still abundant protein-to-protein interacting forces [55]. Since the interaction between proteins in blood plasma is weaker compared to the erythrocyte aggregation in whole blood, the yield stress of blood plasma can be relatively easily broken and overcome even by a small increase of shear force, in

other words, by a small increase of shear rates (i.e. over 10 s^{-1} in Fig. 4-21). Once the yield stress of blood plasma is broken, it would behave as a Newtonian fluid, showing a constant viscosity. As shown in Fig. 4-21, as the coagulated proteins by the corona discharge treatment were removed after filtration, the non-Newtonian behavior of blood plasma has clearly disappeared, showing a constant viscosity down to a shear rate of 5 s^{-1}.

The present study experimentally investigated the effect of corona discharge on the coagulation of LDL. The effect of non-thermal plasma discharge on the coagulation of fibrinogen was investigated by other researchers [108]. The plasma-treated fibrinogen exhibited a multimodal distribution of sizes, with the largest increase in size by about two orders of magnitude as compared to the control [108]. Thus, one can postulate that the coagulated fibrinogen and subsequent removal could also affect the similar improvement in WBV as the coagulated LDL did.

Thus, we can conclude, as in the DBD experiment, that both LDL and fibrinogen molecules in blood plasma might have been oxidized by the corona discharge treatment, and the oxidized macromolecules may tend to precipitate into relatively large size particles and can be removed by filtration. This requires further investigation in the coagulation mechanism of LDL and fibrinogen.

4.4 Limitations

The present study clearly demonstrated that treatments with electrical plasma

discharges (i.e., both DBD and corona discharges) followed by filtration of the coagulated particles could reduce WBV. The results indicated that the non-thermal DBD treatment might have precipitated and coagulated plasma proteins (i.e., fibrinogen) and LDL molecules in blood plasma, contributing the feasibility of the use of electrical plasma technology to improve blood viscosity. However, the potential application still remains theoretical, and several issues still need to be further investigated before the implementation of this technology in vivo.

Thus, a comprehensive study should be performed to investigate 1) the mechanism of the coagulation of proteins and LDL molecules, 2) the biological effects of active species generated by electrical plasma discharge on blood properties, 3) the change of the functional properties of blood plasma after electrical plasma treatment, and 4) the issue of preservation of vital biological properties of blood plasma. Since very few papers have been published about the effect of electrical plasma on blood, it would be an interesting subject for the future study more oriented toward biomedical field.

In addition, the catalytic effect of tungsten electrode material on blood properties also needs to be investigated for a potential application of corona discharge.

CHAPTER 5: A STANDARD VISCOSITY FLUID FOR BLOOD VISCOSITY MEASUREMENTS

5.1 Motivations and Literature Survey on a Standard Viscosity Fluid for Blood Viscosity Measurements

As previously explained in Fig. 1-2 of Chapter 1, one of the most important experimental principles of the SCTV system is that the height difference of fluids moving in two vertical riser tubes is measured using optical detectors, where CCDs are able to detect the rate of the height change as the light emitted from LEDs is blocked by blood in the riser tubes [43].

Even though this system does not require a calibration since the height difference is naturally driven not by any external mechanical forces but by the gravitational force, a standard viscosity fluid (SVF) for the present SCTV system is essential in order to validate its functionality and reliability in operation.

In addition, it is also needed to propose a SVF due to the limitation of using human blood in hemorheological experiments, such as to experimentally investigate the flow characteristics of blood in a stenosis or bifurcation of vessel models or to verify the result of a numerical simulation through in vitro experiments, etc.

A brief summary for the requirements of the SVF to be proposed is as follows:

1) It should to be opaque so that CCD-LED light sensors can detect the height difference of fluid.
2) It should properly behave as a shear-thinning non-Newtonian fluid which

changes its viscosity according to different shear rates.

3) The viscosity levels of the SVF should be controllable and reproducible when prepared with the same formula.
4) It should maintain its viscosity stable for a certain period, in other words, the degradation of the SVF should not take place over time.

As discussed previously, the reason why the blood behaves as a shear-thinning non-Newtonian fluid is due to (1) the aggregation of red blood cells as a result of complicated intermolecular interactions between macro-molecules and red blood cells when shear rate is low and (2) the dispersion of the aggregated red blood cells as the shear rate increases [1-3, 14, 145]. Thus, the blood behaves as a non-Newtonian fluid where its viscosity exhibits shear-thinning characteristics with the change of shear rates, and a proper SVF might have to replicate such characteristics of blood flow [146].

Reviewing previous studies related to SVF, the closest candidate was the development of blood analog fluid. Blood analog fluid is defined as a compound having a structure similar to that of blood, but differing from blood in respect of certain components, such as physical, chemical, or biochemical properties (cited from Wikipedia). The methods of constituting a blood analog fluid have been carried out in several previous studies [145-157], mainly, with water-soluble polymer-based materials. The purpose of using high molecular weight polymer-based materials was to simulate the complicated intermolecular interactions of macro-molecules existing

in blood plasma since the water-soluble polymer-based materials contain long chain structures. Hence, they are expected to behave as those of macro-molecules in blood even though the chemical compositions between macro-molecules and water-soluble polymer-based materials are quite different from each other.

Brookshier et al. first suggested aqueous solutions of Xanthan gum and glycerin as blood analog fluid and compared their flow behavior to that of blood in straight and athergenic-curved artery models by measuring the wall shear rate in a pulsatile flow, suggesting its applicability in replicating the behavior of a non-Newtonian fluid [147].

Thurston investigated the viscoelastic properties of an aqueous polymer solution and developed a rheological model based upon a multiple relaxation process from a generalized Maxwell model [156, 157].

Gijsen et al. utilized an aqueous Xanthan gum solution to give shear thinning and viscoelastic behavior at a Newtonian control fluid, which was a concentrated solution of Potassium Thiocyanate in water (KSCN, 71 wt%) with a viscosity of 2.9 x 103 Pa.s, and a density of 1410 kg/m^3. The effect of the non-Newtonian characteristics on the flow in a carotid bifurcation was studied using optical flow visualization methods. The non-Newtonian behavior between blood and the Xanthan gum solution with KSCN resulted in a good agreement with both shear-thinning and oscillatory-viscous behavior while different in oscillatory-elastic behavior [146].

Nguyen et al. performed the analysis of experimental flow visualization in hydraulic cardiovascular models using Diethyl Phthalate (Purum 99%, Sigma Aldrich)

with Ethanol as blood analog fluid, representing acceptable compatibility with polymethyl methacrylate (PMMA n=1.491). Interestingly, a procedure of selecting blood analog fluid from several initial fluid candidates referred from Handbooks and Material Safety Datasheets (MSDS) was described in detail in the study, considering the conditions required for flow visualization model [152].

With recent advances in MEMS technology, several studies [149, 154, 155] related to the blood flow in a micro-scale channel have recently been performed using blood analog fluid. Sousa et al. [154] investigated the extensional flow of blood analog solutions, using a polyacrylamide (125 ppm weight/weight) and Xanthan gum (500 ppm weight/weight), through microfluidic channels composed of hyperbolic and sudden contradiction or expansions. The flow pattern of the two blood analog solutions were investigated considering both the shear-thinning behavior and elastic characteristics of the fluids at microscale [154].

In a similar manner, Sribastava et al. [155] used polyethylene oxide (PEO), hydrolyzed polyacrylamide (PAM), and Xamthan gum to examine the characteristics of non-Newtonian fluid in micro-channels [155]. In addition, Hu et al. [149] utilized an aqueous Xanthan gum solution as blood analog fluid to study the effect of viscoelastic fluid on the performance of an axial blood pump model [149].

Thus, polymer-based aqueous blood analog fluids have showed a wide applicability to various experiments related to the flow of blood. Their inexpensive cost and easiness in adjusting the viscosity by simply changing the concentration of the compounds were also contributed to their popularity.

Although they properly behaved as a shear-thinning non-Newtonian fluid with the change of blood viscosity over a range of shear rates, no researches have been performed on an opaque blood analog fluid since most of the studies were conducted using a conventional rotating or capillary tube viscometer. Some studies have employed optical techniques to visualize the flow characteristics of blood analog fluids. However, transparent and laser-induced fluorescent substances were utilized in those studies [146, 147]. In addition, the polymer-based aqueous blood analog fluid could be degraded after circulation through a pump within 1-2 days due to its high molecular weight with long-chain structures (i.e, $Mw > 10^6$). Thus, such a fluid shows inadequate flow characteristics by losing their shear-thinning non-Newtonian properties, limiting its applicability. Thus, it does not satisfy the requirements of SVF, mentioned above [151, 155]. Lastly, although the aforementioned blood analog fluids showed possible applications to the experiments related to the non-Newtonian flow, no comprehensive experiments in regards to controllability and reproducibility for different viscosity levels have been performed.

Thus, the objectives of the present study were to propose a new opaque SVF to replicate the non-Newtonian behavior of blood for different shear rates, to investigate the effect of dye concentration on the viscosity change of the new opaque SVF, and to validate the experimental accuracy and repeatability for blood viscosity measurement using the SCTV.

5.2 Experimental Methods

5.2.1 Sample Preparation

In the present study, the maltose with 55% of concentration (i.e., a corn syrup: commercial name of maltose) was prepared. It is commercially produced by adding the enzymes, such as α-amylase, β-amylase, and pullulanase to a mixture of corn starch and water. The advantage of using the maltose with 55 % of concentration was that it contained a certain potion of various types of saccharide molecules with very low molecular weight, i.e. 55% maltose (a disaccharide formed with double-linked glucose), oligosaccharide (a saccharide polymer containing the links of 2-10 monosaccharide), and monosaccharide (glucose), which differed from the polymer-based aqueous blood analog fluid with high-molecular weight (up to 6 x 10^6) [155, 158].

Three different levels of SVFs having high, medium, and low viscosity were prepared to investigate the effect of the corn syrup concentration on the viscosity of the SVFs. In order to prepare SVFs, the syrup and distilled water were mixed in a beaker following the mixing formula as given in Table 5-1. The mixture was first stirred manually until there was no string-like dense syrup observable in the liquid mixture and, then, the beaker with the mixture solution was put on a magnetic stirrer (HSD-180, Mtops) for an automated stirring for 10 min.

Table 5-1. Mixing formula to prepare three different levels of SVFs having high, medium, and low viscosities

Range of viscosity	Formula		Concentration of syrup
High viscosity	Syrup	20.76g	0.5810
	Distilled water	14.97g	
	Dye	0.10g	
Medium viscosity	Syrup	22.00g	0.4889
	Distilled water	23.00g	
	Dye	0.10g	
Low viscosity	Syrup	22.00g	0.4314
	Distilled water	29.00g	
	Dye	0.10g	

The weights of the corn syrup and distilled water were precisely measured using a digital scale (CUX-420H, CAS) with a 0.001 g of resolution. Aqueous soluble food dye (Black color, McCormick) was added to the mixture of the syrup and distilled water to make the SVF opaque. Then, the SVFs were transferred into 4-mL plain vacutainers for viscosity measurements using the SCTV.

Figure 5-1. Magnetic stirrer and a 4-mL plain vacutainer used to prepare SVFs in the present study

5.2.2 Experimental Procedures

In order to investigate the effect of dye concentration on the viscosity of SVFs, high, medium, and low standard fluids at three different viscosity levels, respectively, were prepared with three different dye concentrations (i.e. 0.05g, 0.10g, and 0.15g). The effect of dye concentration less than 2% on the viscosity change of an aqueous solution was reported negligible by Kim et al. [43]. Thus, the specific purpose of the present study was to determine the minimum threshold of dye concentration below which the SCTV system could detect the mixture solution of the corn syrup and the dye as an opaque fluid.

After the completion of dye concentration study, six sets of repeatability test for the SVFs were performed using three different viscosity levels of standard fluids,

i.e., high, medium, and low viscosity fluids.

The degradation of the three different levels of opaque SVFs was also investigated over 6 months by periodically measuring the viscosity of SVFs.

In addition, the present study examined the effect of an anti-coagulant (i.e., EDTA) used in vacutainers, which is a necessary chemical for the blood of a patient to be directly collected and stored prior to WBV measurement. The three different viscosity levels of SVFs were stored in two different kinds of vacutainers, 4-mL plain vacutainer (no additives) and 4-mL EDTA vacutainer and the viscosity of SVFs were measured over 6 months.

The obtained viscosity data were averaged and the coefficient of variation was calculated to quantify the dispersion or scatter of the measured viscosities in terms of a normalized distribution.

5.3 Results and Discussion

5.3.1 Viscosity Profiles of SVFs

Figure 5-2 shows the results of three different viscosity levels of SVFs (high, medium, and low viscosities) together with normal WBV for comparison. All three curves obtained from the SVFs showed typical non-Newtonian characteristics both at high shear rates and at low shear rates. When compared to the viscosity curve produced by normal whole blood, the medium level SVFs showed an excellent agreement with the behavior of normal whole blood.

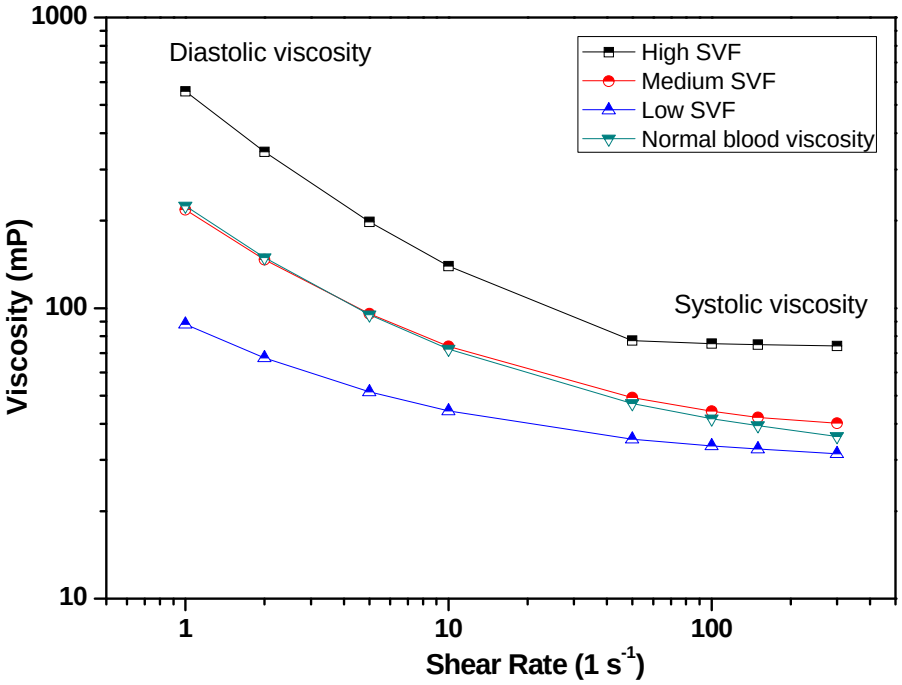

Figure 5-2. Viscosity profiles of three different levels of SVFs and normal whole blood for comparison according to the change of shear rates

Among the three viscosity curves of high, medium, and low SVFs, distinguishable differences in viscosity levels were also observed, indicating that the control of viscosity levels could be achieved by adjusting the syrup concentration on the SVFs (i.e., 0.5810, 0.4889, and 0.4314 of syrup concentration for high, medium, and low viscosities, respectively).

As seen in Table 5-2, the mean systolic viscosities measured at a shear rate of 300 s^{-1} were 74.0 mP for high SVF, 40.2 mP for medium SVF, and 31.5 mP for low SVF, respectively. The mean diastolic viscosities measured at a shear rate of 1 s^{-1}

were 557.8 mP for high SVF, 218 mP for medium SVF, and 87.9 mP for low SVF, respectively. The viscosity values cover the variations found in a clinical range of blood viscosities: high (500~600 mP), medium (200~240 mP), and low (80~100 mP) ranges.

Table 5-2. Results of viscosity measurements from three different SVFs having high, medium, and low viscosities (1cP = 10 mP)

Shear rate ($1\ s^{-1}$)	Viscosity (mP)		
	High viscosity	Medium viscosity	Low viscosity
1,000	73.1	39.3	30.3
300 (Diastolic)	74.0	40.2	31.5
150	74.8	42.0	32.7
100	75.4	44.1	33.5
50	77.3	49.2	35.4
10	139.5	73.9	44.2
5	198.0	95.6	51.4
2	344.5	147.0	67.4
1 (Systolic)	557.8	218.0	87.9

The effect of the syrup concentration on the viscosity change in SVFs is shown in Fig. 5-3. These curves could be used to produce any levels of SVFs within a range from 200 mP to 600 mP in diastolic viscosity, and from 30 mP to 80 mP in systolic viscosity.

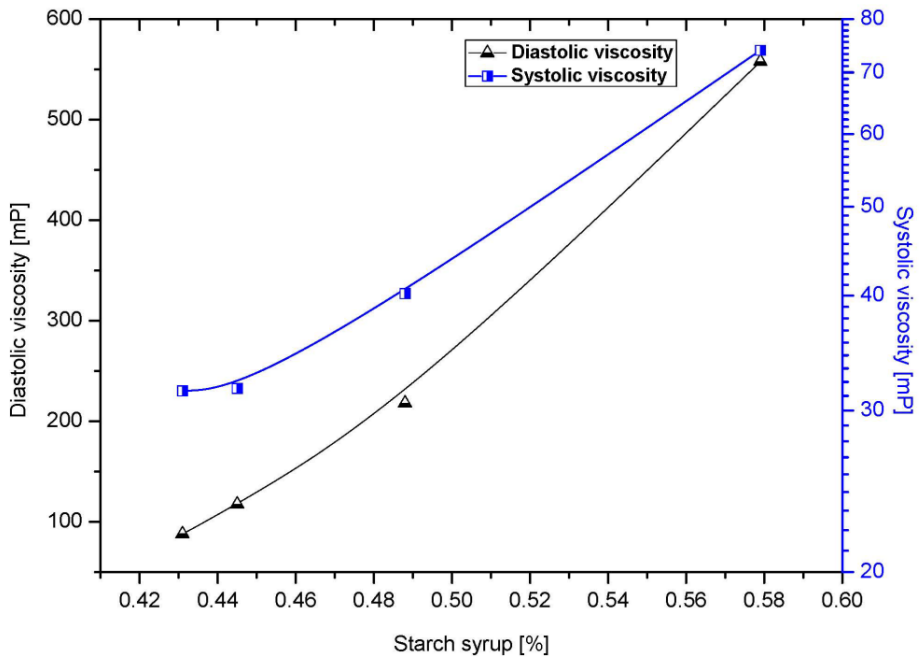

Figure 5-3. Changes of diastolic/and systolic viscosities according to the concentration of syrup used in the present study

5.3.2 Dye Concentration

Figure 5-4 shows the viscosity data obtained from high, medium, and low SVFs with three different dye concentrations (i.e. 0.05g, 0.10g, and 0.15g). The viscosity curves showed that the effect of dye concentration for 0.05g, 0.10g, and 0.15g on the change of viscosity was negligible as was reported by the previous research [43]. In addition, the minimum dye concentration detectable by the SCTV system was achieved to be as low as about 0.2 % by weight as listed in Table 5-3.

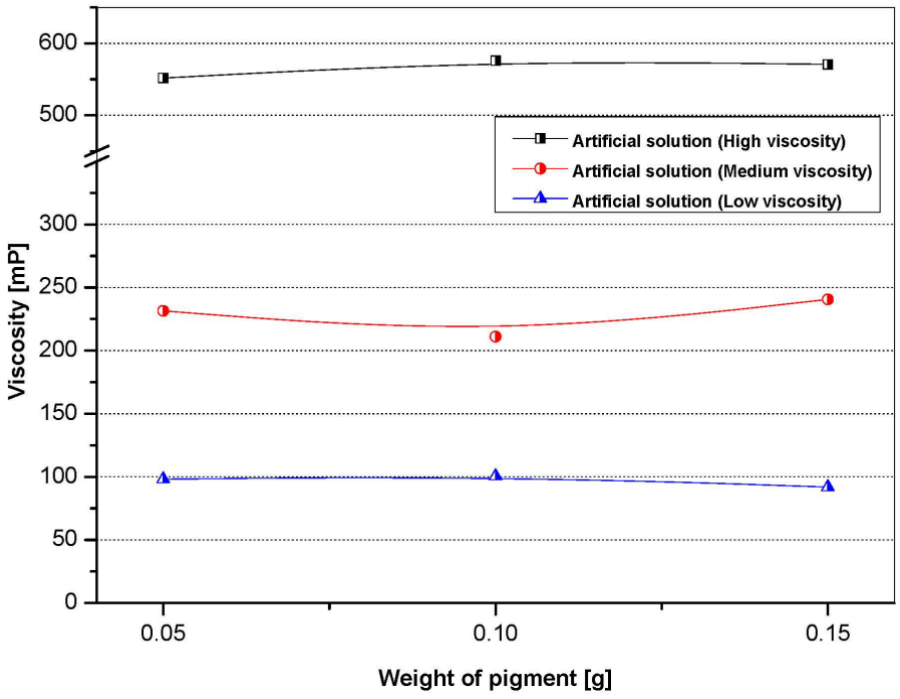

Figure 5-4. Viscosity changes of SVFs according to different dye concentrations (0.05g, 0.10g, and 0.15g)

Table 5-3. Changes of systolic/diastolic viscosities according to different dye concentrations: 0.05g, 0.10g, and 0.15g (1 cP = 10 mP)

Viscosity level	Formula	Amount of dye (g)	Concentration of dye by weight (%)	Systolic viscosity (mP)	Diastolic viscosity (mP)
High viscosity	Syrup 20.76g Distilled water 14.97g	0.05g	0.140	70.2	551.8
		0.10g	0.279	70.2	575.9
		0.15g	0.418	68.8	570.8
Medium viscosity	Syrup 22.00g Distilled water 23.00g	0.05g	0.111	40.5	231.5
		0.10g	0.222	36.4	211.1
		0.15g	0.332	39.9	240.6
Low viscosity	Syrup 22.00g Distilled water 29.00g	0.05g	0.098	30.0	98.1
		0.10g	0.196	31.7	100.5
		0.15g	0.293	31.8	91.9

5.3.3 Repeatability Test

After the effect of syrup concentration and dye concentration on the SVFs were investigated, the repeatability test for the present method in producing SVFs was performed. Two separate samples for high, medium, and low SVFs were prepared according to the same formula listed in Table 5-1, and their viscosities were measured. This procedure was repeated six times, and the results are shown in Figs.

5-5 and 5-8. As listed in Tables 5-4 to 5-6, the results showed less than 5 % of the coefficient of variations over all shear rates, a finding which could effectively validate the repeatability of the present method.

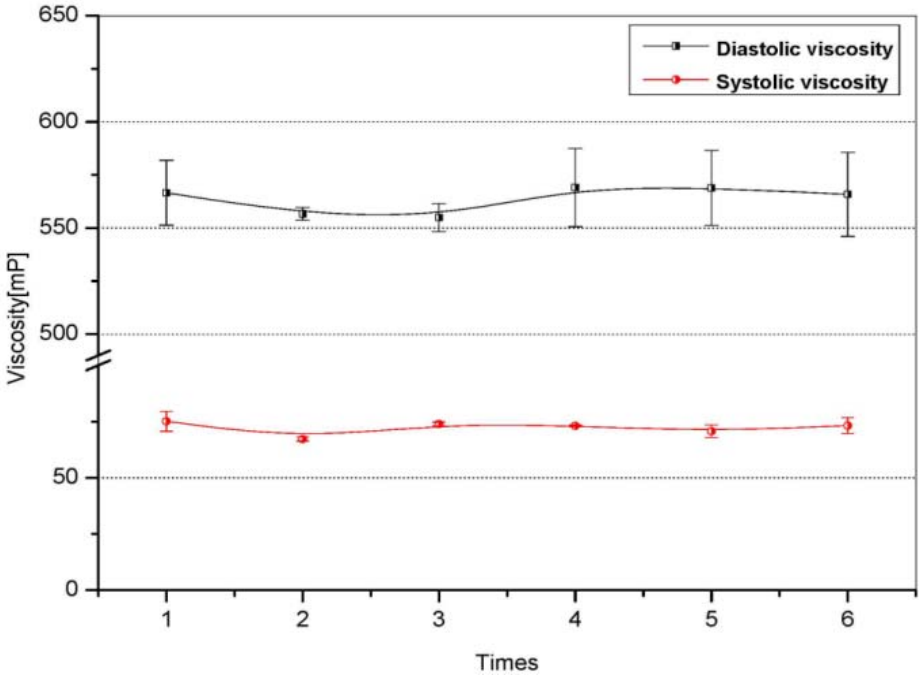

Figure 5-5. Diastolic/systolic viscosity curves obtained from the high level SVF for the validation of repeatability

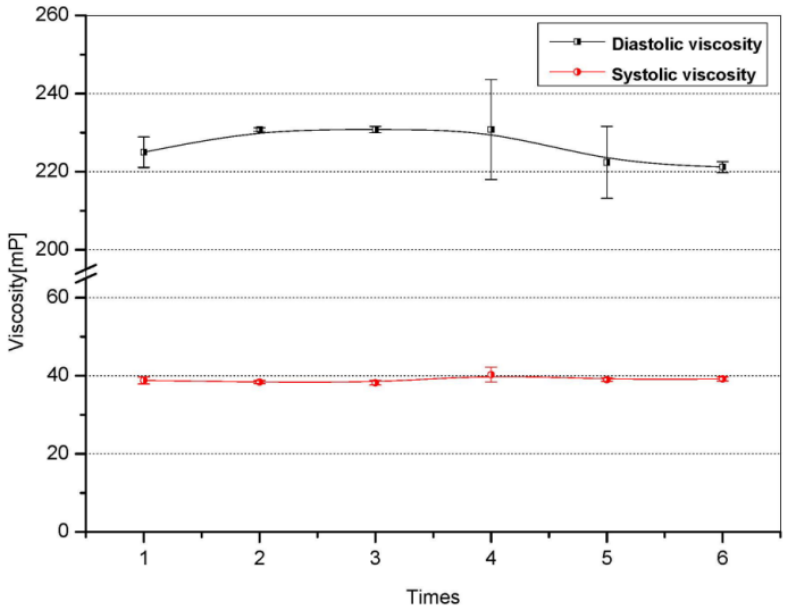

Figure 5-6. Diastolic/systolic viscosity curves obtained from the medium level SVF for the validation of repeatability

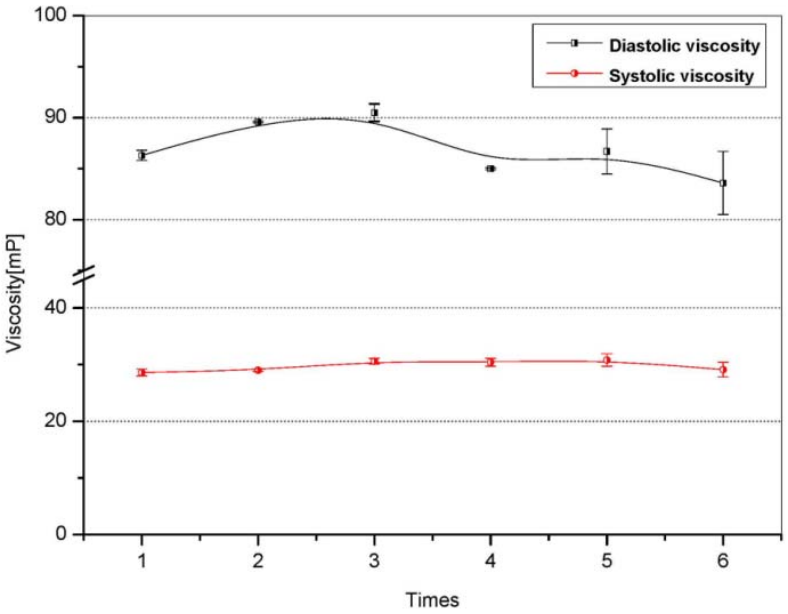

Figure 5-7. Diastolic/systolic viscosity curves obtained from the low level SVF for the validation of repeatability

Table 5-4. The obtained results from high level of SVF for the validation of repeatability (1 cP = 10 mP)

Repeated Number		Shear rate (1/s)								
		1,000	300	150	100	50	10	5	2	1
		Viscosity (mP)	Viscosity (mP)	Viscosity (mP)	Viscosity (mP)	Viscosity (mP)	Viscosity (mP)	Viscosity (mP)	Viscosity (mP)	Viscosity (mP)
1	1-1	77.5	79.6	81.6	83.1	87.1	152.3	213.1	363.9	581.9
	1-2	69.8	70.5	71.2	71.7	73.4	134.6	192.6	338.2	551.2
2	21	65.3	66.3	67.2	67.9	69.9	131.0	189.4	336.9	553.7
	2-2	66.7	68.1	69.5	70.5	73.3	135.3	194.2	342.5	559.7
3	3-1	73.5	74.7	75.8	76.6	78.9	140.2	197.7	340.7	548.3
	3-2	71.8	73.0	74.1	74.9	77.3	139.9	198.8	346.4	561.5
4	4-1	72.1	73.4	74.5	75.4	77.9	143.2	205.0	360.3	587.5
	4-2	71.9	72.7	73.4	74.0	75.7	137.1	194.9	339.7	550.7
5	5-1	72.4	73.5	74.5	75.2	77.4	142.5	204.3	359.5	586.6
	5-2	67.0	67.9	68.7	69.3	71.2	132.3	190.3	336.6	551.2
6	6-1	75.7	76.8	77.8	78.5	80.8	142.0	199.1	340.9	546.1
	6-2	68.6	69.6	70.5	71.2	73.2	137.8	199.6	355.8	585.6
Mean		71.0	72.2	73.2	74.0	76.3	139.0	198.3	346.8	563.7
±S.D.		±3.7	±3.9	±4.1	±4.3	±4.7	±5.8	±6.8	±10.2	±16.7
C.V.		0.052	0.054	0.056	0.057	0.062	0.041	0.034	0.029	0.030

Table 5-5. The obtained results from medium level of SVF for the validation of repeatability (1 cP = 10 mP)

Repeated Number		Shear rate (1/s)								
		1,000	300	150	100	50	10	5	2	1
		Viscosity (mP)	Viscosity (mP)	Viscosity (mP)	Viscosity (mP)	Viscosity (mP)	Viscosity (mP)	Viscosity (mP)	Viscosity (mP)	Viscosity (mP)
1	1-1	36.3	37.9	40.2	42.4	47.7	73.7	96.8	151.9	228.9
	1-2	39.4	39.7	41.3	43.5	48.7	73.7	95.8	148.2	221.0
2	21	37.5	38.7	40.8	43.1	48.5	74.6	97.8	153.1	230.3
	2-2	36.8	38.0	40.1	42.4	47.7	73.9	97.3	153.2	231.3
3	3-1	37.8	38.7	40.5	42.6	47.7	72.1	93.7	144.9	215.9
	3-2	36.9	37.6	39.4	41.5	46.6	71.2	93.1	145.0	217.4
4	4-1	41.7	42.1	44.0	46.4	52.0	79.2	103.3	160.7	240.5
	4-2	37.6	38.4	40.1	42.3	47.3	71.6	93.1	144.2	215.0
5	5-1	38.0	38.5	40.2	42.3	47.3	71.4	92.7	143.2	213.2
	5-2	38.2	39.4	41.5	43.8	49.2	75.4	98.7	154.2	231.6
6	6-1	37.7	38.6	40.4	42.7	47.8	73.0	95.4	148.6	222.6
	6-2	38.7	39.7	41.6	43.8	48.9	73.8	95.7	147.7	219.8
Mean		38.1	38.9	40.8	43.1	48.3	73.6	96.1	149.6	224.0
±S.D.		±1.4	±1.2	±1.2	±1.3	±1.4	±2.2	±3.0	±5.2	±8.4
C.V.		0.037	0.031	0.029	0.029	0.029	0.030	0.031	0.035	0.038

Table 5-6. The obtained results from low level of SVF for the validation of repeatability (1 cP = 10 mP)

Repeated Number		Shear rate (1/s)								
		1,000	300	150	100	50	10	5	2	1
		Viscosity (mP)	Viscosity (mP)	Viscosity (mP)	Viscosity (mP)	Viscosity (mP)	Viscosity (mP)	Viscosity (mP)	Viscosity (mP)	Viscosity (mP)
1	1-1	27.0	28.0	28.9	29.8	31.8	40.8	48.2	64.9	86.7
	1-2	28.2	29.1	30.0	30.8	32.8	41.5	48.8	64.9	85.8
2	21	27.9	29.2	30.3	31.2	33.2	42.4	50.1	67.2	89.5
	2-2	27.2	28.8	30.2	31.1	33.1	42.4	50.1	67.3	89.7
3	3-1	28.7	30.1	31.3	32.2	34.3	43.7	51.5	68.8	91.3
	3-2	29.8	31.1	32.2	33.1	35.1	44.2	51.6	68.2	89.6
4	4-1	30.0	31.1	32.1	32.9	34.8	43.2	50.1	65.4	85.1
	4-2	28.8	29.7	30.7	31.5	33.4	41.9	49.0	64.7	84.9
5	5-1	31.1	31.9	32.8	33.6	35.6	44.5	51.8	68.0	88.9
	5-2	29.0	29.7	30.3	31.1	33.0	41.6	48.6	64.3	84.5
6	6-1	27.1	27.8	28.5	29.2	31.0	39.2	46.0	61.0	80.5
	6-2	29.8	30.3	31.0	31.8	33.7	42.5	49.8	65.8	86.6
Mean		28.7	29.7	30.7	31.5	33.5	42.3	49.6	65.9	86.9
±S.D.		±1.3	±1.2	±1.3	±1.3	±1.3	±1.5	±1.7	±2.2	±3.0
C.V.		0.045	0.042	0.042	0.041	0.040	0.035	0.033	0.033	0.035

5.3.4 Degradation Test with/without EDTA

In order to investigate the degradation of the prepared SVF samples, mostly by deterioration, the SVF samples for high, medium, and low levels of viscosity were prepared according to the formula listed in Table 5-1. In addition, the effect of EDTA on the change of viscosities of the SVFs was investigated by comparing the measured viscosities stored in two different vacutainers, a plain vacutainer (with red cap) and an EDTA vacutainer (with purple cap) as shown in Figs. 5-8 and 5-9, respectively.

Figure 5-8. SVFs in plain vacutainer (right) and EDTA vacutainer (left)

Figure 5-9. Samples of SVFs for degradation test used in the present study

The SVF samples were stored at 4°C and the degradation of the SVF samples was monitored by periodically measuring the viscosities of randomly-selected samples with intervals of 7 days.

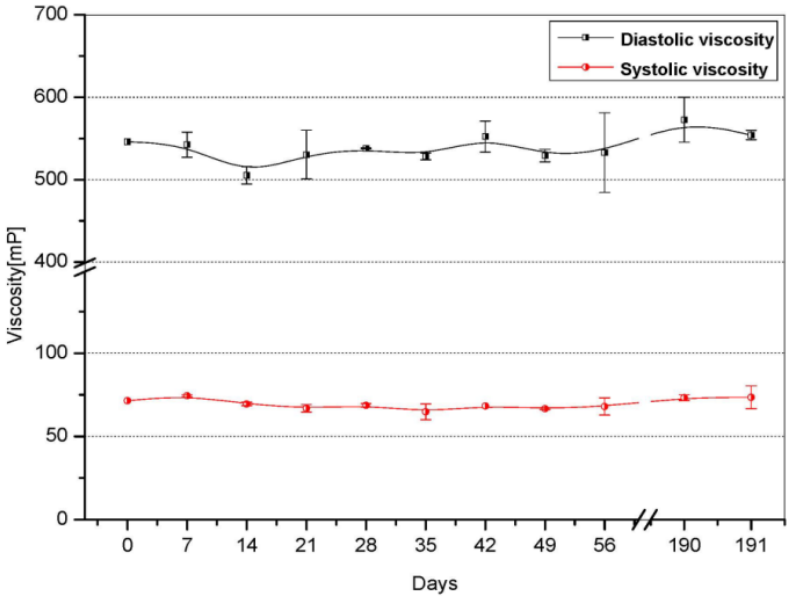

Figure 5-10. Viscosity changes of high level of SVF due to degradation for about 6 months (plain vacutainer)

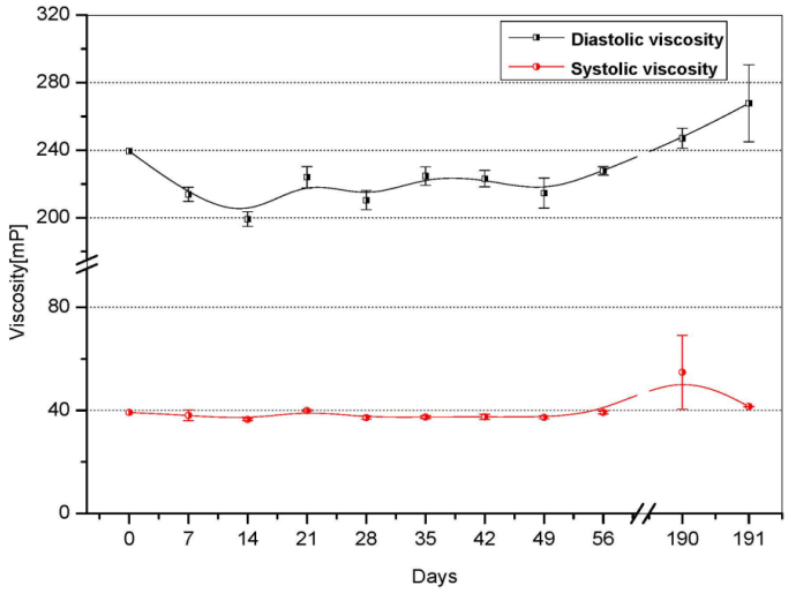

Figure 5-11. Viscosity changes of medium level of SVF due to degradation for about 6 months (plain vacutainer)

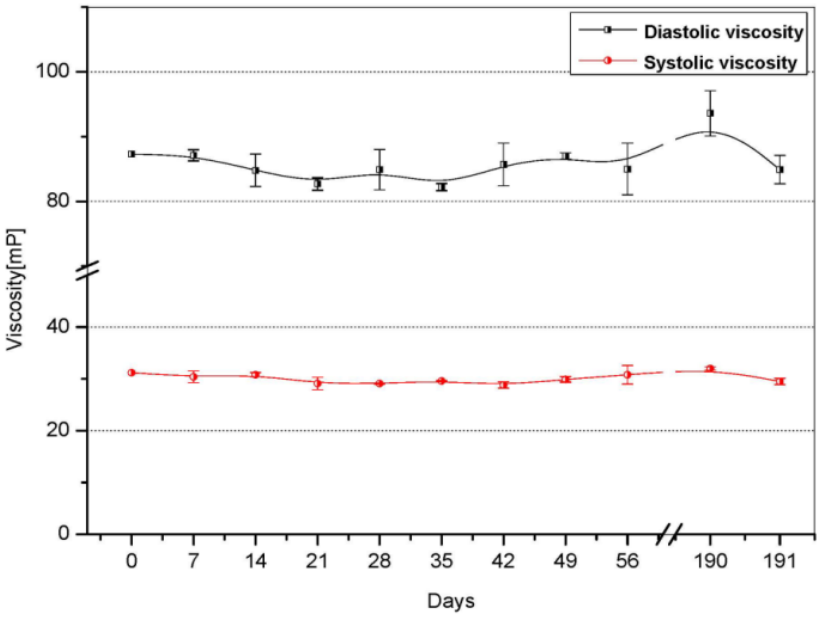

Figure 5-12. Viscosity changes of low level of SVF due to degradation for about 6 months (plain vacutainer)

Table 5-7. Viscosity changes of SVFs due to degradation for about 6 months (plain vacutainer) (1 cP = 10 mP)

Plain vacutainer						
	High viscosity (mP)		Medium viscosity (mP)		Low viscosity (mP)	
	SBV	DBV	SBV	DBV	SBV	DBV
DAY 0	71.5	546.1	39.2	239.5	31.2	87.3
DAY 7	74.9	527.2	36.0	209.7	31.5	87.9
	74.0	557.8	40.2	218.0	29.3	86.2
DAY 14	68.5	494.7	36.9	194.9	31.2	87.3
	70.4	515.8	36.0	203.4	30.3	82.3
DAY 21	69.1	559.9	40.3	217.6	27.9	83.6
	64.7	501.0	39.5	230.3	30.2	81.7
DAY 28	67.7	538.4	37.8	204.8	29.0	81.8
	69.6	537.5	36.6	216.2	29.2	87.9
DAY 35	60.1	524.1	37.9	230.2	29.6	81.6
	69.4	532.3	36.8	219.2	29.5	82.7
DAY 42	68.2	571.1	36.5	218.2	28.2	82.4
	68.3	533.4	38.5	227.9	29.3	89.0
DAY 49	67.2	521.6	37.8	223.6	30.4	86.5
	66.2	536.7	36.7	205.7	29.3	87.5
DAY 56	62.8	484.5	38.5	225.3	32.6	89.0
	73.1	581.1	39.8	230.3	29.0	81.0
…	…	…	…	…	…	…
DAY 190	71.6	545.5	69.0	241.1	32.3	90.1
	75.0	599.8	40.5	253.1	31.7	97.0
DAY 191	66.6	548.3	41.4	245.0	30.1	87.1
	80.3	559.7	41.6	290.5	28.9	82.7

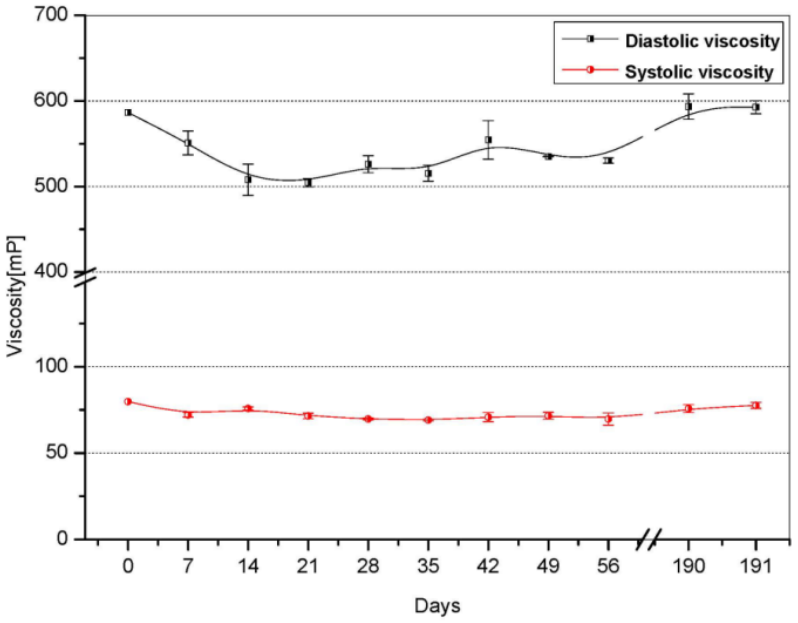

Figure 5-13. Viscosity changes of high level of SVF due to degradation for about 6 months (EDTA vacutainer)

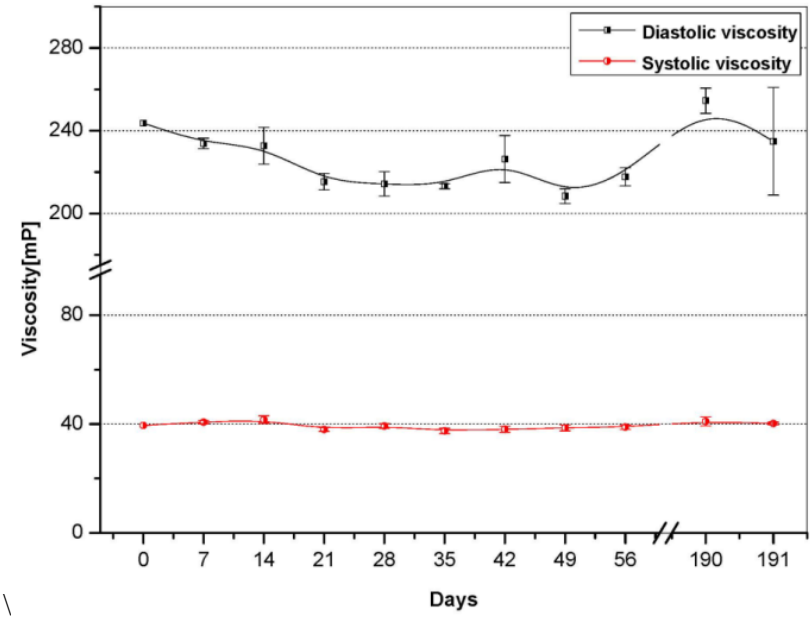

\

Figure 5-14. Viscosity changes of medium level of SVF due to degradation for about 6 months (EDTA vacutainer)

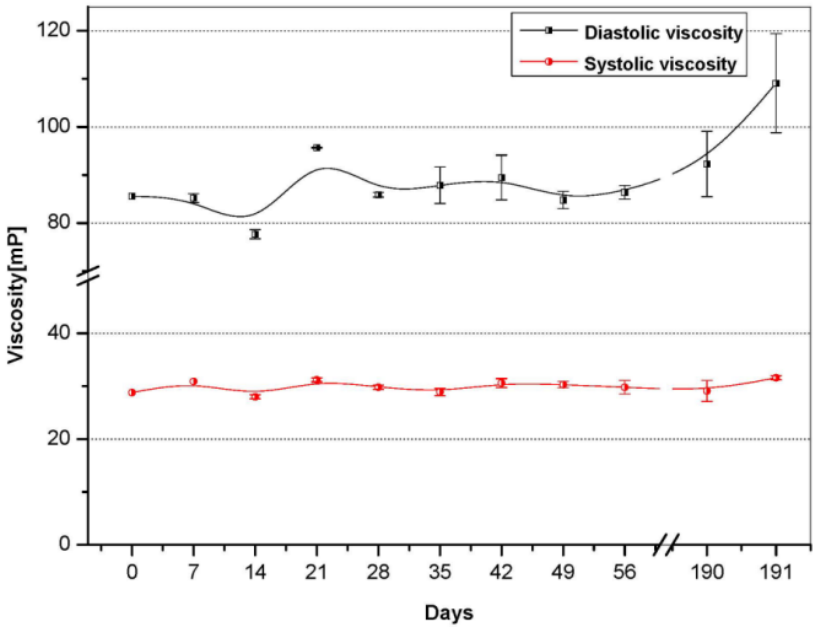

Figure 5-15. Viscosity changes of low level of SVF due to degradation for about 6 months (EDTA vacutainer)

Table 5-8. Viscosity changes of the SVFs due to degradation for about 6 months (EDTA vacutainer) (1 cP = 10 mP)

EDTA Vacutainer						
	High viscosity (mP)		Medium viscosity (mP)		Low viscosity (mP)	
	SBV	DBV	SBV	DBV	SBV	DBV
DAY 0	79.8	586.4	39.5	243.7	28.8	85.6
DAY 7	70.8	564.8	40.1	236.4	30.9	86.1
	73.3	536.9	41.3	231.4	30.9	84.3
DAY 14	76.7	489.6	42.9	241.6	27.6	78.6
	74.9	526.2	40.2	223.8	28.4	76.7
DAY 21	73.0	509.3	38.7	211.4	30.8	95.8
	69.9	499.5	37.3	219.4	31.5	95.6
DAY 28	69.1	536.0	40.0	208.3	30.2	86.4
	70.2	516.0	38.5	220.2	29.4	85.4
DAY 35	68.6	506.1	36.5	212.0	28.2	84.1
	69.5	524.8	38.4	214.4	29.6	91.6
DAY 42	68.2	577.0	37.0	214.9	29.7	84.8
	73.4	531.8	39.2	237.6	31.4	94.1
DAY 49	73.5	535.4	39.6	212.0	30.8	86.5
	69.6	534.7	37.5	204.8	29.7	83.0
DAY 56	66.2	533.3	39.6	213.3	28.5	85.0
	73.2	527.2	38.1	222.1	31.0	87.7
…	…	…	…	…	…	…
DAY 190	73.4	608.4	39.4	248.4	27.1	85.5
	78.0	578.5	42.5	260.5	31.1	99.0
DAY 191	75.9	600.3	40.6	260.8	31.2	98.8
	79.3	585.0	39.7	208.9	32.0	119.3

Figures 5-6 to 5-12 and Table 5-7 showed the results of viscosity change of the SVFs in a plain vacutainer due to degradation measured at intervals of 7 days. Based on the Figs. 5-6 and 5-12, the viscosity of the SVFs in a plain vacutainer began to show a significant change after about 56 days. The coefficient of variation over the period was less than 5% within 56 days, and after 56 days, the variation gradually increased over 5% over time.

The lower the viscosity among the high, medium, and low SVFs, the larger difference due to degradation was observed, indicating that even though the same amount of degradation had been occurred by deterioration, the low SVF might have been affected more significantly due to its low concentration of syrup.

The viscosity of SVFs between plain and EDTA vacutainers showed no significant difference when compared with Figs. 5-13 and 5-15 and Table 5-8.

5.4 Limitations

The present study showed the applicability of new opaque SVFs by dye concentration, repeatability, and degradation tests for blood viscosity measurement using the SCTV.

In degradation tests of the SVFs, it was verified that the sample showed stable viscosity over about 2 months, and after that, its non-Newtonian viscosity property was gradually altered by deterioration. Here, the mechanism of degradation was not

exactly known. Further investigation might be required in order to improve its quality and accuracy of the opaque SVFs over an extended period by preventing the degradation process.

By adopting low molecular-weight materials as used in the present study with various kinds of chain structures, the non-Newtonian viscosity behavior of blood caused by the aggregation of RBCs with intermolecular forces was able to be replicated. It would be also interesting to investigate the mechanism on how to replicate the effects of the deformability of RBCs within the SVF, a task which has not been investigated in the present study.

CHAPTER 6: CONCLUSIONS

Blood viscosity, which represents the frictional resistance between a moving blood and stationary vessel walls, was suggested as the hidden link between cardiovascular disease and the related risk factors from a biomechanical approach [159]. The present study covered the followings: 1) a new hematocrit-correction method of measured WBV profiles, 2) a new in-line method to measure hemorheological property (i.e. hematocrit), 3) the application of DBD and corona discharges to improve blood viscosity, and 4) a new SVF for blood viscosity measurement using the SCTV.

6.1 A New Hematocrit-Correction Model

A new hematocrit-correction model to correct the measured WBV at native hematocrit to a standard hematocrit of 45 % was successfully completed, resulting in less errors and deviations over a wide range of shear rates than the Matrai's model [45]. The new model does not require the measurement of plasma viscosity. The new model showed the maximum negative and positive deviations by -6.7% to 8.5 % from the measured WBV at 45 % hematocrit, which were about 4 to 6 times less than those from the Matrai's model. The applicability of the new model was also visually demonstrated by plotting the corrected WBV profiles to the measured WBV profile at 45 % hematocrit with no significant difference. Thus, it is concluded that once the yield stress and the Casson constant are obtained by either the SCTV or any other means, the corrected WBV can be accurately calculated over a wide range of shear rates using the new model without the need of the plasma viscosity.

6.2 A New On-Line Conductance Cell for Hematocrit Measurements

A new method of measuring the electric conductivity of whole blood for the purpose of hematocrit measurement was successfully validated through experimental tests. The new measurement method of the conductivity of blood produced stable and noise free data, without the usual error associated with the conventional method due to the sedimentation of erythrocytes. The conductivity of whole blood measured from the conductance cell was compared with hematocrits obtained from microcentrifuge over a wide range of hematocrits, 20-65 %. The present study demonstrated that a simple but accurate hematocrit measurement could be achieved by employing a low-frequency square-wave voltage signal in a conductance cell. The present conductivity measurement method could open a door for a possible integration of the present on-line hematocrit measurement to other blood property measuring devices such as a blood viscometer.

6.3 Plasma Discharge Treatment to Improve Hemorheological Properties

A new physical treatment method with the application of high voltage electrical plasma discharges (i.e. DBD and corona discharge) followed by filtration of the coagulated particles was validated through experimental tests in the present study. The results indicated that the plasma discharge treatment could precipitate and coagulate plasma proteins (i.e., fibrinogen) and LDL molecules in blood plasma. The

DBD treatment produced the formation of white layer on the surface of blood plasma, confirming the precipitation and coagulation of plasma proteins and lipids in blood plasma. WBV could be significantly reduced by 9.1 and 17.7 % for SBV and DBV, respectively, from the respective baseline values when DBD-treated blood plasma was filtered prior to mixing with red blood cells. When treated with the corona discharge, DBV dropped by about 30.1 % from the baseline value, whereas the SBV showed no significant change. However, the measurements of LDL molecules in the corona-treated blood plasma for 60 pulses showed a drop in the LDL concentration by 31.5 %, from 132.8 to 90.0 mg/dL after filtration.

6.4 A Standard Viscosity Fluid for Blood Viscosity Measurements

A new opaque SVF was proposed using maltose with 55 % of concentration to replicate the non-Newtonian shear-thinning behavior of blood viscosity for different shear rates. The produced viscosity profiles from three different levels of SVFs gave a good agreement with WBV profiles over a wide range of shear rates. In particular, the medium level SVF gave an excellent agreement with normal blood viscosity profile. The applicability of new opaque SVFs was demonstrated by repeatability test with coefficient of variations less than 5 % , dye concentration test, achieving the minimum detectable concentration of dye as low as about 0.2 % by weight, degradation test with coefficient of variations less than 5 % over approximately 2 months, and anti-coagulant test with no significant difference between plain and EDTA vacutainers.

In summary, the ultimate goal of a blood viscosity study is to utilize WBV as a means to promote health and save lives as the WBV can be used as a biomarker or a risk factor for the prediction, diagnosis, treatment, and prevention of various circulatory diseases.

List of References

1. Baskurt, O.K. and H.J. Meiselman. Blood rheology and hemodynamics. 2003. New York: Stratton Intercontinental Medical Book Corporation, c1974-.

2. Kensey, K.R., The mechanistic relationships between hemorheological characteristics and cardiovascular disease. Current Medical Research and Opinion®, 2003. 19(7): p. 587-596.

3. Cho, Y.I. and D.J. Cho, Hemorheology and microvascular disorders. Korean Circulation Journal, 2011. 41(6): p. 287.

4. Roger, V.L., et al., Heart Disease and Stroke Statistics—2011 Update1. Circulation, 2011. 123(4): p. e18-e209.

5. Xu, J., et al., Deaths: final data for 2007. 2010.

6. Anstey, K.J., D.M. Lipnicki, and L.F. Low, Cholesterol as a risk factor for dementia and cognitive decline: a systematic review of prospective studies with meta-analysis. American Journal of Geriatric Psych, 2008. 16(5): p. 343.

7. Banerjee, A., et al., A six year prospective study of fibrinogen and other risk factors associated with mortality in stable claudicants. Thrombosis and haemostasis, 1992. 68(3): p. 261.

8. Caen, J., et al., Fibrinogen, a vascular risk factor]. Bulletin de l'Académie nationale de médecine, 1993. 177(8): p. 1433.

9. De Simone, G., et al., Relation of blood viscosity to demographic and physiologic variables and to cardiovascular risk factors in apparently normal adults. Circulation, 1990. 81(1): p. 107-117.

10. Kenyeres, P., et al., Low hematocrit per blood viscosity ratio as a mortality risk factor in coronary heart disease. Clinical hemorheology and microcirculation, 2008. 38(1): p. 51-56.

11. Kivipelto, M., et al., Obesity and vascular risk factors at midlife and the risk of dementia and Alzheimer disease. Archives of Neurology, 2005. 62(10): p. 1556.

12. Kivipelto, M. and A. Solomon, Cholesterol as a risk factor for Alzheimer's disease–epidemiological evidence. Acta Neurologica Scandinavica, 2006. 114: p. 50-57.

13. Baskurt, O.K., et al., New guidelines for hemorheological laboratory techniques. Clinical hemorheology and microcirculation, 2009. 42(2): p. 75-97.

14. Cokelet, G. Hemorheology and Hemodynamics. 2011. Morgan & Claypool Life Sciences.

15. Cokelet, G.R., The rheology and tube flow of blood. Handbook of bioengineering, 1987: p. 14.1-14.17.

16. Merrill, E.W., Rheology of blood. Physiol Rev, 1969. 49(4): p. 863-88.

17. Ramping, M.W., The great divide: From viscometer to vasculatureLecture held during the 14th European Conference for Clinical Hemorheology and Microcirculation, Dresden, Germany. Clinical hemorheology and microcirculation, 2008. 39(1): p. 9-20.

18. Stoltz, J.F., M. Singh, and P. Riha, Hemorheology in practice. Vol. 30. 1999: Ios Pr Inc.

19. Chien, S., S. Li, and J.Y.J. Shyy, Effects of mechanical forces on signal transduction and gene expression in endothelial cells. Hypertension, 1998. 31(1): p. 162-169.

20. Davies, P.F., Flow-mediated endothelial mechanotransduction. Physiological reviews, 1995. 75(3): p. 519.

21. Gimbrone, M.A., Vascular endothelium: an integrator of pathophysiologic stimuli in atherosclerosis. The American journal of cardiology, 1995. 75(6): p. 67B-70B.

22. Ishida, T., et al., Fluid Shear Stress-Mediated Signal Transduction: How Do Endothelial Cells Transduce Mechanical Force into Biological Responses? Annals of the New York Academy of Sciences, 1997. 811(1): p. 12-24.

23. Malek, A.M., S.L. Alper, and S. Izumo, Hemodynamic shear stress and its role in atherosclerosis. JAMA: the journal of the American Medical Association, 1999. 282(21): p. 2035.

24. Malek, A.M. and S. Izumo, Control of endothelial cell gene expression by flow. Journal of biomechanics, 1995. 28(12): p. 1515-1528.

25. Traub, O. and B.C. Berk, Laminar shear stress: mechanisms by which endothelial cells transduce an atheroprotective force. Arteriosclerosis, thrombosis, and vascular biology, 1998. 18(5): p. 677-685.

26. Devereux, R.B., et al., Possible role of increased blood viscosity in the hemodynamics of systemic hypertension. American Journal of Cardiology, 2000. 85(10): p. 1265-1267.

27. Frangos, S.G., V. Gahtan, and B. Sumpio, Localization of atherosclerosis: role of hemodynamics. Archives of Surgery, 1999. 134(10): p. 1142.

28. Merrill, E.W., et al., Non-Newtonian Rheology of Human Blood-Effect of Fibrinogen Deduced by" Subtraction". Circulation Research, 1963. 13(1): p. 48-55.

29. Merrill, E., et al., Rheology of Human Blood, near and at Zero Flow:: Effects of Temperature and Hematocrit Level. Biophysical Journal, 1963. 3(3): p. 199-213.

30. Devereux, R.B., et al., Whole blood viscosity as a determinant of cardiac hypertrophy in systemic hypertension. The American journal of cardiology, 1984. 54(6): p. 592-595.

31. Letcher, R.L., et al., Direct relationship between blood pressure and blood viscosity in normal and hypertensive subjects:: Role of fibrinogen and concentration. The American journal of medicine, 1981. 70(6): p. 1195-1202.

32. Tarazi, R.C., et al., Hypertension and high hematocrit:: Another clue to renal arterial disease. The American journal of cardiology, 1966. 18(6): p. 855-858.

33. Lowe, G., et al., Blood viscosity, fibrinogen, and activation of coagulation and leukocytes in peripheral arterial disease and the normal population in the Edinburgh Artery Study. Circulation, 1993. 87(6): p. 1915-1920.

34. Danesh, J., et al., Haematocrit, viscosity, erythrocyte sedimentation rate: meta-analyses of prospective studies of coronary heart disease. European Heart Journal, 2000. 21(7): p. 515-520.

35. Lowe, G., et al., Relation between extent of coronary artery disease and blood viscosity. British medical journal, 1980. 280(6215): p. 673-674.

36. Most, A., N. Ruocco Jr, and H. Gewirtz, Effect of a reduction in blood viscosity on maximal myocardial oxygen delivery distal to a moderate coronary stenosis. Circulation, 1986. 74(5): p. 1085.

37. Simpson, L., Blood viscosity factors-the missing dimension in modern medicine. The Mumford Institute, Highlands, New Jersey, 2008.

38. Walburn, F.J. and D.J. Schneck, A constitutive equation for whole human blood. Biorheology, 1976. 13(3): p. 201.

39. Rosencranz, R. and S.A. Bogen, Clinical laboratory measurement of serum, plasma, and blood viscosity. American Journal of Clinical Pathology. Pathology Patterns Reviews., 2006. 125(Suppl 1): p. S78.

40. Kim, S., et al., A new method for blood viscosity measurement. Journal of non-newtonian fluid mechanics, 2000. 94(1): p. 47-56.

41. Kim, S., et al., A method of isolating surface tension and yield stress effects in a U-shaped scanning capillary-tube viscometer using a Casson model. Journal

of non-newtonian fluid mechanics, 2002. 103(2-3): p. 205-219.

42. Kim, S., et al., A scanning dual-capillary-tube viscometer. Review of Scientific Instruments, 2000. 71: p. 3188.

43. Kim, S. and Y.I. Cho, The effect of dye concentration on the viscosity of water in a scanning capillary-tube viscometer. Journal of non-newtonian fluid mechanics, 2003. 111(1): p. 63-68.

44. Kim, S., et al., Determination of rheological properties of whole blood with a scanning capillary-tube rheometer using constitutive models. Journal of mechanical science and technology, 2009. 23(6): p. 1718-1726.

45. Matrai, A., R. Whittington, and E. Ernst, A simple method of estimating whole blood viscosity at standardized hematocrit. Clin Hemorheol, 1987. 7: p. 261-265.

46. Box, F., et al., The influence of flow, vessel diameter, and non-newtonian blood viscosity on the wall shear stress in a carotid bifurcation model for unsteady flow. Investigative radiology, 2005. 40(5): p. 277.

47. Lee, B.K., et al., Hemorheological abnormalities in stable angina and acute coronary syndromes. Clinical hemorheology and microcirculation, 2008. 39(1): p. 43-51.

48. Lee, A.J., et al., Blood viscosity and elevated carotid intima-media thickness in men and women: the Edinburgh Artery Study. Circulation, 1998. 97(15): p. 1467.

49. Freyburger, G., et al., Rheological properties of commonly used plasma substitutes during preoperative normovolaemic acute haemodilution. British journal of anaesthesia, 1996. 76(4): p. 519-525.

50. Lee, B.K., et al., Microcirculatory dysfunction in cardiac syndrome X: role of abnormal blood rheology. Microcirculation, 2008. 15(5): p. 451-459.

51. Vlastosa, G.A., C.C. Tangneyb, and R.S. Rosensonc, Effects of hydration on blood rheology. Clinical hemorheology and microcirculation, 2003. 28: p. 41-49.

52. Michalska-Malecka, K., et al., Correlations in some pathogenetic factors and values of hemorheological parameters in age-related macular degeneration. Clinical hemorheology and microcirculation, 2008. 38(3): p. 209-216.

53. Walawender, W., T. Chen, and D. Cala, An approximate Casson fluid model for tube flow of blood. Biorheology, 1975. 12(2): p. 111.

54. Zydney, A., J. Oliver III, and C. Colton, A constitutive equation for the viscosity of stored red cell suspensions: Effect of hematocrit, shear rate, and

suspending phase. Journal of Rheology, 1991. 35: p. 1639.

55. Késmárky, G., et al., Plasma viscosity: a forgotten variable. Clinical hemorheology and microcirculation, 2008. 39(1): p. 243-246.

56. Cha, K., E.F. Brown, and D.W. Wilmore, A new bioelectrical impedance method for measurement of the erythrocyte sedimentation rate. Physiological Measurement, 1994. 15: p. 499-508.

57. Cha, K., et al., An electronic method for rapid measurement of haematocrit in blood samples. Physiological Measurement, 1994. 15: p. 129-137.

58. Carallo, C. and A. Pujia, Whole blood viscosity and haematocrit are associated with internal carotid atherosclerosis in men. Coronary artery disease, 1998. 9(2-3): p. 113-117.

59. Rim, S.J., et al., Decrease in coronary blood flow reserve during hyperlipidemia is secondary to an increase in blood viscosity. Circulation, 2001. 104(22): p. 2704-2709.

60. Oshima, S. and Y. Sankai, Improvement of the accuracy in the optical hematocrit measurement by optimizing mean optical path length. Artificial Organs, 2009. 33(9): p. 749-756.

61. Foley, R.N., et al., The impact of anemia on cardiomyopathy, morbidity, and mortality in end-stage renal disease* 1. American journal of kidney diseases, 1996. 28(1): p. 53-61.

62. Ritz, E., et al., Cardiovascular mortality of patients with polycystic kidney disease on dialysis: is there a lesson to learn? Nephron, 1994. 66(2): p. 125-128.

63. Shirakura, T., K. Kubota, and K. Tamura, Blood viscosity and cerebral blood flow in aged. Nippon Ronen Igakkai Zasshi, 1993. 30(3): p. 174-181.

64. Hirsch, F.G., et al., The electrical conductivity of blood : I. Relationship to erythrocyte concentration. Blood, 1950. 5(11): p. 1017-1035.

65. Gram, H., Cell volume and electrical conductivity of blood. Journal of Biological Chemistry, 1924. 59(1): p. 33-40.

66. Velick, S. and M. Gorin, The electrical conductance of suspensions of ellipsoids and its relation to the study of avian erythrocytes. The Journal of General Physiology, 1940. 23(6): p. 753-771.

67. Hebert, L.E., et al., Alzheimer disease in the US population: prevalence estimates using the 2000 census. Archives of Neurology, 2003. 60(8): p. 1119.

68. Horne, R., Theory of electrical conductance in acidic, aqueous solutions,

1964, Little (Arthur D) Inc Cambridge MA. p. 1-17.

69. Steinfelder-Visscher, J., et al., Conductivity-based hematocrit measurement during cardiopulmonary bypass. Journal of clinical monitoring and computing, 2007. 21(1): p. 7-12.

70. Bull, H.B. and K. Breese, Electrical conductance of protein solutions. Journal of Colloid and Interface Science, 1969. 29(3): p. 492-495.

71. Ohshima, H., Electrical conductivity of a concentrated suspension of soft particles. Journal of Colloid and Interface Science, 2000. 229(1): p. 307-309.

72. Zhao, T.X., Electrical impedance and haematocrit of human blood with various anticoagulants. Physiological Measurement, 1993. 14: p. 299-307.

73. Ludt, H. and H. Herrmann, In vitro measurement of tissue impedance over a wide frequency range. Radiation and Environmental Biophysics, 1973. 10(4): p. 337-345.

74. Jaspard, F. and M. Nadi, Dielectric properties of blood. Physiological Measurement, 2002. 23: p. 547-554.

75. Okada, R. and H. Schwan, An electrical method to determine hematocrits. Medical Electronics, IRE Transactions on, 1960(3): p. 188-192.

76. Wu, J. and J. Stark, A high accuracy technique to measure the electrical conductivity of liquids using small test samples. Journal of Applied Physics, 2007. 101(054520): p. 1-7.

77. Fricke, H., A mathematical treatment of the electric conductivity and capacity of disperse systems I. The electric conductivity of a suspension of homogeneous spheroids. Physical Review, 1924. 24(5): p. 575-587.

78. Trutman, E.D. and R.S. Newbower, A practical analysis of the electrical conductivity of blood. Biomedical Engineering, IEEE Transactions on, 1983(3): p. 141-154.

79. Landolfi, R., et al., Polycythemia vera. Internal and emergency medicine, 2010. 5(5): p. 375-384.

80. Kwaan, H.C. and J. Wang. Hyperviscosity in polycythemia vera and other red cell abnormalities. 2003. New York: Stratton Intercontinental Medical Book Corporation, c1974-.

81. Hall, J.E., Pocket Companion to Guyton & Hall Textbook of Medical Physiology E-Book, 2011, A Saunders Title.

82. Burch, G.E. and N.P. DePasquale, The hematocrit in patients with myocardial infarction. JAMA: the journal of the American Medical Association, 1962.

180(1): p. 63.

83. Cokelet, G.R., Experimental determination of the average hematocrit of blood flowing in a vessel. Microvascular research, 1974. 7(3): p. 382.

84. Jan, K.M. and S. Chien, Effect of hematocrit variations on coronary hemodynamics and oxygen utilization. American Journal of Physiology-Heart and Circulatory Physiology, 1977. 233(1): p. H106-H113.

85. Munoz, D.R. and S.C. Berga, An analog electronic interface to measure electrical conductivity in liquids. Measurement, 2005. 38(3): p. 181-187.

86. Zhang, J., P.C. Johnson, and A.S. Popel, Effects of erythrocyte deformability and aggregation on the cell free layer and apparent viscosity of microscopic blood flows. Microvascular research, 2009. 77(3): p. 265-272.

87. Dellimore, J. and R. Gosling, Change in blood conductivity with flow rate. Medical and Biological Engineering and Computing, 1975. 13(6): p. 904-913.

88. Hoetink, A., et al., On the flow dependency of the electrical conductivity of blood. Biomedical Engineering, IEEE Transactions on, 2004. 51(7): p. 1251-1261.

89. Geddes, L. and C. Sadler, The specific resistance of blood at body temperature. Medical and Biological Engineering and Computing, 1973. 11(3): p. 336-339.

90. Hill, D. and F. Thompson, The effect of haematocrit on the resistivity of human blood at 37 C and 100 kHz. Medical and Biological Engineering and Computing, 1975. 13(2): p. 182-186.

91. Wen, Z., et al., A study of RBC aggregation-sedimentation phenomenon with conductivity method. Science in China. Series B, Chemistry, life sciences & earth sciences, 1992. 35(8): p. 950-958.

92. Baskurt, O.K. and H.J. Meiselman, Hemodynamic effects of red blood cell aggregation. Indian journal of experimental biology, 2007. 45(1): p. 25.

93. Bandello, F., et al., Hypercoagulability and high lipoprotein (a) levels in patients with central retinal vein occlusion. Thrombosis and haemostasis, 1994. 72(1): p. 39.

94. Chien, S., et al., Blood viscosity: influence of erythrocyte aggregation. Science, 1967. 157(3790): p. 829.

95. Pasternak, R.C., et al., ACC/AHA/NHLBI clinical advisory on the use and safety of statins. Circulation, 2002. 106(8): p. 1024-1028.

96. Amarenco, P., et al., Stroke Prevention by Aggressive Reduction in

Cholesterol Levels (SPARCL) Investigators. High-dose atorvastatin after stroke or transient ischemic attack. N Engl J Med, 2006. 355(6): p. 549-559.

97. FERRARESE, C., High-Dose Atorvastatin after Stroke or Transient Ischemic Attack. New England Journal of Medicine, The, 2006.

98. Davignon, J., Advances in lipid-lowering therapy in atherosclerosis. Diabetes and Cardiovascular Disease, 2001: p. 49-58.

99. LaRosa, J.C., J. He, and S. Vupputuri, Effect of statins on risk of coronary disease. JAMA: the journal of the American Medical Association, 1999. 282(24): p. 2340-2346.

100. Baigent, C., et al., Cholesterol Treatment Trialists'(CTT) Collaborators. Efficacy and safety of cholesterol-lowering treatment: prospective meta-analysis of data from 90,056 participants in 14 randomised trials of statins. Lancet, 2005. 366(9493): p. 1267-78.

101. Collins, R., et al., Effects of cholesterol-lowering with simvastatin on stroke and other major vascular events in 20536 people with cerebrovascular disease or other high-risk conditions. Lancet, 2004. 363(9411): p. 757.

102. Kearney, P., et al., Efficacy of cholesterol-lowering therapy in 18,686 people with diabetes in 14 randomised trials of statins: a meta-analysis. Lancet, 2008. 371(9607): p. 117.

103. Pasternak, R.C., et al., ACC/AHA/NHLBI clinical advisory on the use and safety of statins. Circulation, 2002. 106(8): p. 1024.

104. Banyai, S., et al., Atorvastatin improves blood rheology in patients with familial hypercholesterolemia (FH) on long-term LDL apheresis treatment. Atherosclerosis, 2001. 159(2): p. 513-519.

105. Antons, K.A., et al., Clinical perspectives of statin-induced rhabdomyolysis. The American journal of medicine, 2006. 119(5): p. 400-409.

106. Kiortsis, D., et al., Statin-associated adverse effects beyond muscle and liver toxicity. Atherosclerosis, 2007. 195(1): p. 7-16.

107. Cohen, D.E., F.A. Anania, and N. Chalasani, An assessment of statin safety by hepatologists. The American journal of cardiology, 2006. 97(8): p. S77-S81.

108. Kalghatgi, S.U., et al., Mechanism of blood coagulation by nonthermal atmospheric pressure dielectric barrier discharge plasma. Plasma Science, IEEE Transactions on, 2007. 35(5): p. 1559-1566.

109. Fridman, G., et al., Comparison of Direct and Indirect Effects of Non Thermal Atmospheric Pressure Plasma on Bacteria. Plasma Processes and

Polymers, 2007. 4(4): p. 370-375.

110. Stoffels, E., I. Kieft, and R. Sladek, Superficial treatment of mammalian cells using plasma needle. Journal of Physics D: Applied Physics, 2003. 36: p. 2908.

111. Stoffels, E., R. Sladek, and I. Kieft, Gas plasma effects on living cells. Physica Scripta, 2004. 2004: p. 79.

112. Fridman, G., et al., Blood coagulation and living tissue sterilization by floating-electrode dielectric barrier discharge in air. Plasma Chemistry and Plasma Processing, 2006. 26(4): p. 425-442.

113. Fridman, G., et al., Applied plasma medicine. Plasma Processes and Polymers, 2008. 5(6): p. 503-533.

114. Chirokov, A., A. Gutsol, and A. Fridman, Atmospheric pressure plasma of dielectric barrier discharges. Pure and applied chemistry, 2005. 77(2): p. 487-495.

115. Kalghatgi, S.U., et al. Non-thermal dielectric barrier discharge plasma treatment of endothelial cells. 2008. IEEE.

116. Dobrynin, D., et al., Physical and biological mechanisms of direct plasma interaction with living tissue. New Journal of Physics, 2009. 11: p. 115020.

117. Ayan, H., et al., Heating effect of dielectric barrier discharges for direct medical treatment. Plasma Science, IEEE Transactions on, 2009. 37(1): p. 113-120.

118. Hall, C.E. and H.S. Slayter, The fibrinogen molecule: its size, shape, and mode of polymerization. The Journal of biophysical and biochemical cytology, 1959. 5(1): p. 11-27.

119. Mora, S., et al., LDL particle subclasses, LDL particle size, and carotid atherosclerosis in the Multi-Ethnic Study of Atherosclerosis (MESA). Atherosclerosis, 2007. 192(1): p. 211-217.

120. El Harchaoui, K., et al., Value of low-density lipoprotein particle number and size as predictors of coronary artery disease in apparently healthy men and women: the EPIC-Norfolk Prospective Population Study. Journal of the American College of Cardiology, 2007. 49(5): p. 547-553.

121. Jidenko, N., E. Bourgeois, and J.-P. Borra, Temperature profiles in filamentary dielectric barrier discharges at atmospheric pressure. Journal of Physics D: Applied Physics, 2010. 43(29): p. 295203.

122. Nozaki, T., et al., Energy distribution and heat transfer mechanisms in atmospheric pressure non-equilibrium plasmas. Journal of Physics D: Applied

Physics, 2001. 34: p. 3383-3390.

123. Bray, J.J., Lecture notes on human physiology. 2nd ed1999: Wiley-Blackwell.

124. Oehmigen, K., et al., The role of acidification for antimicrobial activity of atmospheric pressure plasma in liquids. Plasma Processes and Polymers, 2010. 7(3-4): p. 250-257.

125. Epstein, F.H., et al., The pathogenesis of coronary artery disease and the acute coronary syndromes. New England Journal of Medicine, 1992. 326(4): p. 242-250.

126. Libby, P., P.M. Ridker, and A. Maseri, Inflammation and atherosclerosis. Circulation, 2002. 105(9): p. 1135-1143.

127. Sloop, G. and D. Garber, The effects of low-density lipoprotein and high-density lipoprotein on blood viscosity correlate with their association with risk of atherosclerosis in humans. Clinical science, 1997. 92(5): p. 473-479.

128. Sloop, G. and D. Mercante, Opposite effects of low-density and high-density lipoprotein on blood viscosity in fasting subjects. CLINICAL HEMORHEOLOGY AND MICROCIRULATION, 1998. 19: p. 197-204.

129. Slyper, A., et al., The influence of lipoproteins on whole-blood viscosity at multiple shear rates. Metabolism, 2005. 54(6): p. 764-768.

130. Moriarty, P.M., et al., Effect of low-density lipoprotein cholesterol apheresis on blood viscosity. The American journal of cardiology, 2004. 93(8): p. 1044-1046.

131. Yang, Y., Plasma Discharge in Water and Its Application for Industrial Cooling Water Treatment, 2012, DREXEL UNIVERSITY.

132. Lukes, P., et al., Ultraviolet radiation from the pulsed corona discharge in water. Plasma Sources Science and Technology, 2008. 17: p. 024012.

133. Šunka, P., Pulse electrical discharges in water and their applications. Physics of plasmas, 2001. 8: p. 2587.

134. Rampling, M., Red cell aggregation and yield stress. Clinical blood rheology, 1988. 1: p. 45-64.

135. Baskurt, O.K. and H.J. Meiselman, Cellular determinants of low-shear blood viscosity. Biorheology, 1997. 34(3): p. 235.

136. Meiselman, H., Red blood cell role in RBC aggregation: 1963-1993 and beyond. Clinical hemorheology, 1993. 13(5): p. 575-592.

137. Jung, J.M., et al., Determination of hematocrit using on-line conductance cell.

International Journal of Heat and Mass Transfer, 2011.

138. Bachorik, P.S., et al., Lipids and dyslipoproteinemia. Clinical Diagnosis and Management by Laboratory Methods. 20th ed. Philadelphia: WB Saunders, 2001: p. 224-245.

139. Brooks, D., R. Greig, and J. Janzen, Mechanisms of erythrocyte aggregation. Erythrocyte Mechanics and Blood Flow, 1980. 140.

140. Kobuchi, Y., T. Ito, and A. Ogiwara, A model for rouleaux pattern formation of red blood cells. Journal of theoretical biology, 1988. 130(2): p. 129-145.

141. PULANIC, D. and I. Rudan, The past decade: fibrinogen. Collegium antropologicum, 2005. 29(1): p. 341-349.

142. Wells, R. and H. Schmid-Schonbein, Red cell deformation and fluidity of concentrated cell suspensions. Journal of Applied Physiology, 1969. 27(2): p. 213-217.

143. Evans, E.A. and P.L. La Celle, Intrinsic material properties of the erythrocyte membrane indicated by mechanical analysis of deformation. Blood, 1975. 45(1): p. 29.

144. Mohandas, N. and S. Shohet, The role of membrane-associated enzymes in regulation of erythrocyte shape and deformability. Clinics in haematology, 1981. 10(1): p. 223.

145. Lim, H., et al., Measurement of blood coagulation with considering RBC aggregation through a microchip-based light transmission aggregometer. Clinical hemorheology and microcirculation, 2011. 47(3): p. 211-218.

146. Gijsen, F., F. Van de Vosse, and J. Janssen, The influence of the non-Newtonian properties of blood on the flow in large arteries: steady flow in a carotid bifurcation model. Journal of biomechanics, 1999. 32(6): p. 601-608.

147. Brookshier, K. and J. Tarbell, Evaluation of a transparent blood analog fluid: aqueous xanthan gum/glycerin. Biorheology, 1993. 30(2): p. 107.

148. de Jonge, E. and M. Levi, Effects of different plasma substitutes on blood coagulation: a comparative review. Critical care medicine, 2001. 29(6): p. 1261.

149. Hu, Q.H., J.Y. Li, and M.Y. Zhang, Effects of Fluid Viscoelasticity on the Performance of an Axial Blood Pump Model. ASAIO Journal, 2012. 58(1): p. 32.

150. Kobayashi, S., et al., Development of Blood Analog Fluids Using Human Hair Protein Particles. JSME International Journal Series C, 2005. 48(4): p. 494-498.

151. Naiki, T., Y. Yamai, and K. Hayashi, Evaluation of High Polymer Solutions as Blood Analog Fluid—For the Model Study of Hemodynamics—. J. Japanese Soc. Biorheol, 1995. 9: p. 84-89.

152. Nguyen, T., et al., A method for matching the refractive index and kinematic viscosity of a blood analog for flow visualization in hydraulic cardiovascular models. Journal of biomechanical engineering, 2004. 126: p. 529.

153. Shuib, A.S. Flow regime characterization in a diseased artery model. 2010.

154. Sousa, P., et al., Extensional flow of blood analog solutions in microfluidic devices. Biomicrofluidics, 2011. 5: p. 014108.

155. Srivastava, N. and M.A. Burns, Analysis of non-Newtonian liquids using a microfluidic capillary viscometer. Analytical Chemistry, 2006. 78(5): p. 1690-1696.

156. Thurston, G.B., Rheological parameters for the viscosity viscoelasticity and thixotropy of blood. Biorheology, 1979. 16(3): p. 149.

157. Thurston, G.B., Shear rate dependence of the viscoelasticity of polymer solutions.:: I. Theoretical model. Journal of non-newtonian fluid mechanics, 1987. 9(1-2): p. 57-68.

158. Cho, Y. and K. Kensey, Effects of the non-Newtonian viscosity of blood on flows in a diseased arterial vessel. Part 1: Steady flows. Biorheology, 1991. 28(3-4): p. 241.

159. Kensey, K.R. and Y.I. Cho, The Origin of Atherosclerosis: An introduction to hemodynamics2002: EPP Medica.

VITA

JIN MU JUNG

Drexel University, Philadelphia, PA 19104, USA

Email: jinmu3431@gmail.com

Education

Ph.D. in Mechanical Engineering and Mechanics
Drexel University, Philadelphia, PA — May, 2012
Advisor: Young I. Cho

M.S. in Mechanical Design Engineering
Chonbuk National University, Jeonbuk, Republic of Korea — Jul, 2009

B.S. in Mechanical Design Engineering
Chonbuk National University, Jeonbuk, Republic of Korea — Feb, 2007

Publications

1. **Jin M. Jung**, Yong Yang, Dong H. Lee, Greg Fridman, Alexander Fridman, Young I. Cho, Effect of dielectric barrier discharge treatment of blood plasma to improve rheological properties of blood, Plasma Chemistry and Plasma Processing, 32 (1), 2012, pp. 165-176.

2. **Jin M. Jung**, Dong H. Lee, Ki-Tae Kim, Young I. Cho, Determination of hematocrit using on-line conductance cell, International Journal of Heat and Mass Transfer, 55 (7-8), Mar. 2012, pp. 1836-1843.

3. Won Kim, Sung Kwang Park, Kyung Pyo Kang, Dong Hwan Lee, Sam Yeon Kim, **Jin Mu Jung**, Young I. Cho, Changes in whole blood viscosity at low shear rates correlate with intravascular volume changes during hemodialysis, International Journal of Artificial Organ, 2012, DOI: 10.5301/ijao.5000107.

4. Dong H. Lee, **Jin M. Jung**, Jong H. Ha, Young I. Cho, Improvement of heat transfer with perforated circular holes in finned tubes of air-cooled heat exchanger, International Communications in Heat and Mass Transfer, 39 (2), Feb. 2012, pp. 161-166.

Conferences

1. **Jin Mu Jung**, Yong Yang, Alexander Fridman, Young I. Cho, Mineral Fouling Control by Underwater Plasma Discharge in a Heat Exchanger, International Symposium on Plasma Chemistry, Philadelphia, USA, July 24-49, 2011.

2. Yong Yang, Hyoungsup Kim, **Jin Mu Jung**, Andrei Starikovksiy, Alexander Fridman, Young I. Cho, Application of pulsed spark discharge for mitigation of mineral fouling in a heat exchanger, Proceedings of International Heat Transfer Conference, Washington DC, USA, August 8-13, 2010.